Towards AI-driven Functional Prediction and Diagnosis of Cardiovascular Diseases

心臓血管系疾患の人工知能による機能予測と診断に向かって

July 2023

WANG SIRUI

Graduate School of Engineering

CHIBA UNIVERSITY

（千葉大学審査学位論文）

Towards AI-driven Functional Prediction and Diagnosis of Cardiovascular Diseases

心臓血管系疾患の人工知能による機能予測と診断に向かって

July 2023

WANG SIRUI

Graduate School of Engineering

CHIBA UNIVERSITY

Abstract

Cardiovascular disease (CVD) is a group of diseases involving the heart and the entire vascular system, such as strokes and coronary heart disease, usually resulting from cardiovascular risk factors (e.g., atherosclerosis, hypertension, hyperlipidemia, heart failure, etc.). Presently CVDs caused the highest mortality worldwide, posing a significant threat to human health. Thus, prediction and diagnosis of CVD are clinically important.

Evaluating cardiac function and observing changes in chamber structures through various functional and structural parameters have a positive impact on the prediction and diagnosis of CVD. Although there are numerous types of risk factors, and their diagnosis mainly relies on the measurement of different physiological signals (pulse waves, electrocardiograms (ECG), etc.) and clinical indicators (blood pressure, blood lipids, etc.). Pulse waves contain abundant physiological information related to CVD and functional structures. However, the present clinical application of pulse diagnosis is primarily through qualitative analyses. Assessing cardiac function through pulse wave detection chiefly relies on doctors' subjective experience, and it lacks sufficient support from evidence-based medicine. Furthermore, the variability in pulse waveforms complicates the process of feature extraction and analysis of these waveforms. Thus, devising a robust methodology for feature extraction that can elucidate the relationship between pulse waves and specific aspects of cardiac function and structure is vital for enhancing CVD diagnosis and treatment.

Surgical treatments are the most effective approach for the treatments of severe CVD. For instance, in the case of ischemic stroke caused by carotid artery stenosis (CAS), altering the vascular lumen structure through carotid endarterectomy, carotid angioplasty, and carotid stenting are common and effective treatment methods. Numerous research indicated that obtaining hemodynamics (e.g., blood flow velocity and pressure, etc.) before and after surgery is highly instructive for the selection and optimization of surgical procedures. Currently, although computational fluid dynamics (CFD) is the major method for obtaining hemodynamics, it requires specialized operational skills and high computational costs,

which hinder its clinical application. Thus, it is very important to develop an effective and accurate method for hemodynamic calculations.

Artificial intelligence methods including machine learning and deep learning enables providing new solutions to solve these problems. Leveraging big data and high-performance GPU computing clusters, AI technology is capable of rapidly and accurately extracting underlying features. These features can then be abstracted into high-level attribute features, which further enables the AI to accomplish pattern recognition and logistic regression tasks. Based on the research background, the main content of this thesis is as follows:

Chapter 2: 412 subjects after strict screening, are divided into two datasets according to whether suffering from cardiovascular diseases and high-risk factors. After that, pulse wave data and three cardiac function parameters of the two datasets were collected, while a fully connected network was developed for the ML-based regression analysis, assessing cardiac function status by directly predicting different cardiac function parameters through pulse waves (MAPE<15%). And the Bland-Altman analysis results demonstrating good consistency between ML prediction and clinical measurements. This Chapter revealed the quantitative relationship between pulse wave signal and cardiac function.

Chapter 3: Based on the finding of Chapter 2, we gathered clinical data from 237 patients with heart failure (HF) for further validating the quantitative relationship between pulse wave and specific disease. We selected five parameters that reflect the blood supply capacity in patients with HF. In addition to the previously used fully connected network, we also utilized the DenseNet network. Both networks accurately predicted the blood supply capacity parameters of heart failure patients based on pulse wave signals (MAPE<15%), quantitatively analyzing the relationship between pulse wave signals and blood supply capacity in the patients with heart failure. And besides, the ML prediction is agreed with the clinical measurements. This chapter proposed a new machine learning strategy that revealed the feasibility and possibility of pulse wave-based evaluation for blood supply capability in patients with heart failure, which will be clinically significant in health monitoring and deterioration prevention.

Chapter 4: We established four-point cloud datasets of the cardiovascular

hemodynamics of carotid artery stenosis before and after carotid artery surgery from CFD simulation results. The point cloud dataset can reflect the overall structure and inside flow field distribution of various models with remarkable resolution. We employed a novel deep learning network that enables analyzing and extracting the relationship between global geometric information and inside hemodynamics directly while avoiding the complex operations of CFD. Regrading sample resolution and applicability, our deep learning strategy outperforms previous studies on processing or deep learning. Statistical analysis shows that our deep learning method's predictions of hemodynamics are consistent with the results of the CFD method, but with a significant reduction in computational time. This chapter presents a DL-based strategy that revealed the possibility in real-time monitoring for carotid artery stenosis treatment, which is beneficial for the clinical treatment of ischemic stroke.

In summary, this thesis explores the application of AI approaches in the diagnosis and prediction of cardiovascular diseases, demonstrating high clinical value and application prospects.

Keywords：

Cardiovascular disease (CVD); Deep learning; Machine learning; Hemodynamics; pulse wave; carotid artery stenosis surgical treatments.

Table of Contents

Chapter I

General introduction

1.1 Cardiovascular diseases

1.1.1 Causes of cardiovascular disease (CVD)

Cardiovascular disease (CVD) usually indicates heart, brain, and systemic ischemic or hemorrhagic diseases, such as type 2 diabetes, hyperlipidemia, atherosclerosis, hypertension, ischemic stroke caused by carotid artery stenosis.

1.1.2 The harm of cardiovascular diseases:

CVD poses a serious threat to human health, especially for people over the age of 50. It is characterized by high morbidity, high disability, and high mortality rates. More than 15 million people die from cardiovascular diseases worldwide every year, ranking first among all causes of death. Heart failure is a serious consequence of cardiovascular disease that has not been treated promptly and effectively. Coronary artery disease can lead to insufficient blood supply to the heart, which may cause a myocardial infarction. Myocardial infarction can impair the heart's pumping function, leading to heart failure.

1.1.3 Diagnosis and treatment of cardiovascular diseases:

Currently, cardiovascular disease is the highest mortality disease in the world, posing a serious threat to human health. Therefore, the diagnosis and treatment of cardiovascular diseases are of great significance.

Risk factors and irregular cardiac function are the direct causes of CVD. Hence, detecting various risk factors has a positive effect on the diagnosis and treatment of CVD. There are many risk factors for cardiovascular diseases. Their detection mainly relies on various clinical signals (such as pulse waves, electrocardiograms, and heart sounds) and clinical indicators (such as blood pressure, blood lipids, and blood viscosity). Taking pulse waves as an example, noninvasive hemodynamic detection technology, exemplified by pulse

wave detection and analysis, has become prevalent as a crucial approach for noninvasive cardiovascular function examination due to its convenience, speed, and high reliability. Pulse waves begin with the heartbeat, propagate in the arterial blood vessels, and continuously reflect at various downstream branches. Therefore, pulse waves are influenced not only by the heart but also by a variety of physiological and pathological factors, including vascular resistance and arterial stiffness at different arterial levels and branches. Pulse wave characteristics, such as velocity, shape, amplitude, and period, are very correlated to vascular function conditions. Therefore, distinct physiological and pathological alterations result in diverse pulse wave features. Jin et al. found that pathological events such as atherosclerosis can significantly increase pulse wave velocity. M et al. discovered that hypertension or certain CVDs can lead to wave reflection advances, causing the first and second wave peaks to overlap. Song et al. found that hypertension can also increase the amplitude and duration of the major wave of the pulse shape. Fig. 1-1 shows that cardiovascular function changes caused by CVD risk factors can be reflected in changes in pulse wave waveform.

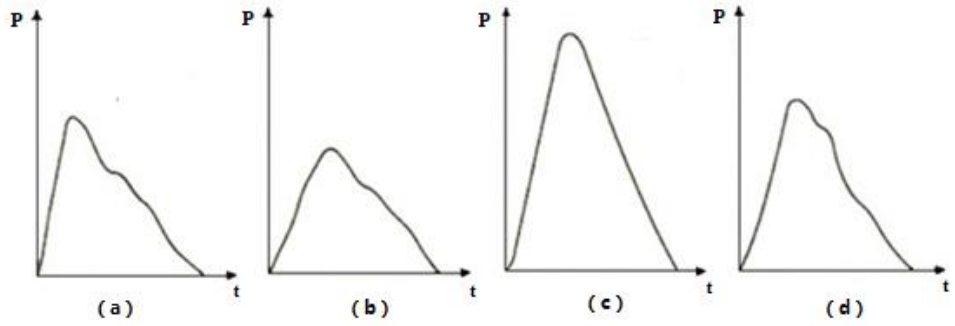

Fig. 1-1 Change of pulse wave under different physiological and pathological. (a) normal (b) aortic stenosis (c) the aortic regurgitation (d) arteriosclerosis. The decrease of arterial elasticity caused by CVD speed up the propagation of pulse wave. Reflected in the characteristics of the waveform is the early appearance of the reflected wave (the second wave peak) or the increase of the amplitude of the main wave peak.

However, multiple risk factors often coexist. In addition, pulse waves are influenced by

age, gender, and lifestyle habits. This makes it difficult to extract pulse waveform parameters related to specific types of CVD risk factors. Therefore, obtaining and analyzing the typical features of pulse waves under specific types of risk factors helps in the effective diagnosis and treatment of different CVDs.

Obtaining lesion site information of CVD patients based on medical imaging technology and further obtaining the patient's hemodynamic parameters based on this information have important significance for the treatment and diagnosis of CVD. Medical imaging techniques such as computed tomography (CT) and digital subtraction angiography are used to examine cardiovascular lesions. Medical imaging technology can noninvasively obtain lesion tissue images (such as coronary artery stenosis) and provide a reliable data basis for establishing personalized 3D cardiovascular models based on precise anatomical structures. Combining computational fluid dynamics (CFD), finite element analysis, fluid-structure interaction (FSI) techniques, etc., accurate hemodynamic parameters of lesion sites can be obtained, thereby realizing the formulation and optimization of related treatment plans. This paper mainly focuses on the calculation of hemodynamics.

Taking ischemic stroke caused by carotid artery stenosis as example, blockage of the common carotid artery (CCA) or internal carotid artery (ICA) caused by atherosclerosis, also known as carotid artery stenosis (CAS), resulting in reduced blood supply to the brain is known as ischemic stroke, accounting for brain stroke 87%. Patients with severe CAS often require revascularization surgery to prevent ischemic stroke. The corresponding commonly used surgical methods as shown in Figs. 1-2, 1-3, and 1-4: carotid endarterectomy, carotid angioplasty, and carotid stent placement [1–4], the following background should be explained:

Carotid endarterectomy is a surgical treatment for carotid artery disease, used to remove plaque in the carotid artery to improve the blood flow of the carotid artery and reduce the

risk of stroke. Plaque accumulation (atherosclerosis) may restrict blood flow to the brain. During surgery, the surgeon makes an incision in the front of the neck, opens the carotid artery, and clears the plaque blocking the artery. Then, the surgeon repairs the artery with sutures or a patch made from a vein or artificial material (graft repair).

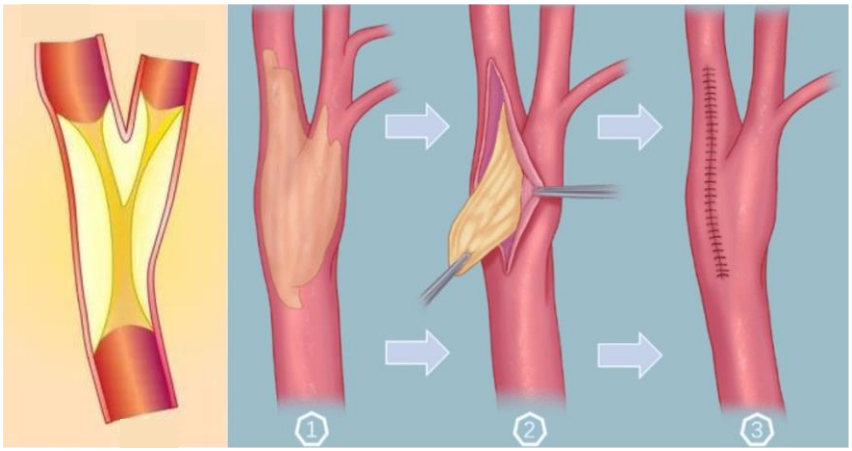

Fig. 1-2 Schematic diagram of carotid endarterectomy

Carotid angioplasty is a medical procedure that involves opening a blocked artery to restore blood flow to the brain. During the procedure, a narrow area is opened using a thin tube with a balloon tip, and a tiny mesh tube called a stent can be placed in the area to help keep the artery open. Carotid angioplasty is considered a non-surgical procedure because it is less invasive than surgery and may shorten recovery time. The procedure is commonly used to treat or prevent strokes, especially when the blockage in your carotid artery reaches or exceeds 70%, and your overall health is not good enough to undergo surgery.

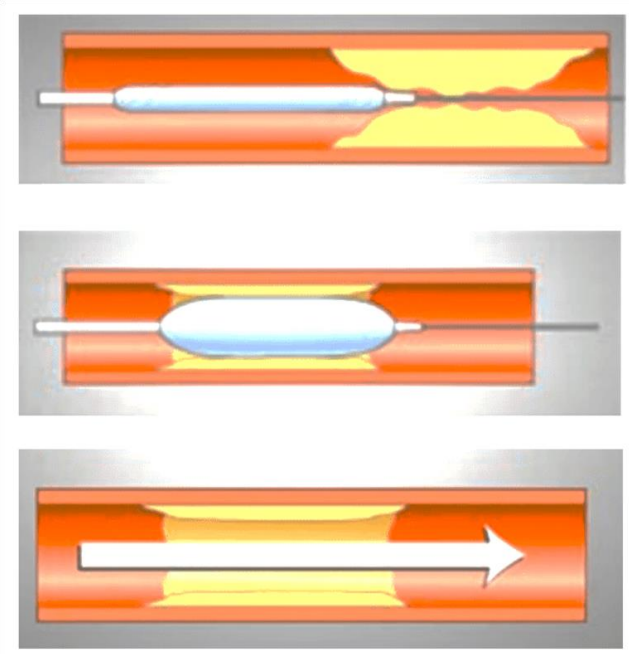

Fig. 1-3 Schematic diagram of carotid angioplasty

Carotid artery stent placement is a medical procedure used to treat carotid artery stenosis, which is the narrowing of the carotid artery caused by plaque accumulation. During the procedure, a small metal coil called a stent is placed in the blocked artery to support it and reduce the chances of it narrowing again. Carotid angioplasty and stenting can be used when traditional carotid surgery (carotid endarterectomy) is not possible, or the risks are too high. Compared to carotid endarterectomy, this procedure is considered a less invasive option with a quicker recovery time. However, as with any medical procedure, there are risks involved, and patients should discuss the risks and benefits with their doctor.

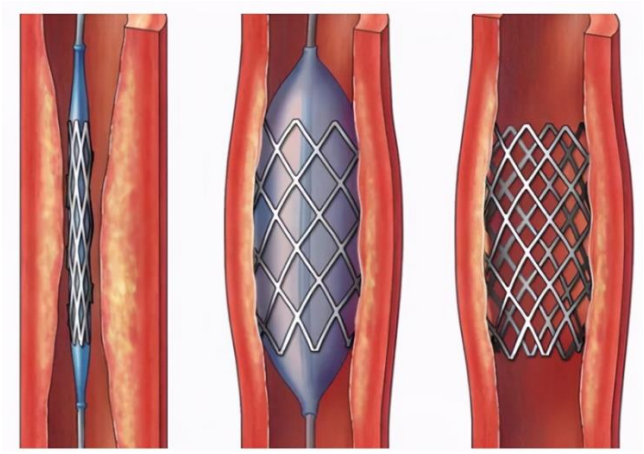

Fig. 1-4 Schematic diagram of carotid artery stent placement

Numerous studies and clinical practices have demonstrated that obtaining accurate hemodynamic parameters of cardiovascular lesions before and after surgery is crucial for the selection and optimization of surgical plans [5–7]. These three surgeries can effectively improve the issue of a narrowed carotid artery lumen. Therefore, obtaining hemodynamic parameters of the blood flow in the lumen before and after surgery can provide guidance for the optimization of surgical plans.

Computational Fluid Dynamics (CFD) is a major method for obtaining hemodynamics [8–11]. However, CFD typically requires specialized operational skills and high computational cost [12,13]. CFD methods usually take several hours to calculate the hemodynamic parameters of a patient's individualized model, which is difficult to accept for clinical applications, especially for real-time surgical guidance.

1.2 Artificial intelligence (AI)

1.2.1 Definitions and classifications.

Artificial Intelligence (AI) involves the imitation of human cognitive abilities in machines or computer systems, allowing them to think, learn, and tackle problems similarly

to humans [14]. This interdisciplinary field merges computer science, mathematics, cognitive psychology, and other areas to develop algorithms, models, and systems capable of executing tasks that generally require human intellect [15].

Essential elements of AI encompass machine learning, deep learning, and natural language processing. These components allow AI systems to acquire knowledge from data, refine their performance over time, and engage with humans in a more intuitive manner. [16]

1.2.2 Machine learning and deep learning

Machine Learning (ML) is a subset of AI, which enables computers to learn automatically through accumulated experiences [17]. ML algorithms typically build a mathematical model based on sample data, known as "training data", to make predictions or decisions without being explicitly programmed to perform the tasks, and to uncover key insights in data. These algorithms improve their performance as the number of samples available for learning increases. They identify patterns within the given data, learn from them, and then apply what they've learned to make informed decisions [18]. This process begins by feeding the algorithm high-quality, relevant data and allowing it to learn and make predictions.

Deep Learning (DL) is a subset of AI and ML [19], employs multi-layered neural networks to simulate human brain behaviour. These models automatically and adaptively learn from data through the creation and optimization of artificial neural networks. Unlike ML, DL combines basic features to generate a lot of abstract, complicated representations, enabling it to discover distributed feature representations in data. This makes it especially effective for handling large volumes of unstructured or unlabelled data, positioning it as a valuable tool in big data analytics.

1.2.2 Detection of CVD conditions or factors via AI approaches

Utilization of AI approaches to detect cardiovascular disease conditions or cardiac function mainly by processing physiological signals related to the cardiovascular system. In this paper, we choose the pulse wave as the research object. The main reason is compared with other physiological signals (such as heart sounds, etc.), pulse wave contains richer physiological and pathological information. The pulse wave is often influenced by various CVD risk factors, complications, and clinical parameters. In contrast, most previous studies have primarily concentrated on examining the relationship between pulse waves and various cardiac function parameters using statistical analyses, which are typically of a qualitative nature. And because of the uncertainty of noise and interference, it is impossible to quantitatively and accurately predict cardiac function parameters to provide clinicians with various information about pulse waves. Although several studies based on physical-mathematical models could capture our body signals, like aortic pressure and cardiac output, however they usually have limitations in selecting and simplifying reliable governing differential equations to accurately calculate complicated mechanisms and these physical-mathematical models sometimes require additional input of various physiological factors, and the calculation cost is very high.

For machine learning methods, for this long-standing and challenging topic, the recent rapid development of AI technology may be able to provide a solution because of its powerful feature extraction ability and significant success in various signal analysis. They have been successfully applied for medical signals analysis, such as pulse wave, electrocardiogram (ECG), and heart sound: Hannun et al. reported an accurate diagnosis of arrhythmia based on the feature extraction of dynamic ECG signals [20]; Chen et al. confirmed the recognition of different heart sound signals [21]; Li et al. realized the classification task of five cardiovascular disease risk factors based on pulse wave [22]. These

studies have however paid a specific attention to the pattern classification while not being able to provide a direct and accurate prediction on the values of the cardiac function parameters through medical signals, which remains challenges.

1.2.3 Prediction of cardiovascular hemodynamic based on deep learning

Several studies have evaluated the potential of deep learning for predicting hemodynamics. For example, Itu et al. implemented fraction flow reserve (FFR) calculations using machine learning[18], while Guo et al. employed a deconvolution network to anticipate changes in the flow field around simple geometric obstacles [23]. Liang et al. utilized deep learning to predict the hemodynamics of an ideal thoracic aortic model [24].

Compared to conventional Computational Fluid Dynamics (CFD) methods, deep learning enhances computational speed for hemodynamic parameters and simplifies complex operations. However, these studies share a common limitation: their reliance on overly simplistic and idealized flow datasets. The low resolution of these datasets inadequately represents the intricate geometry and flow field distribution of the cardiovascular system, as illustrated in Fig. 1-5.

Furthermore, the proposed deep learning networks require adjustments for different hemodynamic parameters, limiting their universality. Hence, the application of deep learning to predict patient-specific cardiovascular hemodynamics remains challenging.

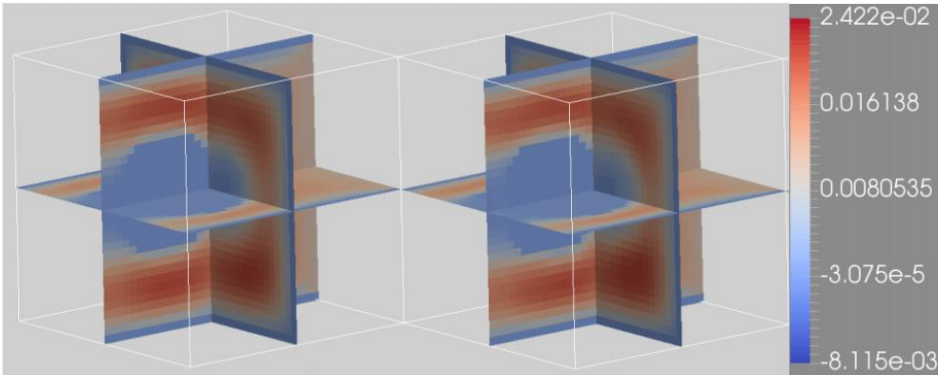

Fig. 1-5 Guo's study presented a 3D flow velocity field prediction, with CFD simulation on the left and DL prediction on the right. The pixel-level resolution was insufficient to accurately depict the cardiovascular system's geometry and hemodynamic distribution.

1.3 Objectives

Based on the above research background, this study separately collected 412 subjects' pulse wave signals physiological and pathological information, 237 patients with heart failure's pulse waves and their in-hospital clinical information, and 297 subjects' cerebral and carotid CT data. On this basis.

(1) For the predication of cardiac function of different populations:

- Select cardiac function parameters: artery compliance (AC), total peripheral resistance (TPR), and stroke volume (SV).
- Use machine learning to quantitatively analyze the relationship between pulse wave and cardiac function.
- Develop a machine learning-based strategy for predicting cardiac function parameters.

(2) For the predication of blood supply capability of patients with heart failure:

- Select parameters left ventricular ejection fraction (LVEF), left ventricular end-diastolic diameter (LVDd), left ventricular end-systolic diameter (LVDs), left atrial dimension (LAD), and peripheral oxygen saturation (SpO2).
- Use two machine learning networks to quantitatively reproduce the relationship between pulse wave and blood supply capability of patients with heart failure.
- Employed two machine learning networks for predicting blood supply capability parameters.

(3) For cardiovascular hemodynamic prediction of carotid artery stenosis:

- Select CVD: carotid artery stenosis.
- Use deep learning to bridge the correlation between hemodynamics and geometry of artery stenosis.
- Employed a fast, accurate and high-resolution deep learning approach to predict hemodynamics of carotid artery stenosis before and after surgical treatments.

1.4 Thesis contents

The contents of this thesis are outlined as follows:

- Chapter I: an introduction of cardiovascular diseases, artificial intelligence methods, and a proposal of research objectives of this thesis;
- Chapter II: a study utilizing machine learning approach for the prediction of cardiac function for different populations through pulse wave;
- Chapter III: a study utilizing two machine learning networks for the evaluation of blood supply capability specifically for patients with heart failure through pulse wave;
- Chapter IV: a study to predict the internal hemodynamics of carotid artery stenosis before and after a surgical treatment via deep learning;
- Chapter V: a conclusion of this study and the outlook beyond the content in this thesis.

Chapter II

Machine learning-based strategy in fast predicting cardiac function using peripheral pulse wave

2.1 Introduction

Pulse wave (Fig. 2-1-a) has been extensively used for the initial clinical diagnosis of cardiovascular diseases (CVDs) owing to its convenient and rapid measurement with high reliability[25] [26]. Pulse wave starts from the heart and propagates from the aorta to all levels of branched arteries (Fig. 2-1-c), and it contains a large amount of information (Fig. 2-1-I) associated with the cardiovascular status under normal and abnormal conditions. It is pointed out that the cardiovascular function is characterized by pulse wave [27]; the arterial stiffness degree of patients with type 2 diabetes can be judged via pulse waves through conducting quantitative wave analysis [28]; and there exist specific discrepancy in the harmonics of pulse waves between hypertension patients and healthy people based on frequency-domain analysis method [29].

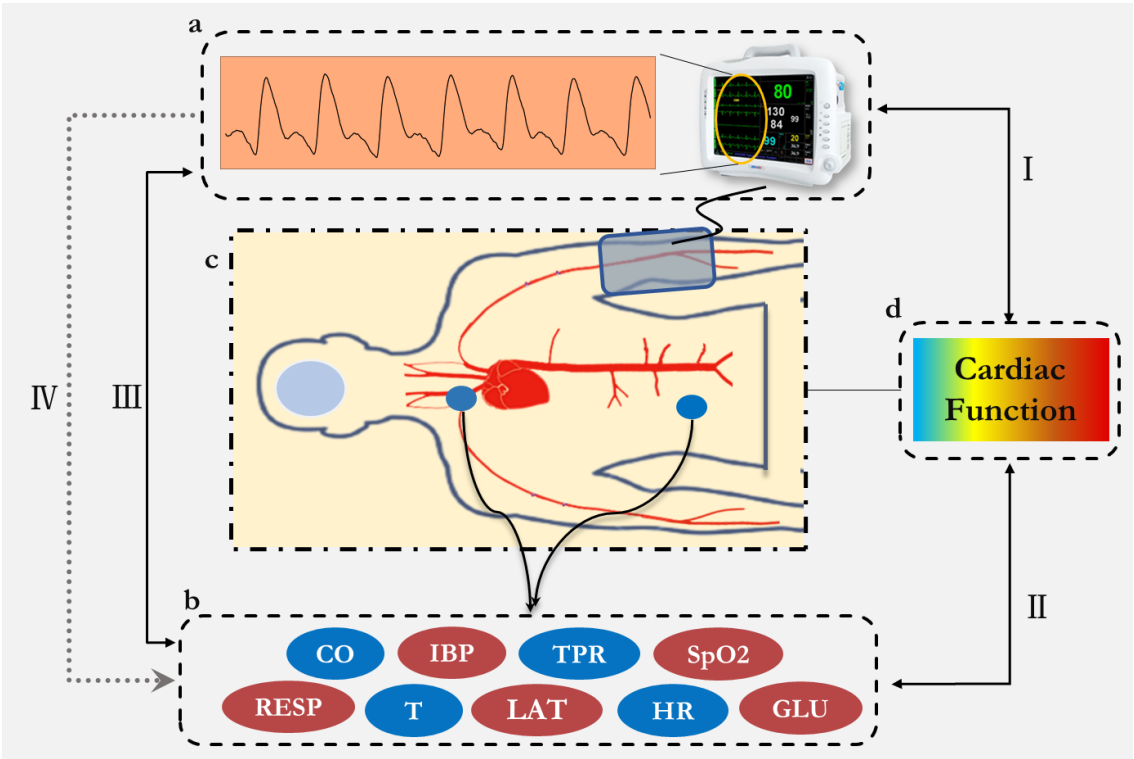

Fig. 2-1 Relationship among pulse wave, cardiac function parameters, and cardiac function. CO: Cardiac Output; IBP: Invasive Blood Pressure; TPR: Total Peripheral Resistance; SpO2: Blood Oxygen Saturation; RESP: Respiration; T: Temperature; LAT: Lactate; HR: Heart Rate; GLU: Blood Glucose.

As illustrated in Fig. 2-1-II, compared with pulse wave, cardiac function parameters (Fig. 2-1-b) can reflect the functional state of CVS more accurately and directly in terms of total peripheral resistance (TPR), stroke volume (SV), arterial compliance (AC), etc. For instance, SV directly represents the outcome of heart-pumping ability, is a perioperative monitoring indicator during cardiovascular surgery [30]; AC reflects the ability of the artery to passively expand during ventricular systole to accommodate most of the stroke volume while continuing blood flow during diastole [31]; and TPR is the amount of afterload on circulating blood exerted by the circulation system [32]. However, directly measuring cardiac function parameters usually requires specialized and expensive equipment along with the guidance of clinical technicians, and even in an invasive manner [33][34], which hinders the clinical application. Patients with CVDs normally suffer from several CVDs or pathogenic high-risk factors simultaneously [35][36], which may result in rapid deterioration or even sudden death without obvious symptoms [37][38][39]. Thus, timely while feasible diagnosis and treatment are of great importance for the patients. On the other hand, the diagnosis process associated with CVDs is normally of high complexity requiring professional physicians to perform with consideration of multi-cardiac function parameters [40][41][42]. Therefore, clarification and quantification of the correlations between pulse wave and cardiac function parameters (Fig. 2-1-IV) is of great clinical significance in health monitoring and CVD diagnosis, which remains however poorly studied yet.

Previous studies have mainly focused on analyzing the correlations between pulse wave and various cardiac function parameters through statistical analyses [43][44][45], which are normally qualitative and fail to provide clinicians with a quantitative and accurate prediction on various cardiac function parameters because of the uncertainties due to noise and interference information in concern with pulse waves. While a variety of physical-mathematical models of the CVS have been also proposed to capture the physiological

signals such as aorta pressure and cardiac output [46][47][48], they usually share limitations in the difficulties of selecting and simplifying reliable control differential equations to accurately capture the complex mechanisms in CVS, and of appropriate defining and adjusting the many various parameters [49][50]. These physical-mathematical models sometimes also need additional input of multiple physiological factors with high computational costs [51]. For this long-standing and challenging topic, recent rapid developments in machine learning (ML) methods may be able to provide a solution because of its powerful feature-extracted capability and significant success in various signal analyses [52][53][54][55]. An ML strategy may make this possible through setting the personalized pulse wave signal as input and quantitatively predicting the cardiac function parameters as output. The ML-based methods normally comprise more abstract high-level features of the signal with multi-layer perceptions of the network or through integrating low-level features, thus capable of achieving signal classification or prediction tasks [56]. They have been successfully applied for medical signals analysis, such as pulse wave, electrocardiogram (ECG), and heart sound: Hannun et al. reported an accurate diagnosis of arrhythmia based on the feature extraction of dynamic ECG signals [20]; Chen et al. confirmed the recognition of different heart sound signals [57]; Li et al. realized the classification task of five cardiovascular disease risk factors based on pulse wave [22]. These studies have however paid a specific attention to the pattern classification while not being able to provide a direct and accurate prediction on the values of the cardiac function parameters through medical signals.

In this study, we aim at for the first time proposing an ML strategy that enables a fast while accurate noninvasive prediction of the cardiac function parameters based on pulse waves. We collected pulse wave signals from 412 subjects while recording their relating cardiac function parameters and clinical information. To accurately predict the cardiac

function parameters with the limited clinical data, we inflicted high requests in our datasets and ML structure to fit the flexibility of the input signal formats, which is also the major technical matter and hence the advantage of this study. Based on various cardiovascular statuses, we established two high-quality pulse wave datasets and developed a novel ML-based framework for predicting three selected cardiac function parameters (AC, TPR, and SV). Error analysis results verify that our ML model can achieve high accuracy in the prediction of TPR and SV (MAPE<15%) and the predictions are well consistent with the clinical measurements.

2.2 Methods

2.2.1 Data collection and ethics approvals

All data employed in this study was taken from a previous study [4], in which the original wrist-based pulse wave data of 412 subjects were collected along with the related clinical information. For all the subjects, pulse waves and blood pressure were measured and recorded with the Blood Pressure/Pulse Wave Examining Apparatus -Fukuda VS-1500A under doctors' guidance with each pulse wave collected comprising more than five valid periods, while the cardiac function parameters were measured and recorded with the CHM-T3002 Cardiac Hemodynamic Monitoring device (manufactured by Shandong Baolihao Medical Appliances, Ltd, China) taken by clinicians and the related clinical information involving height, weight, age, gender, etc. were also collected (Fig. 2-1), All subjects were informed of the detection date and were asked not to eat irritating food or drink alcohol until the collection was completed. All the subjects were registered at Beijing University of Technology Hospital in 2015, and their medical records were also collected associated with CVDs and related risk factor information.

The Clinical Research Ethics Committee of the Beijing University of Technology

approved the study. All measurements were carried out under the related regulations and guidelines. We obtained the signed informed consent.

2.2.2. Data screening

To verify whether our machine learning method is universally applicable for both healthy people and CVD patients, based on the pathological information, we classified the datasets into two subject groups: a healthy-subject group and a CVD-subject group. Fig. 2-2 illustrates the procedure of data screening. For the CVD-subject group, 138 subjects fulfilled the criteria: 1) the detection of the pulse wave and the cardiac function parameters was completed; 2) the patients with congenital heart disease, heart failure, aortic aneurysm, and other uncommon CVDs were excluded, according to medical interviews, physical examinations, and medical history information checks (due to the sample data limited, we further excluded few patients with diseases such as congenital heart disease that had significant effects on pulse waves and cardiac function parameters [58]); 3) the group subjects solely suffered from one or more of the five cardiovascular diseases or high-risk factors among coronary heart disease, hypertension, hyperlipidemia, arteriosclerosis, and type 2 diabetes. For the healthy-subject group, 126 subjects fulfilled the criteria: 1) the detection of the pulse wave and the cardiac function parameters was completed; 2) the patients involved in the CVD-subject group were excluded, according to medical interviews, physical examinations, and medical history information checks. In addition, taking into consideration that the basic physiological parameters can affect the pulse wave characteristics [59], we carried out an independent sample t-test for the basic physiological parameters of the two subject groups to exclude the impact of multiple noise factors on the two data groups. Moreover, we conducted a Pearson's chi-squared test to investigate whether the gender distributions have significant correlations with cardiac function [38] in our

datasets.

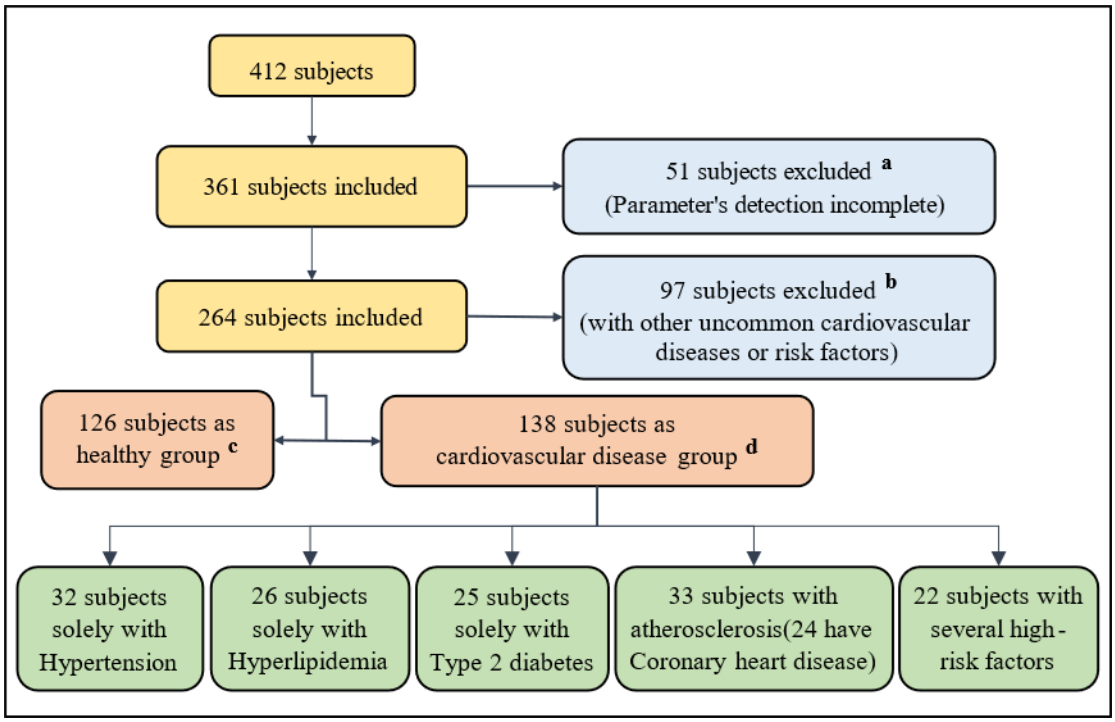

Fig. 2-2 Data screening procedure. Screening criteria [a,b,c,d]: for [a], 51 subjects with incomplete relevant information are excluded; for [b], with a focus on the effects of common CVDs and high-risk factors, 97 patients with uncommon CVDs or risk factors are excluded; for [c,d], a healthy-subject group of 126 subjects and a CVD-subject group of 138 subjects are created.

2.2.3 Pulse wave preprocessing and dataset creation

As reported by previous studies there often exist various noises and interrupt signals introduced during the pulse wave sampling procedure [60][61][62], thus the preprocessing of the pulse wave signals that mainly contain denoising and normalization was performed by averaging the pulse waveforms of the targeted pulse waves of each subject based on the data of all the valid cycles (more than five cycles at a stable state)[63][64]; and the noise was eliminated with the wavelet transform decomposition method [28], [65]. Since the pulse-wave sampling points were confirmed to convert from 1000 to 100 according to the

Nyquist theorem and the actual sampling frequency (1000Hz), substantially the pulse wave amplitude was normalized to a range of 0-100. As a result, two pulse wave datasets were created comprising a 126 healthy-subject dataset and a 138 CVD-subject dataset, and they were further separated to training set and test set by the division ration of 4:1. Details of the two datasets for the machine learning analysis are summarized in Table 1.

Table 2-1: The details of ML analysis data sets.

Pulse wave datasets	Cardiac function parameters	Total pulse number	Training number	Test number
H-subject dataset	AC	126	101	25
	TPR	126	101	25
	SV	126	101	25
CVD-subject dataset	AC	138	111	27
	TPR	138	111	27
	SV	138	111	27

Note: AC: Arterial Compliance; TPR: Total Peripheral Resistance, SV: Stroke Volume.

2.2.4 Machine learning network

To choose an appropriate ML network for this study, we conducted many preliminary experiments for testing and comparison of prediction stability and performance among different networks (e.g., CNN and other machine learning networks). As a result, a fully connected network was substantially chosen and employed in all the simulations, which was further optimized in terms of the network parameters, e.g., number of hidden layers, neurons of each hidden layer, loss function, et al., as illustrated in Fig. 2-3. The network is composed of three parts: an input layer, five hidden fully connected layers, and an output layer. In addition, the neuron quantity in the five fully connected layers was set to be 1024, 256, 64, 16, and 4, respectively. And the ReLU was employed as the activation function after each

layer. The mean-square error (MSE) was used as the loss function; adam optimizer was employed with a learning rate of 0.001, $\epsilon = 0.001$, $\rho 1 = 0.9$, $\rho 2 = 0.999$, and $\delta = 1E\text{-}8$, respectively [66]. The ML network was trained with TensorFlow (v2.0.0rc, Python 3.7 on a Nvidia GeForce GTX 1660 Ti GPU).

The training process for the ML network was accomplished by separately setting the three parameters (AC, TPR, and SV) as output while employing the corresponding pulse waves of two subject groups as input, which resulted in six training times in total for the prediction of the three cardiac function parameters of the two subject groups. The input layer length is taken as 100, which is equal to the sampling number of each pulse wave after normalization, while the length of the output layer is 1, namely the single selected cardiac function parameter in each training time. Since all the parameters for the six training networks were chosen and adjusted based on the prediction performance among the huge networks, we further optimized the configuration and stored the set of parameters associated with the six training networks for other predictions. Error analysis and consistency analysis were also conducted for each corresponding test dataset.

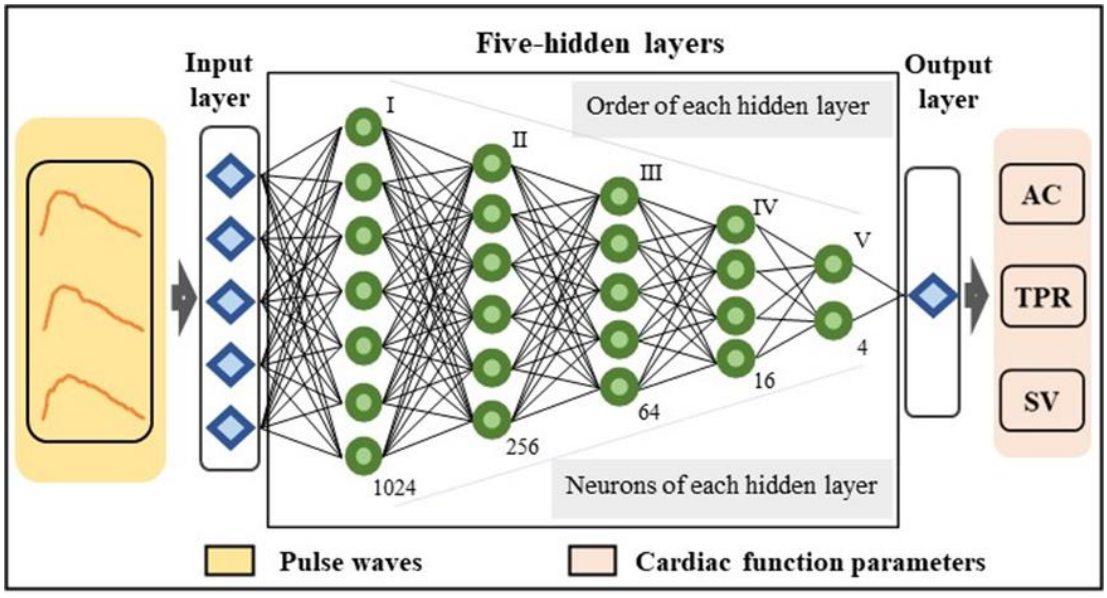

Fig. 2-3 The architecture of machine learning network. The network contains an input layer,

an output layer and five hidden layers. The numbers represent the neuron quantity of each hidden layer. AC: Arterial Compliance; TPR: Total Peripheral Resistance, SV: Stroke Volume.

2.2.5 Error functions and consistency analysis

To evaluate the ML model, we employed the Mean Absolute Percentage Error (MAPE) as the error function:

$$\text{MAPE} = \frac{100\%}{n}\sum_{i=1}^{n}\left|\frac{\hat{y}-y}{y}\right|, \quad (1)$$

where y and $\hat{y}$ denote the clinical-measured value and the ML-predicted value of the cardiac function parameters, respectively; n is the quantity of the test dataset. The MAPE was calculated for the test datasets with the accuracy defined as:

$$\text{Accuracy} = 1 - \text{MAPE}, \quad (2)$$

In addition, we utilized the Bland-Altman method for the consistency analysis of the clinical measurement and ML-based prediction. The Bland-Altman method can dissect the discrete tendency, the agglomeration tendency, and the relevance of the three cardiac function parameters between two datasets based on the two different methods. When the three parameters fall within the allowable range, it can be considered that the two data sets have a good consistency, and the two methods can be substituted for each other [67]. See details in the results section.

2.3 Results

After the data screening and preprocessing, two high-quality pulse wave datasets of a healthy-subject group (H-group) and a CVD-subject group (CVD-group) were successfully built up, which were adapted to the flexible input data format and the datasets. As illustrated in Fig. 2-4, five pulse waves were plotted along with their averages from the two subject

groups, respectively, which obviously display distinguishable waveform features between them. To clarify the featured discrepancy between the two groups associated with the three cardiac function parameters (SV, AC, TPR) along with the related clinical information, we further performed the t-test for the two subject groups. As summarized in Table 2, the mean values of the H-group and CVD-group differ significantly in terms of blood pressure and cardiac function parameters ($p<0.05$), but there is no dissimilarity between the two groups regarding basic physiological parameters (age, height, weight, and BMI (Body Mass Index)) ($p>0.05$). Besides, the Pearson's chi-squared test results indicate that there exist some significant correlations between gender distribution and cardiac function ($\chi^2>3.84$, $p<0.05$) (Table 2).

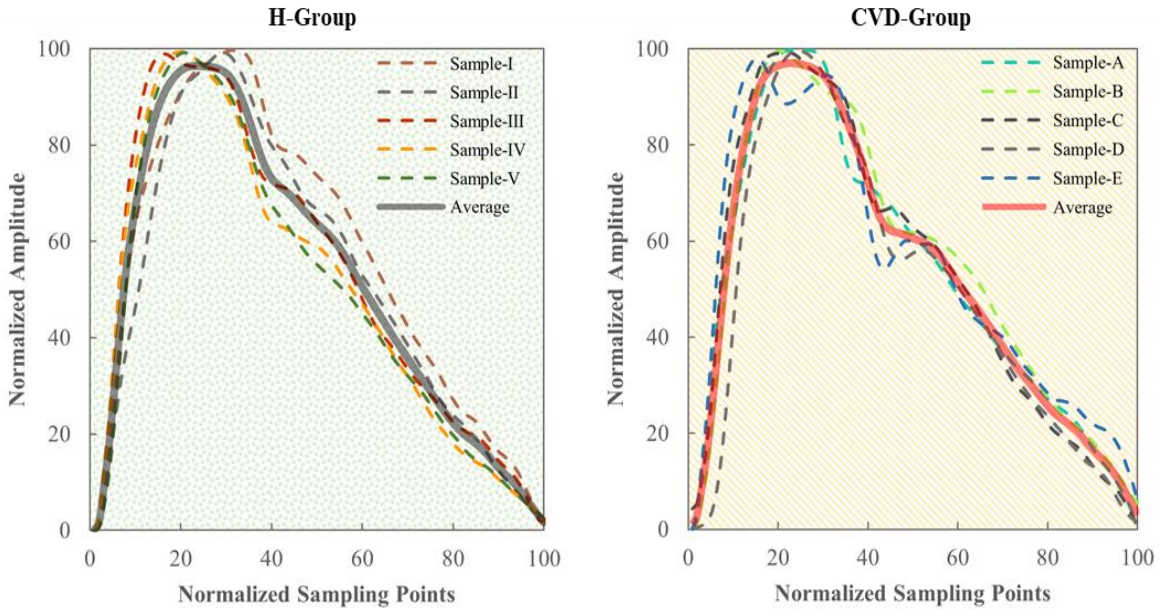

Fig. 2-4 Five samples (dashed lines) of the preprocessed pulse waves from H-group and CVD-group along with their averages (solid lines), respectively.

Table 2-2: Basic characteristics in H-Group and CVD-Group.

Characteristics	All subjects	H-group	CVD-group	p

Age	61.6 ± 7.1	60.7 ± 6.0	62.5 ± 8.1	0.102
Heights	161.2 ± 6.9	161.1 ± 7.0	161.4 ± 6.9	0.809
Weight	66.2 ± 9.9	65.7 ± 9.5	66.7 ± 10.7	0.541
BMI	25.5 ± 3.6	25.6 ± 3.9	25.4 ± 3.4	0.735
BPS	140.8 ± 19.0	125.8 ± 8.9	155.8 ± 13.8	0.000
BPD	83.0 ± 10.5	77.3 ± 6.7	88.6 ± 10.6	0.000
SV	76.7 ± 17.7	80.8 ± 18.4	72.9 ± 16.1	0.005
AC	1.7 ± 0.6	1.9 ± 0.5	1.4 ± 0.5	0.000
TPR	1585.3 ± 400.0	1479.3 ± 376.0	1686.0 ± 402.2	0.001
Male	63	22	41	χ^2=5.440, p=0.020
Female	201	104	97	

Note: Data are presented as mean± SD; p values were calculated based on the independent samples t-test; and Pearson's chi-squared test results for gender distributions are also given. BPS: Blood Pressure-Systole (mmHg); BPD: Blood Pressure-Diastole (mmHg); AC: Arterial Compliance (ml/mmHg); TPR: Total Peripheral Resistance (dyn·s/cm^5), SV: Stroke Volume (ml/Beat).

For the three cardiac function parameters (SV, AC, TPR) we constructed three datasets separately for each of the two subject groups, resulting in six datasets in total, and applied the six datasets to the ML model to train and optimize the model through minimizing the loss function during each epoch of the training process. As depicted in Fig. 2-5, the six learning curves all converge well with a monotonously declining trend without overfitting at the training phase. In addition, to avoid overfitting caused by using the limited datasets, we employed the early stopping strategy for all the ML analyses i.e., terminating the iteration during the training phase to prevent overfitting [68][69]. As shown in Fig 2-6, the accuracy of the test dataset for every 20 epochs was recorded with the training loss function. When the accuracy of the test dataset could not be improved in the continuous 100 to 200 iterations

(more than 50 epochs), we introduced the early stopping strategy to stop the redundant training work to avoid overfitting. After the training, the optimal parameters of each ML model were stored for further use in predicting the three cardiac function parameters of two subject groups at the test phase. The error analysis was further made and as summarized in Table 3, both TPR and SV of the two subject groups demonstrate a low error level with MAPE<15%, indicating that the present ML model is capable to achieve a sufficiently accurate prediction of the two key cardiac function parameters.

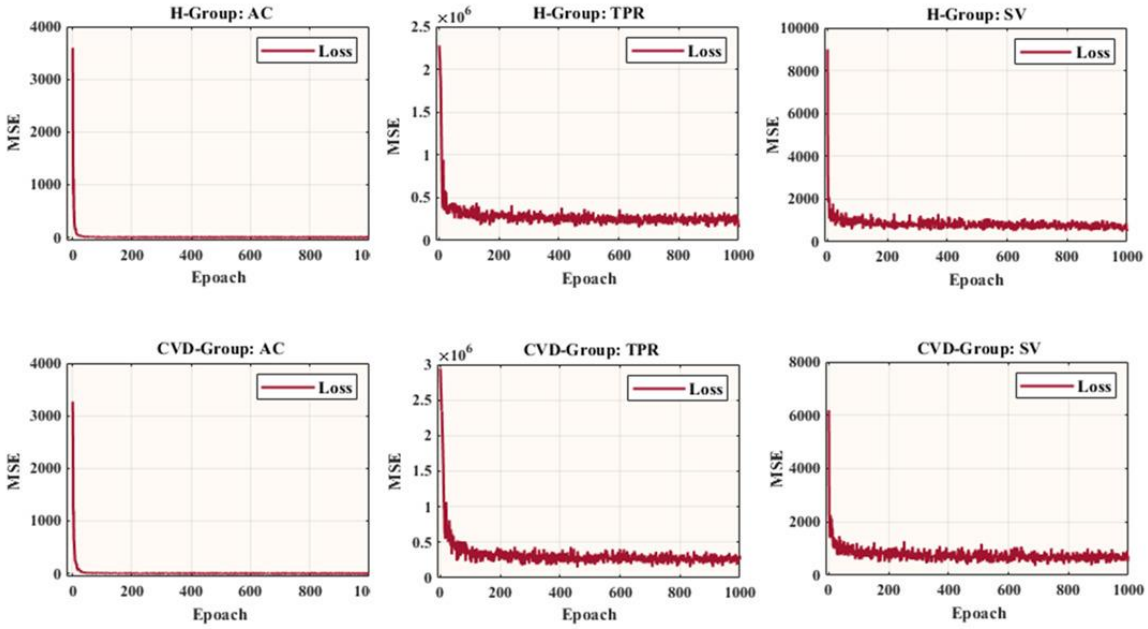

Fig. 2-5 Learning curves for two subject groups in terms of cardiac function parameters of arterial compliance (AC), total peripheral resistance (TPR), and stroke volume (SV).

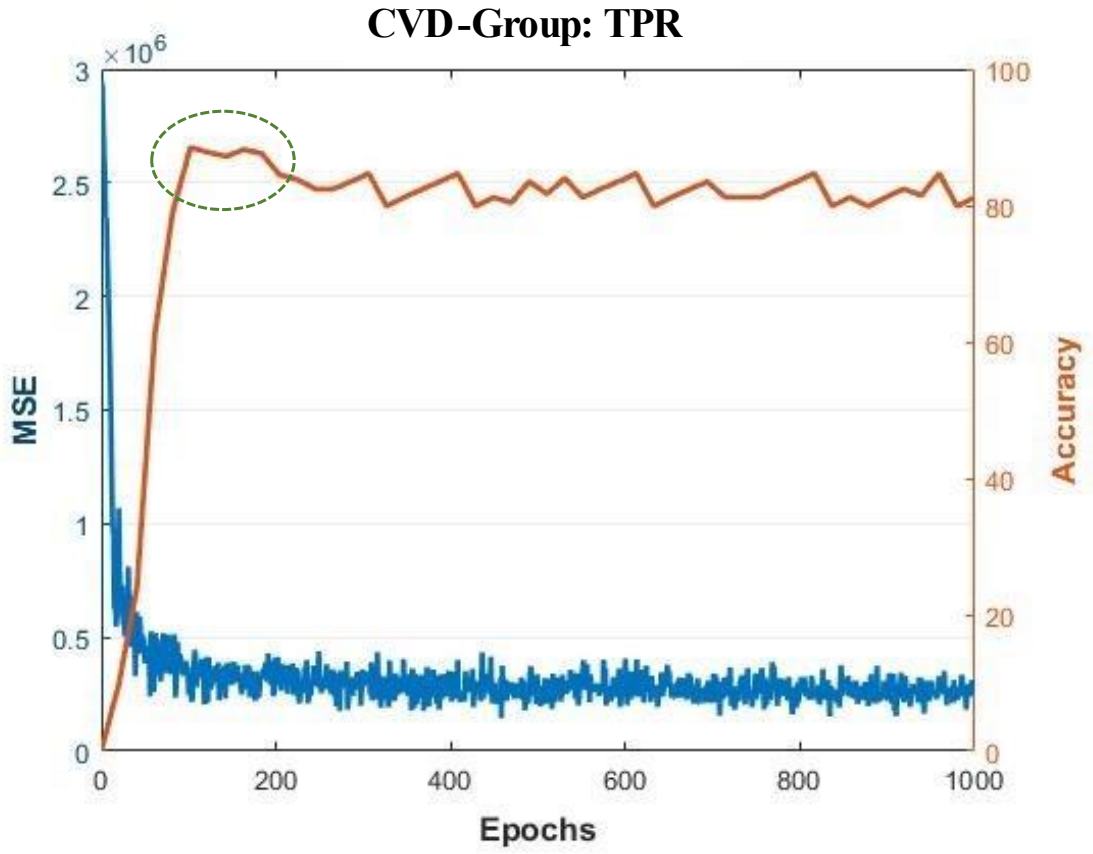

Fig. 2-6 Illustration of the early stopping strategy for avoiding overfitting and redundant learning.

Agreement between ML-predicted and clinically measured results was further verified through the Bland-Altman method-based analysis. As plotted in Fig. 2-7, the relationship between the average (horizontal axis) and the difference (vertical axis) is illustrated in a manner of scatter plot; and the 95% distribution range, i.e., the confidence interval was examined. Note that the two methods are generally considered to be consistent well enough when there are 95% more points in the scatter plot within the confidence interval that does not exceed the professionally acceptable critical value range [70]. It is seen that for the three cardiac function parameters of AC, TPR, and SV, 24 of 25 sets in H-group and 26 of 27 sets

in CVD-group fall in the 95% confidence interval, respectively, results of the two methods are consistent with each other. Our results thus demonstrate that the ML-based predictions are well consistent with the measurements in both healthy and CVD subject groups whereas the errors (MAPE) also display a relatively high level (>10%), which is expected to be further improved by use of larger datasets as our future task.

Table 2-3. Error analysis of ML-based three cardiac functions parameters of arterial compliance (AC), total peripheral resistance (TPR), and stroke volume (SV) in two subject groups.

Dataset	Error Function	AC (%)	TPR (%)	SV (%)
H-group		28.5	14.7	13.1
CVD-group	MAPE	23.1	11.7	10.8
Differences		5.4	3.0	2.3

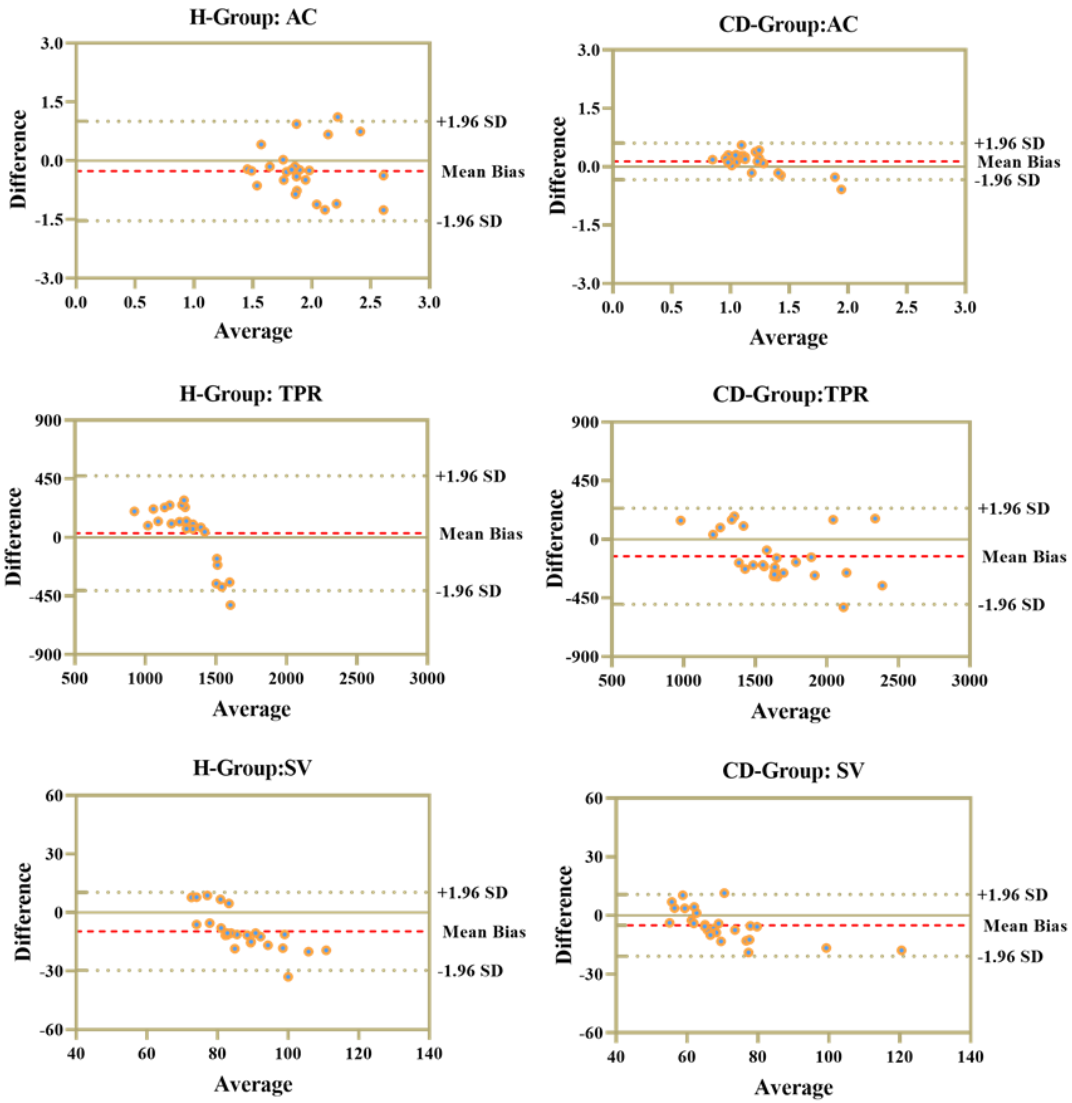

Fig. 2-7 Bland-Altman analysis-based comparison between two subject groups in terms of cardiac function parameters of arterial compliance (AC), total peripheral resistance (TPR), and stroke volume (SV). Relationship between the average (horizontal axis) and the difference (vertical axis) is illustrated in a manner of scatter plots.

2.4 Discussion

In this study, we developed a novel ML-based model with a multi-layered, fully connected network, which is validated to be capable of achieving a pulse wave-based high-

accurate prediction of three cardiac function parameters for both healthy-subject group and CVD-subject group. The model-based prediction is very fast that enables an output of the predicted cardiac function parameters within merely one second. The error analysis indicates that the ML model-based prediction is of high performance particularly for TPR and SV, achieving a low level of MAPE in both the healthy-subject group (MAPE: 14.7%, 13.1%) and the CVD-subject group (MAPE: 11.7%, 10.8) (Table 3). The consistency analysis further verifies a reasonable agreement between the ML model-based and the clinically measured results, demonstrating the validity of our model for clinical application. According to what we know, our study based on ML method first revealed the feasibility and potential in predicting cardiac function through pulse wave.

Compared to conventional methods mostly based on wave analysis strategy, the ML strategy proposed enables the extraction and reproduction of the complicated correlations between pulse wave signal and cardiac function parameters. On the other hand, with consideration of that many factors may affect and even lead to uncertainties in the pulse-wave characteristics such as age, weight, CVDs and other diseases, we herein carried out a strict data-screening (Fig. 2-2) in a manner of trial and error to ensure that the selected two subject groups could reflect the various cardiovascular statuses of the represented subjects, which was verified through the independent t-test (Table 2-2). We further excluded the noise interference likely induced from basic physiological parameters and other uncommon cardiovascular diseases, e.g., coronary aneurysms on the pulse-wave characteristics (Fig. 2-2). As a result, two high-quality pulse-wave datasets were successfully constructed for both the healthy- and CVD-subject groups with the essential features well captured and the high accuracy achieved in the prediction of the three cardiac function parameters.

On a basis of the error analysis, we found that the CVD-group shows a relatively lower error level outperforming the H-group (Table 2-3; Fig. 2-7). It is reported that the CVDs or

risk factors normally cause specifically featured variations (Fig. 2-2) in pulse wave and cardiac function parameters [28][71], which in this study likely works positively to enhance the performance of the ML network-based training in clarifying the correlations between pulse wave and cardiac function parameters and hence improve the prediction accuracy. Yet, it is observed of a high accuracy for the H-group in terms of TPR and SV with an error level of less than 15%. This indicates that our ML model is of capability and validity in predicting the cardiac function parameters for different subject groups.

Cardiac function parameters are common indicators of clinical examination, which can directly reflect the patient's cardiac state. Direct measurements of cardiac function parameters are usually implemented in an invasive manner along with expensive and precise medical devices. Such high clinical costs are thought to be a key reason to hinder many CVD patients from receiving timely diagnosis and treatment. The measurement of pulse waves however is normally non-invasive and processed conveniently at a much lower cost, which is patient-friendly. Recently, it turns to be even possible to capture/measure pulse wave signals with portable electronic devices such as the Apple Watch which enables physiological signal detection [72]. We foresee a trend that the hardware of various low cost while high precision portable devices capable to accurately measure pulse waves will emerge in near future. Therefore, the ML-based method capable of achieving accurate prediction of cardiac function parameters based on pulse wave could provide a feasible and effective software, which is of great clinical significance and importance in health monitoring and CVDs diagnosis.

With respect to the limitations of this study, compared to previous ML-based studies on physiological signal analysis involving ECG, heart sound and et al. [73][74], a major limitation lies in the yet insufficiently large-size subjects and the related clinical information. In principle, given the comparatively large and strictly screened datasets, the proposed ML

model can create relatively high-quality pulse-wave datasets and accomplish a high-accurate prediction of the three featured cardiac function parameters. Here the limited datasets did bring challenges to our ML model: firstly, it was impossible to clarify whether the ML model is capable to classify the patients in terms of specific CVDs, e.g., of aneurysms, aortic stenosis and so on. A diagnostically important application of the current method may be the group classification of healthy and CVDs individuals while quantitatively evaluating the severity of specific CVDs, which will be explored in our future work when large-size datasets are available and more cardiac function parameters are increased to be predictable. In addition, because of the inherent difference between males and females in cardiac function and CVDs [75], [76], the correlations between gender and cardiac function owing to unbalanced sex distributions (Table 2) should be eliminated in future studies through constructing larger and balanced datasets. Moreover, the current ML model could not achieve the prediction on other cardiac function parameters, e.g., those parameters commonly used as the gold standard to diagnose CVDs such as fractional flow reserve (FFR) for detecting the myocardial ischemia [77], B-type natriuretic peptide (BNP) for monitoring heart failure [78], etc. It is also important to comprehensively assess the cardiovascular risk of patients through CV risk scales (e.g., Framingham Risk Score) [79] for CVD-specific classified patient groups, which is more clinically operable and complete rather than group classification merely through CVSs/high-risk factors. Thus, whether setting compare group according to different risk scales could achieve a better prediction performance needs further verification. In addition, it was hard to verify whether an increased training dataset can improve the prediction accuracy for AC and even other parameters. Therefore, with a high goal to apply our ML-based strategy and model for clinical applications, improvement of the prediction accuracy through optimizing and specifying the proposed ML methods with larger datasets and broad aspects of related clinical information will be our next research target.

2.5 Conclusion

In this study, we proposed a ML strategy for the prediction of cardiac function parameters through pulse waves, which points to the feasibility and potential of the pulse wave-based prediction of physiological and pathological CVS conditions in clinical application.

Chapter III

Machine learning-driven, pulse wave-based evaluation of the blood-supply capability of patients with heart failure

3.1 Introduction

Heart failure (HF) has become a significant health concern affecting approximately 26 million people worldwide, particularly older adults who normally require lifelong treatment [80–82]. HF is characterized as “a condition in which the heart cannot adequately pump blood to fulfill the body’s requirements” or “a condition leading to an abnormality in cardiac structure or function that results in the failure of effective oxygen transport for metabolic requirements” [80]. HF is clinically diagnosed using the Framingham criteria, which are primarily used in most research [83]. Because patients with HF have poor blood circulation throughout their bodies, most of them suffer from concurrent cardiovascular diseases from an early stage [84]. The cardiac chambers of patients with HF are generally morphologically remodeled, causing dysfunctions with a significant decline in the pump function of the heart and reduced blood-supply capability [85–88]. Consequently, the oxygen levels in the arterial blood vessels throughout the body decrease, showing symptoms, such as shortness of breath, fatigue, weakness, and decreased exercise capacity, which severely affect the patients’ daily lives and necessitate long-term medication to maintain normal daily activities [89].

Patients with severe HF require hospital visits for prompt medical diagnosis and comprehensive evaluation by clinicians. Various physiological signals and medical images are normally obtained using medical devices, such as the echocardiography test, which is the most standard tool to assist physicians in assessing patients’ conditions every three to six months [90]. Digital imaging of cardiac chambers is crucial for evaluating the blood-supply capability in patients with HF, including the left ventricular ejection fraction (LVEF), left ventricular end-diastolic diameter (LVDd), left ventricular end-systolic diameter (LVDs), and left atrial dimension (LAD), because patients with HF show irregular characteristics of lower LVEF and higher values of LVDd, LVDs, and LAD [84][91]. However,

echocardiography tests are time consuming and expensive, posing challenges for patients with HF [92]. For instance, in the United States, even a 45 min to 1 h ECHOCARDIOGRAPHY test may cost approximately 2000 dollars for a patient, and it is unavailable for the daily monitoring of patients with HF [93–95]. When patients temporarily suffer from severe chest pain, fainting, weakness, arrhythmia, or severe shortness of breath [96], a timely diagnosis of their blood-supply capability to appropriately decide on a medical intervention is crucial to avoid overtreatment and prevent deterioration. Thus, it is necessary to utilize the limited medical resources for accomplishing real-time home health monitoring of patients with HF and providing them with a timely deterioration warning.

Physiological signals, such as pulse waves, have been widely used for health monitoring and disease prediction [22,28,97–100]. Pulse waves provide vital physiological information associated with the blood supply capacity and delivery efficiency [26,44]. The non-invasive and convenient nature of pulse wave measurements allows the employment of various low-cost home electronic devices for the initial diagnosis of cardiovascular diseases and related complications [101,102]. Considering that the abnormal heart chamber geometry typically observed in patients with HF alters the ejection fraction, ultimately impacting blood production and delivery efficiency [84], it would be an effective and patient-friendly tool to achieve non-invasive assessments of the heart's blood supply capacity through physiological and pathological information embedded in pulse waves. Such assessments provide significant potential for health monitoring and prevent disease deterioration in patients with HF.

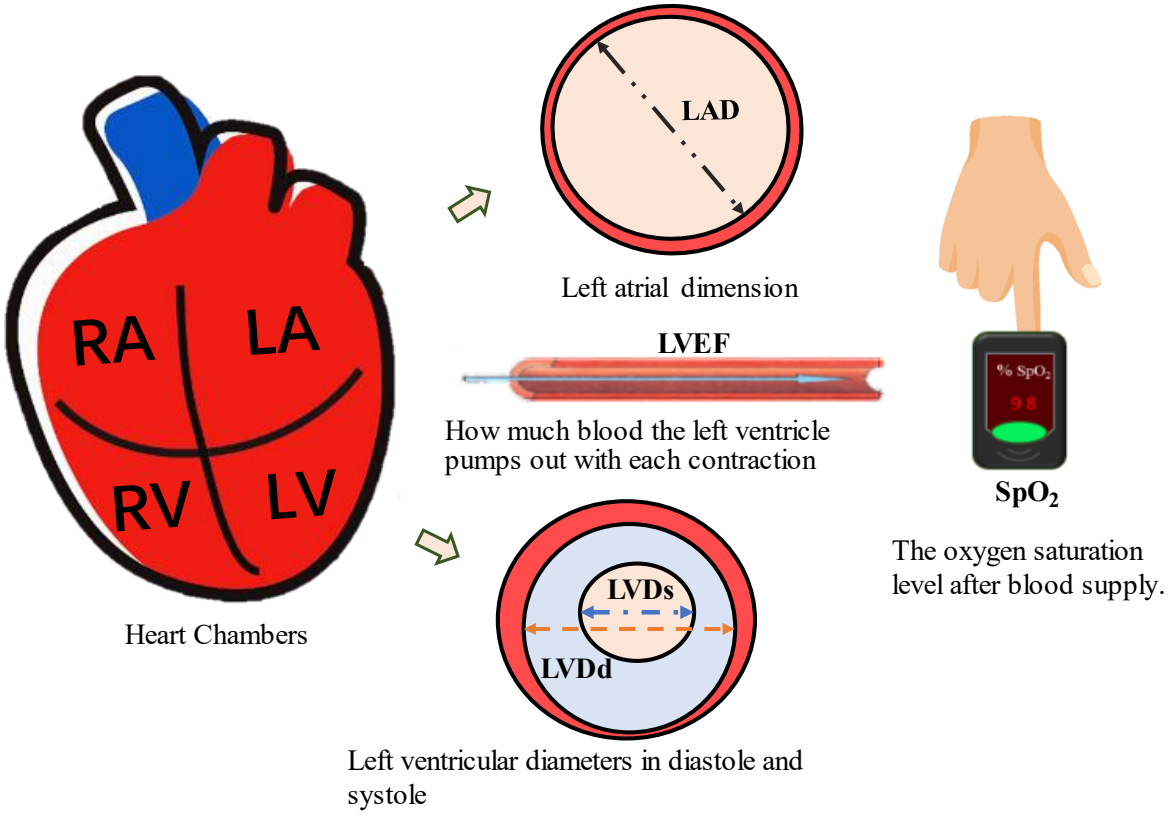

Fig. 3-1 Schematic of blood-supply capability. RA: right atrium; LA: left atrium; RV: right ventricle; LV: left ventricle; SpO_2: peripheral oxygen saturation; LVDd: left ventricular end-diastolic diameter; LVDs: left ventricular end-systolic diameter; LVEF: left ventricular ejection fraction; LAD: left atrial dimension.

Although quantitative analysis of pulse wave signals has been applied to certain cardiac functions or specific diseases [22,41,92], previous studies only targeted healthy subjects and other patients without HF. In particular, the quantitative evaluation of the pulse wave-based blood-supply capability of patients with HF remains unexplored [103]. Owing to the uncertainties caused by the noise and interference generated in the pulse-wave sampling process [104], such pulse-wave-based prediction of blood-supply capability is normally restrained by the limitations of conventional qualitative statistical methods [105,106]. To

establish a fast and non-invasive strategy for effectively predicting the blood-supply capability of patients with HF, we proposed a machine learning (ML)-based model in this study to predict five representative cardiovascular function parameters associated with the heart's blood-supply capacity [107]. As illustrated in Fig. 3-1, the parameters, i.e., LVDd, LVDs, and LAD, directly evaluate the morphological condition of the heart chamber and the heartbeat functions at systole and diastole; the LVEF quantifies the ratio of blood supply from the heart; and the SpO_2 determines the patient's blood oxygen level at the end of the blood supply as well as the supply efficiency. It has been broadly recognized that the ML methodology has powerful and feasible capabilities in robust feature extraction [106,108–112]. Remarkable achievements have been accomplished in various research fields, such as intelligent medicine, medical image processing, and autonomous driving, by integrating multiple basic features into complex features, enabling the mapping of the image or multi-dimensional signal data onto different prediction targets [113–117]. Our previous study verified that the ML-based strategy enabled the fast and efficient prediction of cardiac functions based on peripheral pulse waves [118], demonstrating the high potential and capability of multilayer feature extraction in accurately predicting the relevant indicators for clinical application owing to ML methods. In this study, we further explored the capability and feasibility of ML-driven, pulse wave-based prediction of the blood-supply capability of patients with HF for clinical application.

3.2 Methods

3.2.1 Ethics approvals

This study was approved by the Ethics Review Board of Chiba University Graduate School of Medicine in 2021, with an approval number M10089. The measurements of

clinical data complied with relevant guidelines and regulations.

3.2.2 Clinical data acquisition and screening

All data used in this study were obtained from 237 patients with HF and included raw extremity pulse wave data and relevant clinical, physiological, and pathological information. HF was diagnosed based on the Framingham heart failure diagnostic criteria [83]. All the participants were admitted to Chiba University Hospital between January 2019 and August 2021. After the acute HF condition stabilized, blood pressure/pulse wave detection equipment (Omron 203RPEIII) was used to measure and record the pulse wave and blood pressure during the operation. The SpO_2 was measured using a Nonin Onyx Vantage 9590 Finger Pulse Oximeter (Nonin Medical Inc., USA). All patients underwent transthoracic echocardiography (Vivid E9; GE Healthcare, Horten, Norway) within one week before or after the pulse wave tests. The measured parameters consisted of LVEF, LVDd, LVDs, and LAD, and relevant clinical information (e.g., age and body mass index (BMI)) was also collected. None of the patients consumed spicy food or alcoholic drinks during hospitalization.

3.2.3 Dataset creation

As shown in Fig. 3-2, we performed rigorous data screening to ensure the quality of the data, and 215 patients with HF complied the following screening criteria: 1) the pulse wave data were collected from the left upper arm, 2) more than five valid pulse wave cycles were recorded, and 3) the five parameters (i.e., SpO2, LVEF, LVDd, LVDs, and LAD) associated with blood supply capacity were concurrently measured and recorded for each patient. To ensure the validity of the screened data, we applied the summary-independent sample t-test

method to implement a statistical analysis of the consistency of the data with previous studies [119–121], which were examined in terms of the mean ± standard deviation, resulting in $p > 0.05$, thus a reasonable dataset [21,87,122].

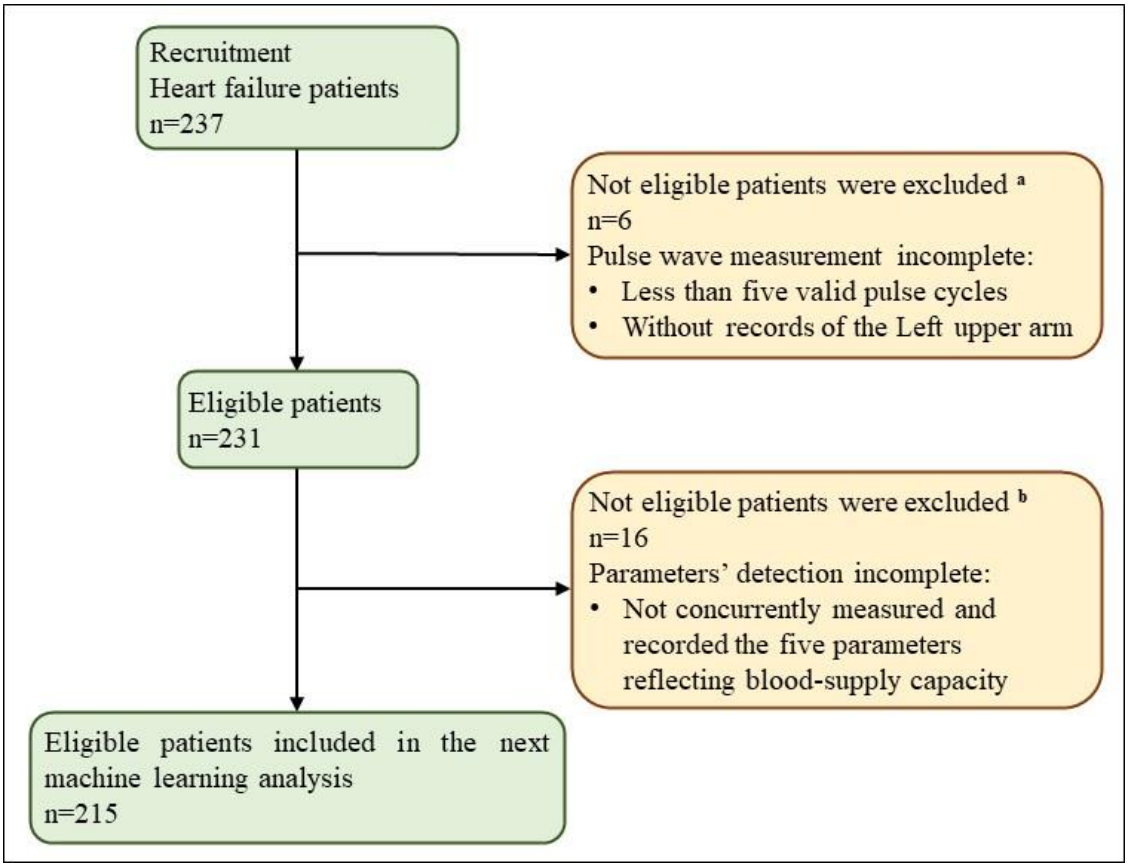

Fig. 3-2 Flow-chart of patient screening. Screening criteria: (1) six patients without complete pulse wave measurement were excluded, and (2) 16 patients without simultaneous measurement and recording of the five parameters were excluded.

The pulse wave data preprocessing methods developed in previous studies [60,61] were employed to eliminate various noise and interference signals during the pulse wave sampling process: 1) using the averaged target pulse wave of over more than five valid heartbeat cycles in a steady state [63,64], wavelet transform decomposition was conducted to remove noise [28,118]; 2) according to Nyquist's theorem and the sampling frequency (1000 Hz), the pulse

wave sampling nodes were converted from 1000 to 100; and 3) normalization of the pulse wave amplitude was undertaken over a range of 0–100. A pulse wave dataset was created from the data of 215 patients with HF, which was further divided into training and testing datasets at a ratio of 9:1. The details of the dataset used for the machine learning analysis are summarized in Table 1.

Table 3-1: Machine learning datasets for five parameters.

Parameters	SpO_2	LVEF	LVDs	LVDd	LAD
Total number of included patients	215	215	215	215	215
Training set	193	193	193	193	193
Testing set	22	22	22	22	22

3.2.4 Machine learning network

In this study, two machine learning (ML) network structures were employed and optimized, as shown in Fig. 3-3. It comprised a fully connected network and a densely connected convolutional network (DenseNet). A fully connected network is an efficient network that is widely used in various research fields [123,124]. A DenseNet is a recently proposed novel network that enables effective feature extraction and has high performance in terms of regression prediction tasks [125].

In the fully connected network, the input layer consisted of 100 neurons, which were identical to the sampling nodes of the input pulse waves. There were three fully connected

layers with 256, 64, and 16 neurons. The deepest layer was composed of one neuron, with five evaluation parameters selected separately as the output of five training times. Except for the input layer, the calculation process for each neuron in the (n+1)th layer of the fully connected network is described as

$$Output^{n+1} = F(\sum_{j=1}^{m_n} W_j^{n+1} Output^n + B_n), \quad (1)$$

where F denotes the activation function ReLU, which was introduced to alleviate gradient vanishing during ML training and to accelerate the convergence of loss functions [126]. m_n and B_n are the number of neurons and the bias in the nth layer, respectively, and W_j^{n+1} is the weight of the jth neuron in the nth layer.

The DenseNet shared the same input and output layers as in the fully connected network and utilized three dense block modules to connect all the layers while transferring various features between the layers. The methodology was verified to be capable of effectively increasing the usage of data features and achieving high performance even with limited data, while avoiding overfitting [125]. The input and output of the $(n+1)$th layer (featured map) associated with the dense block module can be expressed as follows:

$$Output^{n+1} = \text{ feature map } = G^n\left(Output^1, Output^2, \dots, Output^n \right), \quad (2)$$

where G denotes multiple operations including the ReLU, batch normalization, and convolution.

The mean square error (MSE) was employed as a loss function to evaluate the two ML networks combined with the Adam optimizer. The two ML networks were trained using TensorFlow (v2.0.0rc, Python 3.7) on an NVIDIA GeForce GTX 1660 Ti GPU. During the ML training, the utilization of different amounts of data associated with the back-propagation algorithm for adjusting the parameter configuration of the network (e.g., the number of network layers and neurons) may lead to a decline in the loss function and an

alteration in the prediction accuracy. Thus, the network structure size was adjusted to ensure promising convergence in the loss function during network training. The Adam optimizer was chosen [66] under the following conditions: learning rate = 0.001, $\varepsilon = 0.001$, $\rho 1 = 0.9$, $\rho 2 = 0.999$, and $\delta = 1E{-}8$, and the epoch parameter was set to 500. After training, each loss function curve and the relevant optimal configuration of the networks associated with the five parameters (SpO2, LVEF, LVDd, LVDs, and LAD) were recorded and stored. For testing, the ML-predicted parameters were used for statistical analysis and comparison with clinical measurements.

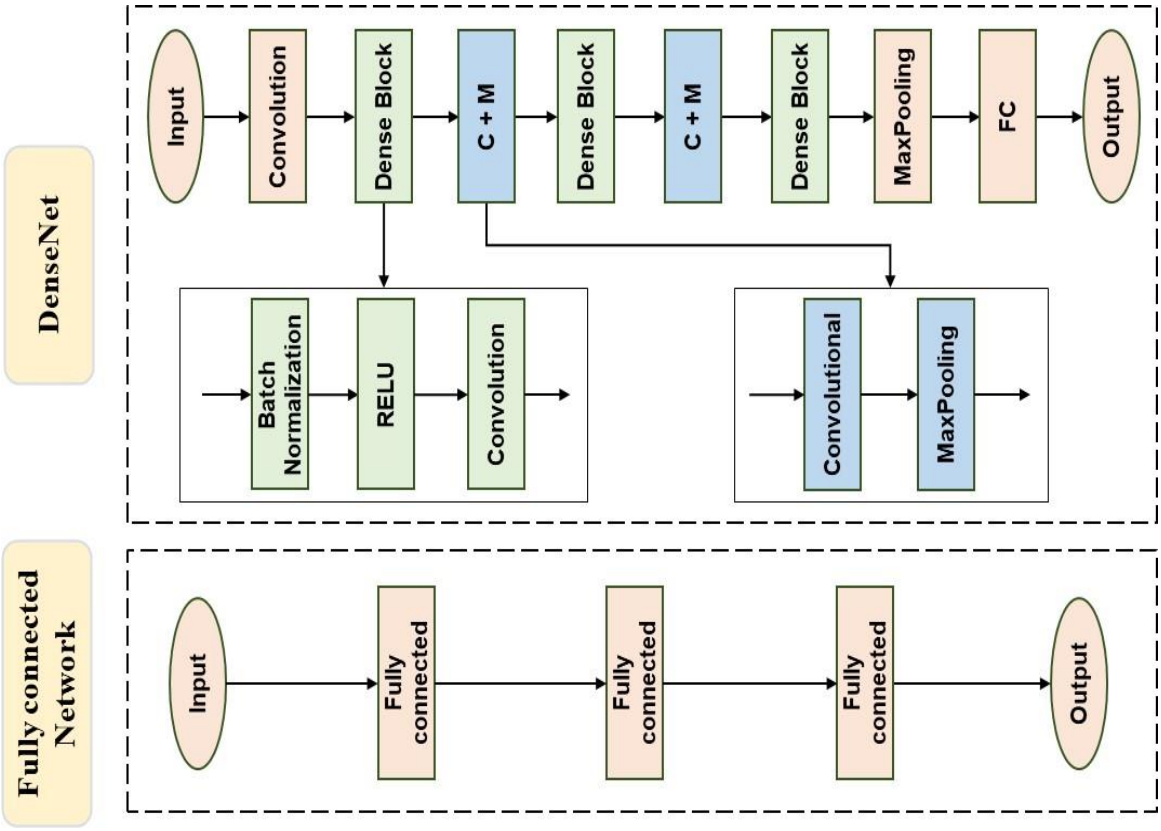

Fig. 3-3 Structures of two machine learning networks.

3.2.5 Performance evaluation

Following previous studies [118,127,128], we employed the mean absolute percentage

error (MAPE) as the error function to verify the ML-based prediction for the test datasets.

$$\mathrm{MAPE} = \frac{\sum_{n=1}^{N} \left|(y_n - \hat{y}_n)\frac{1}{\hat{y}_n}\right| \times 100\%}{N}, \quad (3)$$

where y_n and $\hat{y}_n$ are the clinical-measured and ML-predicted values of the five parameters, respectively, and *n* is the size number of the test dataset.

In addition, the Bland–Altman method was used for consistency analysis of clinical measurements and ML-based predictions. The Bland–Altman can dissect the discrete trend, clustering tendency, and correlations of the five parameters between the two datasets of clinical measurements and ML-based predictions. When the five parameters fell within the allowable range, the two datasets were considered to have good consistency, and the two methods can be substituted for each other [47].

3.3 Results

After critical screening and preprocessing of the pulse wave data of the 237 patients with HF, a high-quality ML dataset was successfully constructed in a suitable manner for flexible input data formats and datasets. To ensure that the screened patients fit in the clinical statistics of the patients with HF associated with the five parameters (SpO_2, LVDd, LVDs, LVEF, and LAD) for evaluating blood-supply capacity and the relevant clinical information summarized in Table 2, we conducted a summary-independent sample t-test based on the statistical results and a comparison with reliable data of previous studies [119–121]. Our results showed good consistency in terms of *p* value ($p > 0.05$) (Table 2) in the test analysis for the five parameters and other physiological information.

Table 3-2: Characteristics of patients with heart failure (HF).

Characteristics	Range	Others' reports	*p* values
Age (Years old)	66.4 ± 16.4	68.0 ± 15.0	0.162
BMI	24.2 ± 5.7	23.5 ± 3.9	0.076
BPs	129 ± 35.4	133.0 ± 29.9	0.105
BPd	80.2 ± 22.7	79.6 ± 18.6	0.703
HR	76.8 ± 15.1	76.0 ± 14.0	0.447
SpO_2	96.9 ± 2.6	97.2 ± 1.8	0.501
LVDd	56.8 ± 10.7	55.9 ± 14.9	0.604
LVDs	46.5 ± 12.9	48.7 ± 11.9	0.153
LVEF	38.3 ± 15.3	38.0 ± 15.0	0.779
LAD	44.4 ± 9.1	42.3 ± 9.4	0.074

Note: Data are presented as mean± SD. BMI: blood mass index (kg/m2); BPs: blood pressure systole (mmHg); BPd: blood pressure diastole (mmHg); HR: heart rate (beats/min).

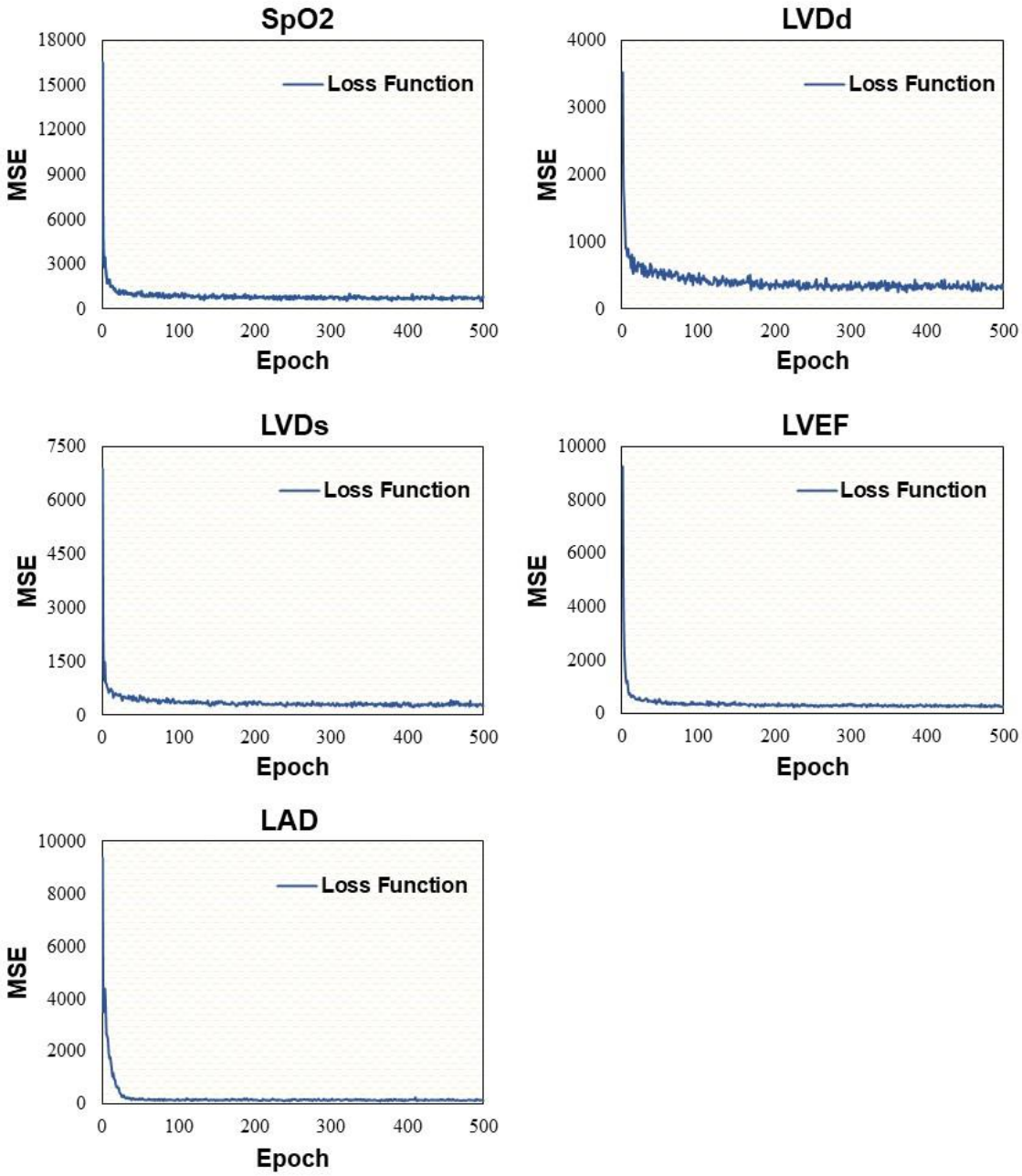

Fig. 3-4 Illustration of DenseNet model-based learning curves.

Five parameters were used to evaluate the blood supply capacity of the two selected ML structure models. During ML training, 10 network optimizations were accomplished, in which reduction in the loss function MSE resulted in a rapid and monotonous decline in each epoch. Using DenseNet as an example, as shown in Fig. 3-4, the MSE curves for every

evaluation parameter with a training epoch of 500 exhibited a constantly decreasing trend to the minimum level. This indicates that the relevant parameters and weights of the network were eventually optimized when the training process converged to a stable stage, which was then stored for ML-based testing. Moreover, the MSE curves of the fully connected network exhibited a decreasing trend, similar to that of DenseNet. In the test phase, both ML models outputted the predicted values for the five parameters within 1 s using the input of the pulse wave signals in the test set.

Table 3-3: Comparison between the predictions of the two ML models for the values of the five parameters associated with blood-supply capability.

ML networks	Error function	Predicted values				
		SpO_2	LVDd	LVDs	LVEF	LAD
Fully connected network	MAPE	6.6	14.7	17.3	21.2	14.9
DenseNet		5.6	12.9	14.6	18.2	12.0

To examine and compare the prediction performance of the two network structures, we summarized the results of the error functions for the five parameters in Table 3. It is worth noting that all the errors were calculated based on the sample data in the corresponding test datasets, which were divided randomly for the error calculation. The larger the error, the larger the deviation of the ML predictions from the clinical measurements. Although the two ML models exhibited reasonably high performance for the selected parameter prediction in evaluating the blood-supply capability, the DenseNet achieved a better performance than the

fully connected network for all five parameters. In particular, the DenseNet exhibited higher performance (MAPE < 15%) for four parameters: SpO_2, LVDd, LVDs, and LAD; the fully connected network had higher performance in three parameters: LVDd, SpO_2, and LAD (MAPE < 15%); and both models predicted SpO_2 more accurately (MAPE < 7%) than for the other four parameters.

We further applied the Bland–Altman method to examine the consistency between the ML predictions and clinical measurements by analyzing the average values and mean bias, which were visualized in a scatter plot, as shown in Figs. 3-5 and 3-6, where the horizontal and vertical axes represent the average value and the difference (with a 95% distribution range, that is, the confidence interval), respectively. It is worth noting that good consistency between the two methods occurs only if the points within a confidence interval of the scatter plot account for more than 95% of all points, and the confidence interval does not exceed the range of critical values for clinical applications [129]. Most sets of the predictions of the two ML networks were within the 95% confidence interval. For the DenseNet, those excluding the sets of LAD were fell into the 95% confidence interval, other parameters (i.e., SpO2, LVDs, LVEF and LVDd) only had one set of data samples outside the 95% confidence interval. For the fully connected network, although the LVDs had two sets not within the 95% confidence interval, the other parameters (SpO2, LVDs, LAD, and LVDd) contained only one set outside the 95% confidence interval. Thus, the ML-network-based predicted results agreed well with the clinical measurements.

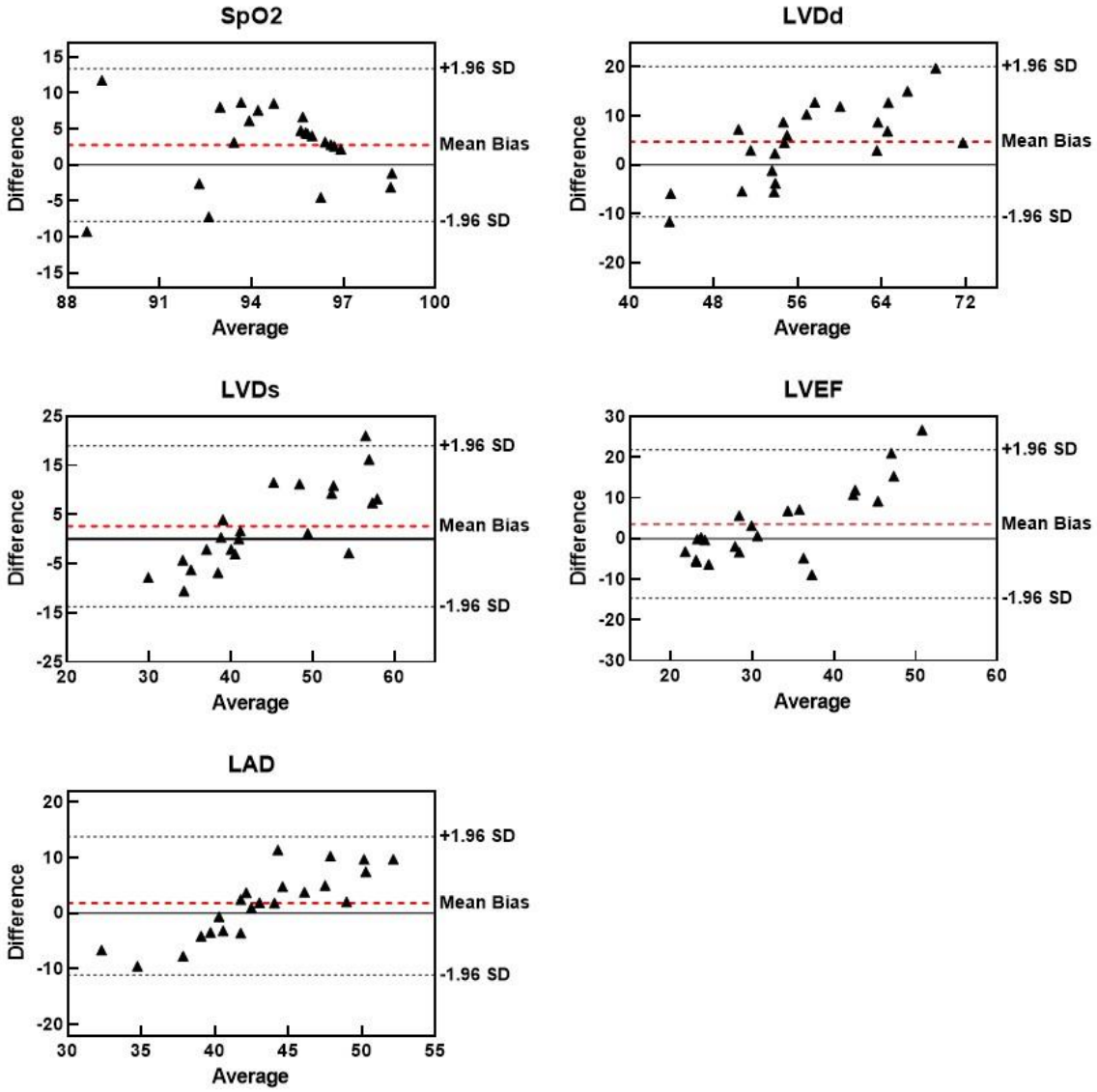

Fig. 3-5 Bland–Altman analyses between DenseNet-based predictions and clinical measurements for five parameters: SpO_2, LVDd, LVDs, LVEF, and LAD.

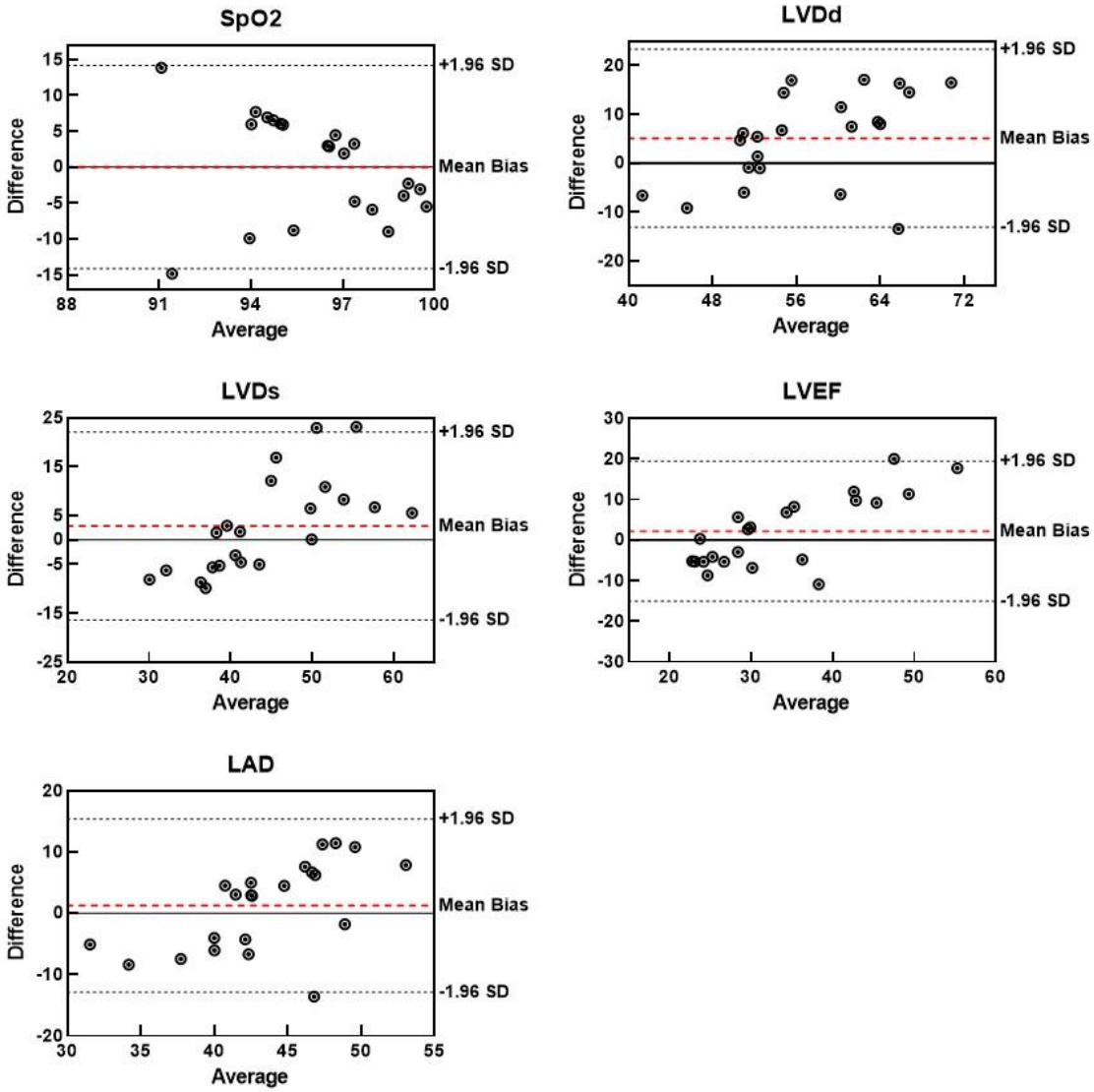

Fig. 3-6 Bland–Altman analyses between fully connected network-based predictions and clinical measurements for five parameters of SpO_2, LVDd, LVDs, LVEF, and LAD.

3.4 Discussion

In this study, for the first time, we applied a machine learning (ML) method to perform a non-invasive evaluation of blood-supply capability through pulse wave signals without

performing echocardiography in patients with HF. It was verified that ML networks have high potential and feasibility for achieving good performance in predicting five cardiovascular function parameters: LVEF, LVDd, LVDs, LAD, and SpO_2. In clinical practice, patients with HF have various cardiac functions that distinguish them from healthy people, making it difficult for expert physicians to make a reasonable diagnosis. Therefore, the ML model-based evaluation methodology developed in this study can be used as a fast and effective tool to assist physicians in providing patient-specific diagnoses and medical treatments. Moreover, LVEF and LAD are crucial factors for physicians to determine the indication for treatment; for instance, patients (less than 40%) with LVEF are normally recommended to use cardioprotective medications, whereas LAD is important for ablation therapy in patients with HF having atrial fibrillation [80].

The dataset used in this study were collected only from patients with HF without information on healthy subjects, and physiological information such as age and other cardiovascular function-related parameters may interfere with pulse wave signals after data screening, as pointed out by Scolletta et al. in a study of the correlation between pulse waves and LVEF [130]. To resolve the issue on methodological consistency associated with the ML model-based analysis, we performed a summary sample t-test to validate the filtered data-based results with reliable datasets. The DenseNet model achieved a high-prediction performance owing to rigorous data screening, which was verified to be capable of successfully ruling out the potential interference of numerical discrepancies in the datasets used for ML analysis, thus ensuring the validity and quality of the datasets.

Clinical measurements of blood supply capacity parameters are normally performed using various expensive and high-tech medical devices under the guidance and operation of highly skilled technicians, which likely hinders patients with HF from receiving timely diagnosis and monitoring. Although configurations of ML networks, such as epochs, batch

size, and the Adam optimizer, require a considerable amount of training and testing, as well as manual adjustments to improve the prediction accuracy and performance, the ML-based strategy proposed here can reduce the time, cost, and usage of medical devices. In addition, recent portable and multifunctional electronic devices such as smartwatches and smartphones have been innovating non-invasive measurements of various physiological signals in a more convenient and cost-effective manner [72,131–133]. Therefore, using these portable electronic devices, the pulse-wave-based ML methodology proposed here could provide an inexpensive and patient-friendly tool to achieve fast and accurate evaluation of the blood supply capacity of patients with HF for real-time monitoring and diagnosis.

The pulse-wave-based ML strategy was verified to have high clinical potential and feasibility. Based on the pulse wave signals of 237 patients with HF, together with clinical information on their heart's blood-supply capability, a high-quality dataset was constructed after rigorous data screening and preprocessing of the pulse waves. Using five selected cardiovascular function parameters: LVEF, LVDd, LVDs, LAD, and SpO_2, which were based on pulse waves using the fully connected network model and DenseNet model, **t**he non-invasive predictions agreed well with the clinical measurements. The prediction performance, which was evaluated through statistical analysis in terms of the error function and consistency, indicated that the proposed ML model achieved a highly accurate prediction (MAPE < 13%) for LVDd, LAD, and SpO_2.

The limitations of this study were mainly caused by the insufficiency of datasets in terms of the clinical parameter scope and data quantity in comparison with previous studies of HFs or physiological signal analyses [73,134,135]. Although we had a comparatively large and rigorously screened dataset, it was difficult to interpret whether the classification of patients with HF considering specific cardiovascular diseases, such as arrhythmia or heart valve problems, could improve or reduce the prediction performance of the ML models. In addition,

other clinically important indicators, such as B-type natriuretic peptide, a hormone produced by the heart in response to increased pressure and volume that is commonly used for diagnosing patients with HF [58], have yet to be considered. In addition, the diversity of patients with HF may also be an essential factor affecting the generalizability and flexibility of our findings, because this study used patient data collected only from a single institution, and pulse wave signals were obtained from the same device. The demographic and clinical characteristics of the patient population [136] may alter the prediction performance of the ML methodology. To explore real-time health monitoring and deterioration prevention in patients with HF, our future task will focus on the optimization of the proposed ML networks, the use of larger datasets for training and testing, and incorporation of relevant clinical information.

3.5 Conclusion

In this study, we developed a novel ML-based strategy to achieve non-invasive and accurate evaluation of blood-supply capability in patients with HF based on pulse waves. It was verified that the ML-based prediction was capable and feasible for real-time health monitoring and deterioration prevention in patients with HF.

Chapter IV

Hemodynamic prediction of 3D carotid artery stenosis pre- and post-surgical treatment using deep learning

4.1 Introduction

Stroke is a high-risk medical condition that seriously threatens human life. For the adverse consequences of stroke, brain cells and tissues can degenerate or die within a few minutes owing to insufficient oxygen and nutrient provision caused by the interruption or reduction of the blood flow from the carotid artery flow to the brain [137,138]. Stroke can be of two types based on the causality: ischemic stroke and hemorrhagic stroke, and according to clinical statistics, ischemic stroke accounts for a large proportion (about 87%) [139,140]. The primary reason for ischemic stroke is the blockage of the common carotid artery (CCA) or internal carotid artery (ICA) induced by atherosclerosis, also known as carotid artery stenosis (CAS), which causes intracranial reduced blood supply [141–143] and usually requires revascularization surgery to prevent ischemic stroke for the patients with severe CAS. Revascularization surgeries for CAS mainly include carotid endarterectomy, carotid angioplasty, and carotid stenting [1–4]. While the operating procedures of these three surgeries are different, i.e., by removing the plaque through surgery, temporarily expanding the stenotic lumen with a balloon, and placing an adaptive vascular stent after balloon dilation, respectively, the ultimate goal of the three surgeries is to enlarge the flow cavity enabling blood flowing through the stenosis to improve the insufficient blood supply problem for preventing ischemic stroke [5–7,144]. The clinical diagnosis and postoperative prognosis of these surgeries often need to be guided by multiple hemodynamic variables such as pressure, velocity and wall shear stress [48,145], which are utilized to diagnose the severity of CAS and evaluate the surgical effect.

To accurately predict the hemodynamic characteristics for the diagnosis of cardiovascular diseases and the prognostic assessment of various revascularization surgeries, computational fluid dynamics (CFD) has now been widely used as an efficient method [8–11,48,146]. CFD modeling is normally conducted in three-fold [147]: (1) pre-processing to

construct three-dimensional (3D) anatomic/geometric models based on medical images of CT, MRI, etc. and to discretize computational domain; (2) computation of flow fields in terms of pressures and velocities by solving the Navier-Stokes equations under certain boundary conditions [11,148–151]; and (3) post-processing to visualize flow fields while calculating hemodynamic parameters such as wall shear stresses. Thus, the CFD-based simulations are of high computational cost due to the requirements of mighty computing resources, large-scale computing time, and highly skilled experts [12,13]. Moreover, the simulation is generally performed in a patient-specific manner by using the image-based geometric model for each individual under specific boundary conditions, which needs to be conducted for all patients and is usually very time-consuming [10,152–155]. Thus, it is a crucial issue to pay the expensive computational costs for real-time simulations of complex blood flows in association with the realistic clinical applications of CFD methods for surgical treatments such as CAS.

Given the powerful feature-extraction capabilities in multidomain regression and pattern recognition, both machine learning (ML) and deep learning (DL) methods have shown successful applications in various fields, such as physiological signal diagnosis, medical image separation, smart medical care, etc [22,53,113–116,118]. The ML and DL-based methodology is also considered as an alternative to the CFD method for blood flow analysis [156] because it is of high potential to implement the mapping of anatomic geometries and CFD-driven flow fields, which enables accomplishing fast and accurate hemodynamic prediction for clinical applications. Recently, the ML/DL models have been verified capable of predicting the reduced-order simulation results in a computationally inexpensive way when merely employing some limited flow information, i.e., the velocities and pressures at the centerline or cross-section of a vessel [18,157,158]. However, from the viewpoint of clinical applications, an accurate prediction of the detailed information on 3D and transient

local flows before and after surgical treatments is needed to provide sufficient clinical references for surgery-decision making, which remains poorly studied yet. With a high goal of the diagnosis of CAS disease and the effect prognosis of surgical treatments, we applied the DL methodology to the CAS disease to accomplish a fast and accurate prediction of the hemodynamic characteristics in association with carotid stenotic artery before and after the surgical operation due to the flow cavity variation. With consideration of the intense vortical flow structures induced by the complex morphology of carotid bifurcation and stenosed carotid arteries [159,160], a flexible data format is thus employed, which is capable of accurately mapping both the carotid artery geometry and the complicated flow field.

The data format utilized in DL and ML methods is usually given in terms of pixels or voxels to deal with the irregular shape and connectivity information, which has resolution limitations in accurately representing the complex arterial geometry and hence reasonably predicting the CAS hemodynamics via CFD simulations [23,24]. While there still exists the accuracy issue in the boundary representation (BRep) with smoothened boundaries, the point cloud dataset has the advantage of being easily generated through converting and transforming from a 3D scanned dataset by means of CAD conversion software (e.g., Solidworks, USA) [161]. The point-cloud data format enables the characterization of both complex geometry of the vessel model and the complicated flow fields with high resolution; and the high-density point cloud capable of conducting potential feature-extraction can be achieved with a small size dataset [53,110,162,163]. Furthermore, a novel DL network can be employed using dual input-sampling channels, which enables the high-performance analysis and establishment of the correlation between arterial geometries and velocity and pressure fields through abstracting and incorporating global and local characteristics of the point cloud dataset [53,110].

In this study, a total of four point-cloud datasets were established and utilized to validate

the CFD simulations and perform the hemodynamic prediction of the CAS models before and after surgical treatments in terms of the flow cavity variation. To match the CFD-based point cloud datasets, we employed a DL network with dual input-sampling channels. After the DL training, the optimal weight configurations were stored for the DL-based hemodynamics prediction of the CAS in the testing process. Compared with previous studies, the evaluation of prediction performance and the DL analyses indicated that the DL strategy proposed here enables uncovering the association between transient blood flow characteristics, including velocity and pressure fields and artery cavity geometric information before and after surgical treatments of CAS. A remarkable reduction of 7200 times is achieved in the computational cost, and the DL-based predictions are well consistent with the CFD simulations in terms of mean velocity in the stenotic region for both the preoperative and postoperative datasets. Our study thus points to the potential and feasibility of the CFD-driven, DL-based methodology in predicting the 3D and transient hemodynamics associated with CAS before and after treatments, which may provide an effective and useful tool for the diagnosis of ischemic stroke and prognosis of surgical treatments.

4.2 Methods

4.2.1 Ethics approvals

This prospective investigation was carried out following the principles outlined in the Declaration of Helsinki and aligned with medical ethics standards. The research received approval from the Ethical Review Committees of Beijing Friendship Hospital, demonstrating compliance with ethical requirements All measurements and collection of the data were carried out under relevant regulations and guidelines. We obtained signed informed consent forms.

4.2.2 Clinical data collection

All clinical data used in this study were taken from Beijing Friendship Hospital. The raw CTA data of the carotid artery for 298 subjects who visited Beijing Friendship Hospital in 2021 and 2022 to examine the cerebral and carotid arteries were collected and collated by professional clinicians at 128-CT (Brilliance iCT, Philips Health care, The Netherlands). In addition, technicians reconstructed 3D anatomic models by importing CT images into MIMICS 20.0 (MIMICS, Leuven, Belgium) for arterial segmenting and repairing. Eventually, 280 3D geometric models with no stenosis of carotid bifurcate arteries were built up, and among them 18 heterogeneous cases were excluded due to incomplete information.

Table 4-1: Geometric parameters of carotid arteries and stenoses

Parameter	Description	Range
Diameter of CCA	Increased or decreased the diameters of the original artery uniformly	6.7-9.0 mm
Diameter of ICA	Increased or decreased the diameters of the original branch artery (for brain) uniformly	4.6-6.3 mm
Diameter of external carotid artery (ECA)	Increased or decreased the diameters of the branch artery (for face and ears) uniformly	3.8-5.2 mm
Bifurcation angle between ICA and CCA	The angle formed by the two branches in the first 10 mm of their course was measured	20–120°
Stenosis location	Random positions on ICA and CCA	
Number of stenosis	ICA and CCA	1-2

Stenosis severity	Severity of stenosis	0-80%
Stenosis length	The length of the stenosis on the ICA or CCA	5-20 mm

3.2.3 Preoperative and postoperative CAS models

It was difficult to perform accurate and efficient DL analyses on the hemodynamic characteristics in association with geometric features of carotid artery stenosis (CAS) by using the mere 280 realistic carotid artery models. Moreover, most patients were found not suffering from surgery treatment for CAS. On the other hand, it has been recognized that the key parameters significantly impacting the CAS hemodynamics consist of the diameter of common carotid artery (CCA), the diameter of internal carotid artery (ICA), the diameter of external carotid artery (ECA), the bifurcation angle between ICA and CCA, the stenosis location, the number of stenoses, the stenosis severity, and the stenosis length [164–167]. Therefore, with the clinicians' agreement and on a basis of the 280 CA models, we reconstructed more models artificially through adjusting these SEVEN parameters as summarized in Table 1, and substantially built up 1000 geometric models. It is worth noting that for the 1000 geometric models, the CAS models were then constructed by randomly changing the stenosis-related parameters within a given range (Table 1) using the modeling software SolidWorks 14.5 (Solidworks, USA), substantially resulting in a dataset of 1000 CAS models.

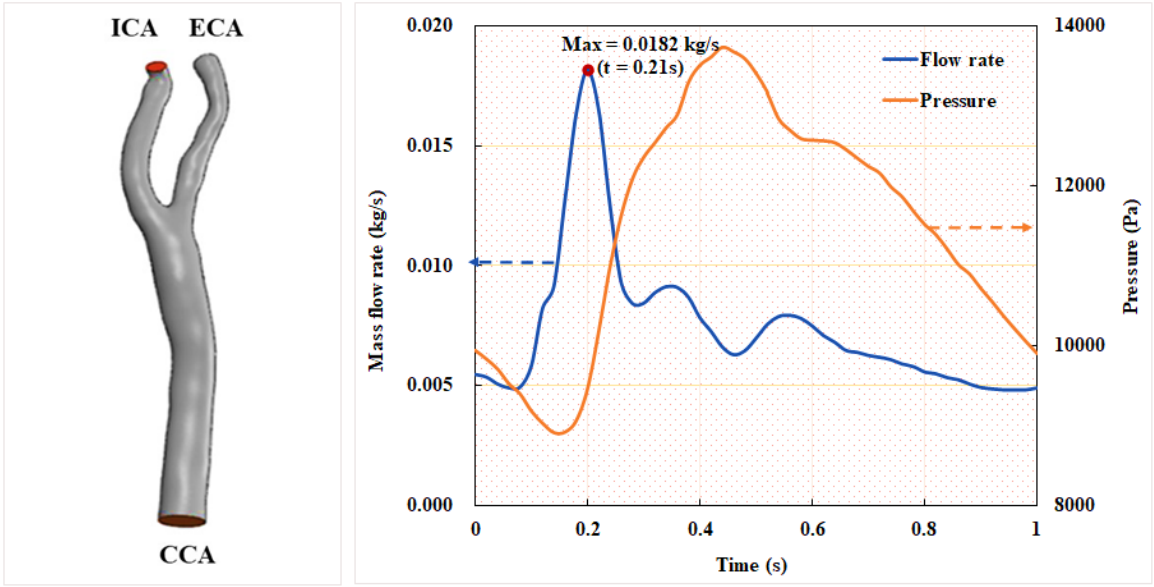

Fig. 4-1 Geometric model and boundary conditions of the carotid bifurcated artery. A. Geometric model of carotid bifurcate artery with branches CCA, ICA and ECA; B. Unsteady boundary conditions comprising a mass flow rate profile at CCA inlet and a pressure waveform at ICA and ECA outlets [168,169]

4.2.4 CFD simulation of CAS before and after surgical treatments

After geometric model augmentation, we carried out CFD simulations to resolve the flow fields and make the hemodynamic prediction for the 1000 CAS models (Fig. 4-1-A). The blood flow was treated as an incompressible, laminar, and Newtonian viscous fluid with the density of 1060 kg/m^3 and the viscosity of 0.0035 Pa·s [168,169]. All arterial walls were treated as rigid boundaries and the nonslip condition was imposed. The commercial software ANSYS-Meshing was utilized for discretizing the computational domains in terms of a tetrahedral mesh with a minimum size of 0.0455 mm. The mesh independency convergence analysis was conducted in terms of the minimum mesh spacing adjacent to the walls and the

mesh number, and it was verified that the results (See details in the Results section) were well consistent with the previous studies [168].

At the inlet of the CCA models, a pulsatile mass flow rate profile (Fig. 4-1-B) with the waveform taken from the previous studies [168,169] was defined, which was spatially uniform while pulsating with time. A transient pressure waveform was simultaneously imposed at the outlets of the ECA and ICA. Given the dimension of the CCA part with a cross section area of 45.23 mm^2 and a diameter of 7.318 mm, and the average flow velocity in a cardiac cycle (Fig. 4-1-A), the Reynolds number was calculated to be approximately 346. It is worth noting that a peak Reynolds number based on the peak mass flow rate (0.182 kg/s) among all our models was approximately 2200. The numerical simulations were performed with ANSYS-CFX 16.0 (ANSYS, Canonsburg, USA) by solving the unsteady Navier-Stokes equations and the continuity equation. The time step was set as 0.01 s, and the maximum iteration number was set to 200 for each time step, which was confirmed capable of ensuring a numerical convergence with the residuals less than 10^{-4}. In addition, all the simulations were performed up to four cardiac cycles, when the flow field was confirmed to reach a stable and converged state. The results of the fourth cycle were used for further hemodynamic analysis.

4.2.5 Creation of DL datasets

This study is attributed to developing a DL strategy to implement the mapping of anatomic geometries and CFD-driven flow fields to achieve the hemodynamic prediction of 3D carotid artery stenosis (CAS) before and after surgical treatments. Thus, both creations of the DL datasets and the construction of a suitable DL network play crucial roles. Therefore, the point cloud data were employed herein to characterize the 3D CAS models (mesh nodes).

The point clouds of two types were extracted from the CFD-based results, representing the geometric features of the CAS cavity and the hemodynamic characteristics, respectively. A suitable DL network with dual input and sampling channels was then developed and employed for the DL analysis.

Because the flow field data comprising velocities and pressures at each mesh obtained through ANSYS software can be directly converted into a high-density point cloud data, we extracted all the CFD results at the instant of 0.21 s, i.e., the systole peak of the fourth cycle. We then established two types of point clouds, namely, the cavity point cloud $\{N_1*P_1\}$ extracted from the innermost layer of the carotid artery wall (i.e., geometric information of flow cavity) and the fluid point cloud $\{N_2*P_2\}$ extracted from the inside of the CA model. Here, N_1 denotes the total number of grids in the lumen shell, P_1 denotes the coordinate information of the carotid lumen, N_2 denotes the total number of grids of the internal fluid, and P_2 denotes the comprehensive properties of the internal fluid, including the information of spatial coordinates and flow fields of velocity and pressure.

In general, any variations in the 3D CAS models would alter their wall surface meshes and hence the mesh distributions in the computational domain, substantially resulting in the change of the spatial distribution of point cloud. The point cloud data thus consists of both the geometric information of the spatial coordinates (x, y, z) and the corresponding CFD-based flow field information of velocities and pressures, which can be collected and stored simultaneously at each discrete point of the point cloud data [53,110,170].

Based on the treatment condition and flow field information, we built up four datasets of the CAS models in terms of either velocity field data or pressure field data, with two preoperative datasets for before surgical treatment and two postoperative datasets for after surgical treatment with the cavity geometry changed, which are summarized in Table 2. All samples in the four datasets contain both fluid point clouds and cavity point clouds. After

the establishment of the four datasets, we randomly divided each dataset into a training set and a testing set by a 9:1 ratio for DL analysis. Thus, each training set includes 900-point cloud sets from CFD simulation results, and each testing set includes 100-point cloud cases. These four datasets were used for training and testing in four independent DL networks.

4.2.6 DL network

According to the characteristics of the established point cloud datasets, we employed a matching dual-input-sampling channel DL network. As shown in Fig. 4-2, the network has two inputs and sampling channels that receive and process the overall outer cavity and inner fluid point clouds of the carotid artery model, respectively. For the sampling module, to enhance the correlation between the point clouds of the two channels while improving the network prediction performance, the first two feed-forward fully connected layers, i.e., FC1 and FC2 (Fig. 4-2) are utilized to share the weights, i.e., the same preliminary feature extraction method. After the step of FC2, the two types of point clouds enter their respective independent feed-forward fully connected layers, i.e., FC3 and FC4 (Fig. 4-2). They are used to extract the overall features from the outer cavity point cloud and to characterize the flow field information from the inner fluid point cloud. After being processed by the sampling module, the characteristics of both outer cavity geometry and the inner fluid flow are extracted as 512-dimensional $\{N_1 * 512\}$ and 128-dimensional $\{N_2 * 128\}$-dimensional vectors, respectively, which are first encoded in the feature stitching module as a $\{N_3 * (512 + 128) = 640\}$ dimensional vector. Then, the dimensional vector $\{N_3* (512 + 128) = 640\}$ containing the two characteristics in the output module (FC5 and FC6) is decoded into $\{N_2, P_2\}$, i.e., the flow field information of the internal fluid, which functions as a convolutional neural network decoding operation. By employing the network with the two matched point

clouds to bridge the fluid's overall cavity and spatial coordinates, the flow field data of velocity and pressure at each point, can be substantially determined.

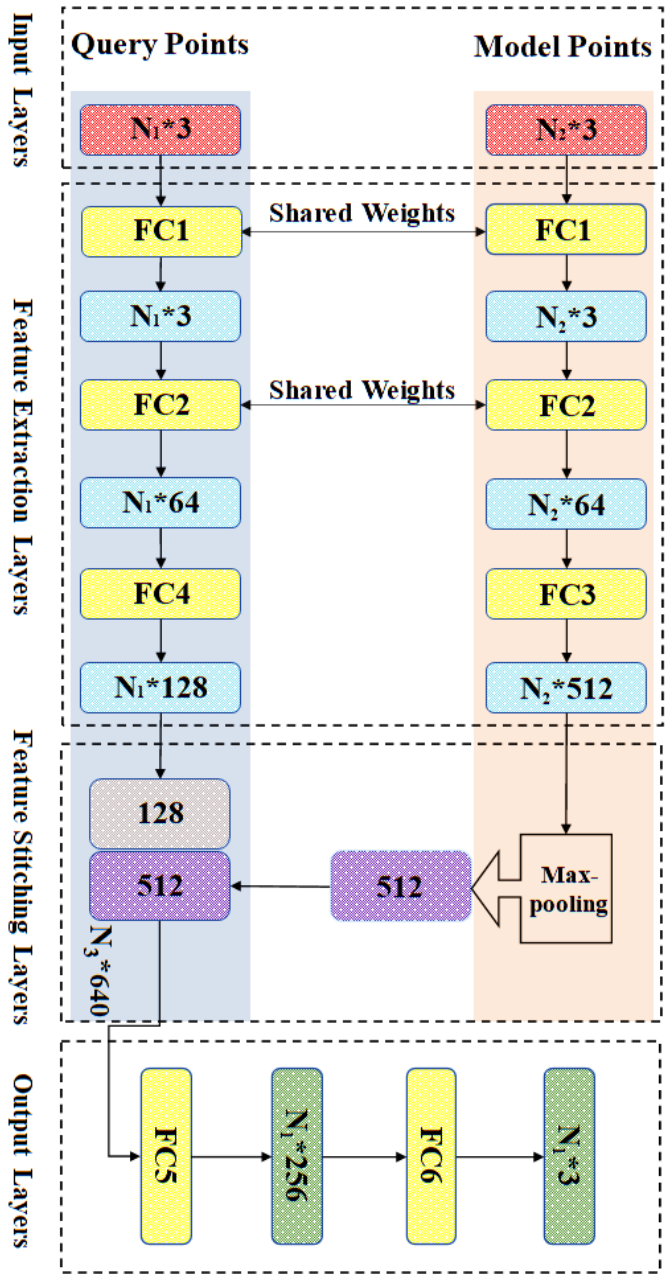

Fig. 4-2 Structure of the proposed network.

With the utilization of a dual-channel rather than a single-channel and sharing weights in the fully connected layers instead of nonshared weights, Li [53] investigated the prediction

performance through testing with control variables in previous work. Here, we focused on the feature extraction and processing point clouds over the network. We added a max pooling part in the sampling module as a symmetric function (Fig. 4-2) to resolve the disorder issue of the input point clouds [162,171]. In addition, the mean absolute error (MSE) was chosen as the loss function**;** the Adam optimizer was utilized as a learning rate=0.001, ε=0.001, $\rho 1$=0.9, $\rho 2$=0.999, and δ=1E−8 [22,66].

4.2.7 Network training and testing

Four DL datasets were trained separately using independent networks in the environment of TensorFlow (v2.0.0rc, Python3.7) on an Nvidia GeForce GTX 1660 Ti GPU with a batch size of 1 and epoch of 1000. In the training phase, we stored the optimal weight configuration by optimizing the loss function to the minimum value, which resulted in four trained networks for the DL prediction at the testing stage. For the testing phase, the hemodynamic results of fluid points in P_2 were predicted by only importing the spatial coordinated information of the cavity point cloud in P_1 and the spatial coordinate information of the fluid point cloud in P_2 using the stored optimal configuration.

Table 4-2: Four DL datasets

Stage	Hemodynamic	Training number	Testing number
Preoperative	Velocity	900	100
	Pressure	900	100
Postoperative	Velocity	900	100
	Pressure	900	100

4.2.8 Evaluation of prediction performance

To quantitatively evaluate the difference between the DL-predicted results and the CFD simulation results, we drew on previous studies to employ the mean radial error (MRE) and the normalized mean absolute error (NAME) to determine the error at each mesh point [24,53,110]. MRE can characterize the error of the DL prediction value relative to the actual value at all query points of the model. The NMAE can characterize the error of the DL-based result relative to the actual value of the overall flow field (CFD result). The definitions of MRE and NAME are given in Equation (1) and Equation (2):

$$MRE(y,\hat{y}) = \frac{1}{N_2}\frac{\sum_{i=1}^{N_2}\sqrt{(y_i-\hat{y}_i)^2}}{\sqrt{{y_i}^2}} \times 100\%\,, \quad (1)$$

$$NMAE(y,\hat{y}) = \frac{1}{N_2}\frac{\sum_{i=1}^{N_2}|y_i-\hat{y}_i|}{Max|y|-Min|y|} \times 100\%, \quad (2)$$

where y_i and $\hat{y}_i$ denote the *i*-th inner fluid point values of pressure or velocity obtained by DL-predicted values and CFD-simulated results, respectively. *i* is the point spatial sequence. N_2 is the total number of fluid point clouds. Max|y| and Min|y| represent the maximum and minimum magnitudes of the corresponding hemodynamic parameters among all points in the selected area, respectively.

4.3 Results

First, the mesh convergence analysis was conducted by investigating the mesh independency of the CFD simulation in terms of minimum mesh spacing adjacent to the wall and mesh number. For the sake of simplicity, a stenotic carotid artery model, as shown in Fig. 4-1-A, was used for the mesh convergence analysis. It was verified that a minimum mesh spacing/size of 0.0455 mm of the tetrahedral meshes at the wall surface was good enough to capture the hemodynamic characteristics of the flow field accurately; and the mesh number exceeding 1.2 million could achieve a marginal difference in association with the

velocity magnitude at the systole peak (Fig. 4-3), less than 3% with increasing the mesh number. With consideration of the balance between numerical accuracy and computational cost for the CFD simulation, we thus selected the number of mesh nodes (point cloud) ranging from 0.18 to 0.25 million, identical to a mesh number exceeding 1.2 million in total across different cases, which were verified capable of accurately and effectively representing the geometric features and flow field details of the CAS models.

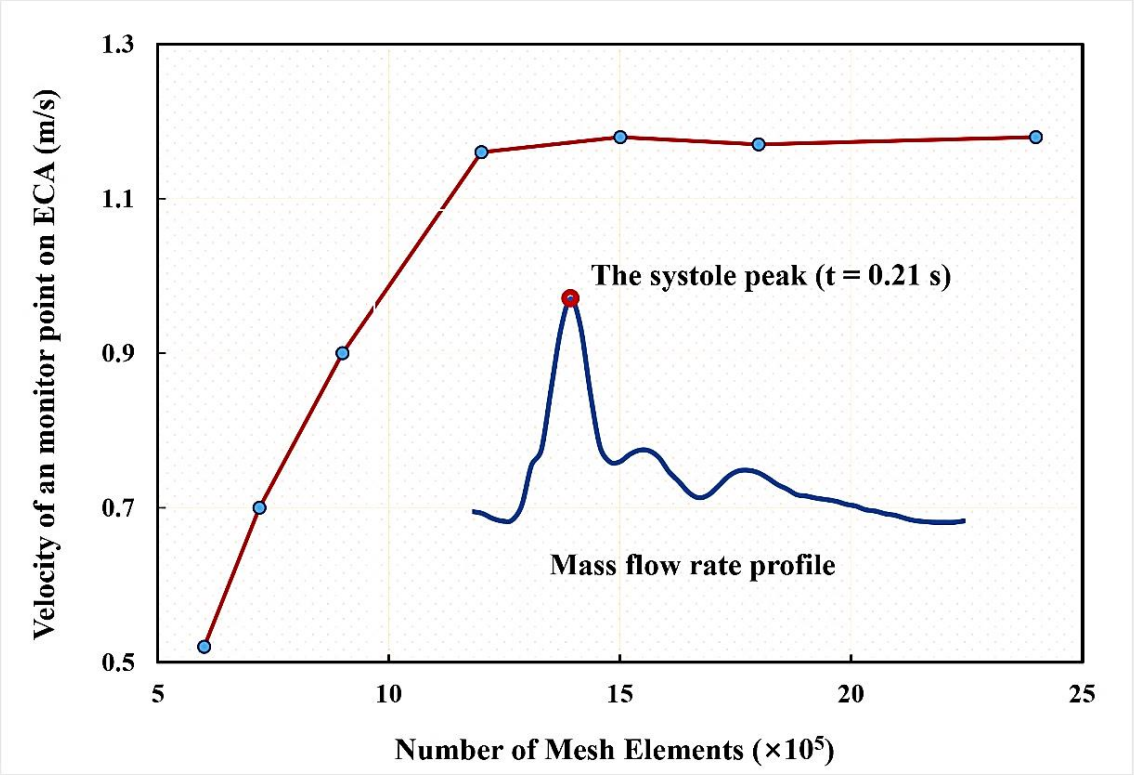

Fig. 4-3 Mesh convergence analysis in terms of mesh independency associated with a specific velocity at the systole peak of the fourth cycle.

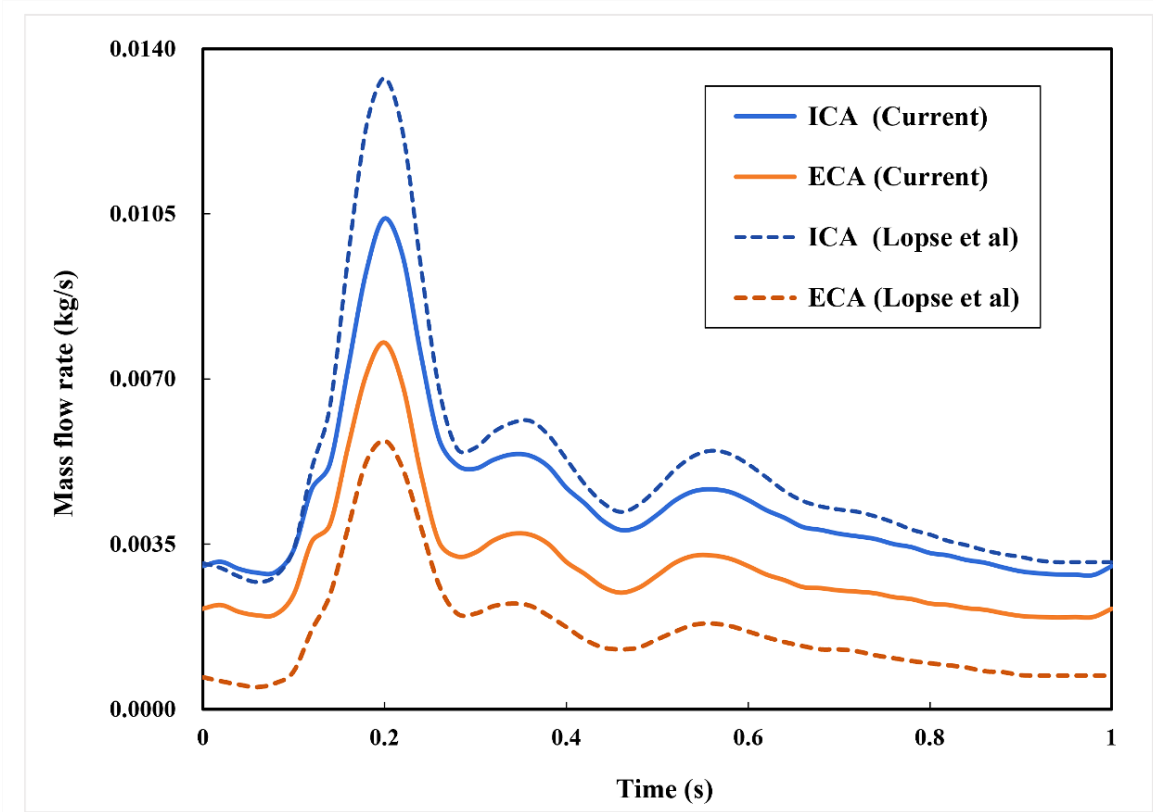

Fig. 4-4 Comparison of simulated mass flow rates at two outlets with published data [168].

Because the DL analyses in terms of accuracy and validity are highly dependent upon the data quality, particularly in the present case of the unsteady flow field, which could exert a significant impact on the point cloud data converted by CFD simulation results. Therefore, we validated the time accuracy of the CFD simulation through a comparison of the mass flow rate at the ICA and ECA outlets in Fig. 4-4. The current CFD-based results are in reasonable agreement with reliable published data [168] in terms of the time-varying mass flow rates at the two outlets of the carotid model even though some noticeable differences exist in the amplitudes mainly due to the discrepancy in the two models.

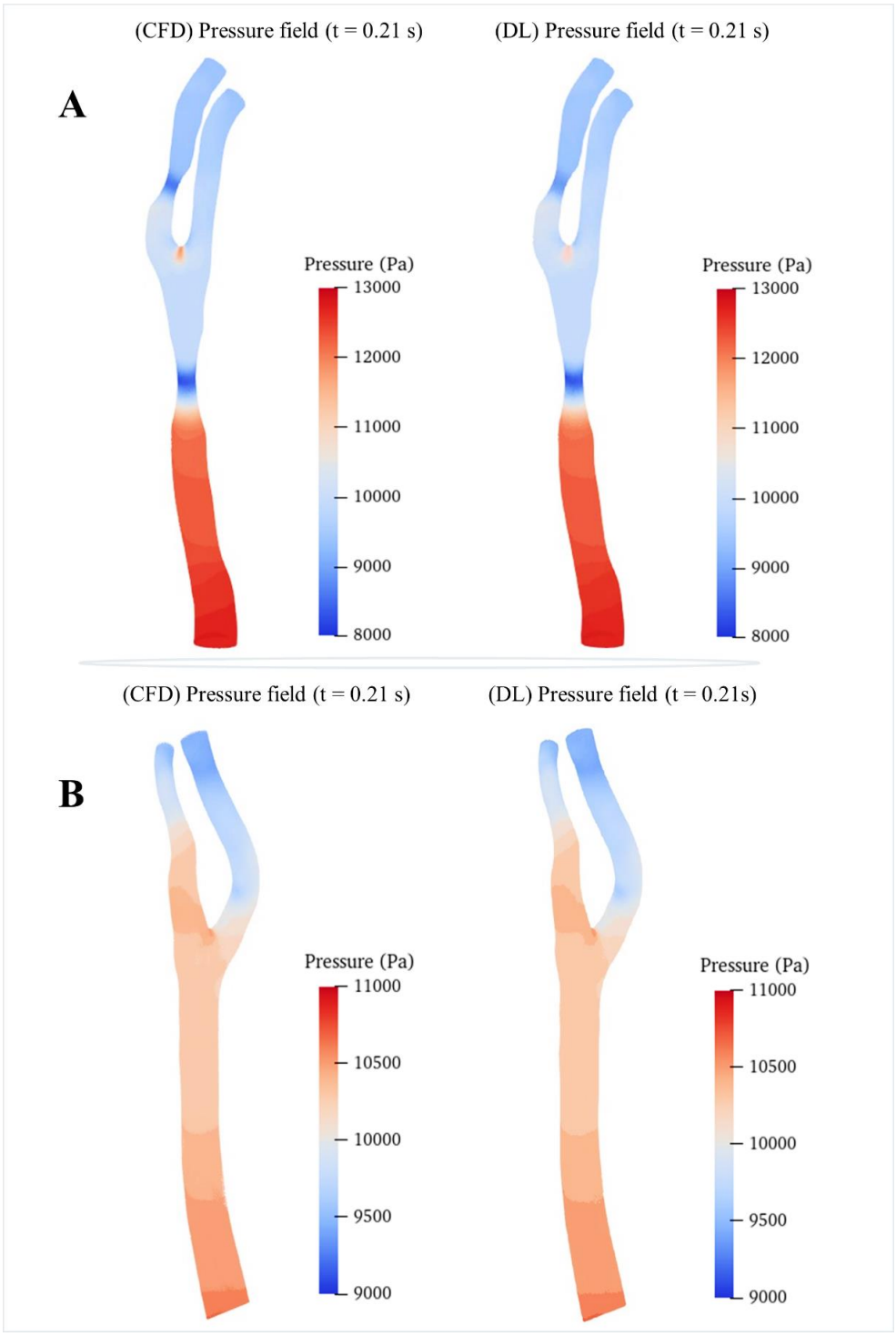

Fig. 4-5 Comparison of pressure fields between CFD simulation and DL prediction. A. Carotid stenotic artery model; B. Carotid artery model without stenosis (cavity changed model).

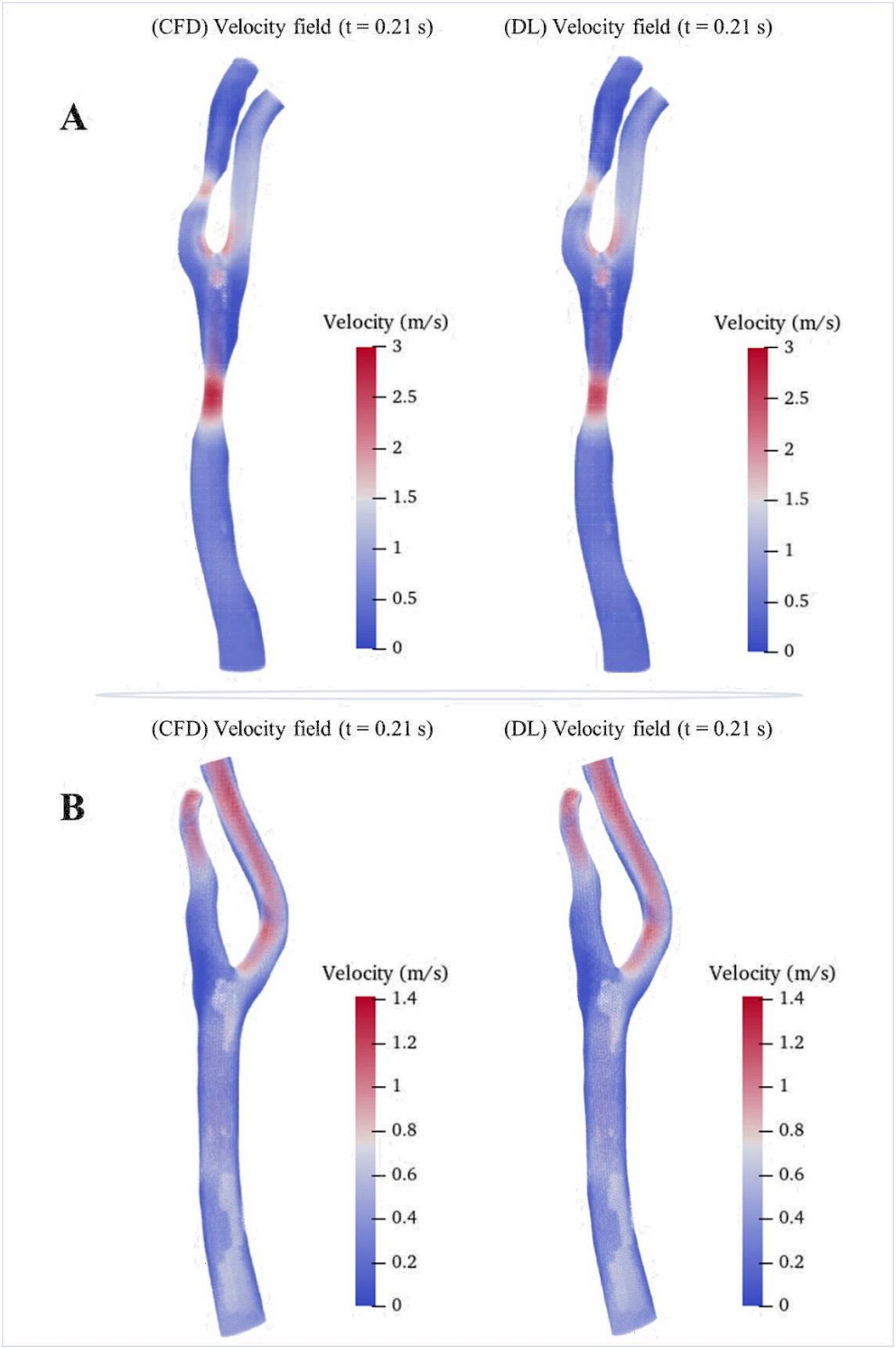

Fig. 4-6 Comparison of velocity fields between CFD results and DL prediction. A. Carotid stenotic artery model; B. Carotid artery model without stenosis (cavity changed model).

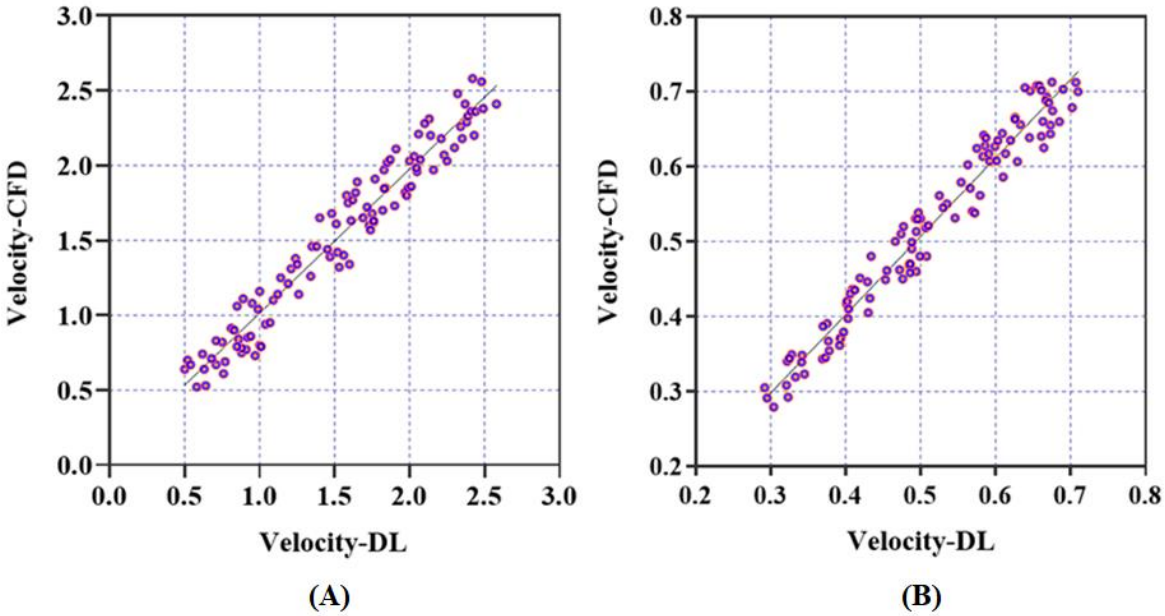

Fig. 4-7 Comparison of averaged velocities in the vicinity of stenosis between DL- and CFD-based results. A. Scatterplot of averaged velocities for preoperative models in terms of Velocity-CFD and Velocity-DL. B. Scatterplot of averaged velocities for postoperative models in terms of Velocity-CFD and Velocity-DL.

We then randomly selected a preoperative model and a postoperative (cavity changed) model from the testing sets as samples to intuitively illustrate the predicted hemodynamic results in terms of pressure and velocity distributions of the maximum inflow rate (t = 0.21 s in Fig. 4-1-B) as illustrated in Figs. 4-5 and 4-6. It is observed that both the pressure fields (Fig. 4-5) and velocity fields (Fig. 4-6) associated with the CAS model and the normal carotid artery model (i.e., the cavity changed model) display excellent consistency between the CFD-based and DL-predicted results.

Table 4-3: Error functions of pressure and velocity fields

Types	Locations	Hemodynamic Parameters	NMAE	MRE
Preoperative	Whole Model	Pressure	3.34 ± 1.31	6.47 ± 1.42
		Velocity	4.53 ± 1.45	8.03 ± 1.57
	Stenosis	Pressure	6.31 ± 2.72	10.42 ± 3.69
		Velocity	7.16 ±1.50	11.48 ± 3.86
	Bifurcation	Pressure	5.34 ± 1.69	10.63 ± 2.64
		Velocity	6.88 ± 2.25	12.35 ± 3.61
Postoperative	Whole Model	Pressure	1.77 ± 1.12	3.81 ± 1.47
		Velocity	2.83 ± 1.33	4.29 ± 1.67
	Bifurcation	Pressure	3.91 ± 2.39	7.87 ± 2.05
		Velocity	5.47 ± 1.74	9.73 ± 2.60

In addition, we summarized the error function results of the velocity and pressure fields in Table 3 in terms of the mean radial error (MRE) (Equation (1)) and the normalized mean absolute error (NAME) (Equation (2)) to investigate the error at each mesh point of the testing set models. Except for the overall error, we also segmented the narrow stenotic portion of the CAS model and calculated the corresponding errors. The error function results indicate that our DL method can achieve reasonable and effective hemodynamic prediction with the maximum error of less than 12.5% throughout the flow field inside the CAS model. The prediction errors for the pressure field are noticeably lower than those of the velocity field, which may be due to the DL-based prediction of the three velocity components at each point can significantly increase the computational cost associated with the corresponding

network, substantially leading to high errors. Besides, the errors of the stenotic models are noticeably larger than the normal carotid artery model (the cavity changed model), probably because of the complex transient flow structures in the vicinity of the stenosis, which may lower the DL-based prediction accuracy. With respect to the computational cost between CFD simulation and DL-based prediction, it is obvious that the DL method is superior, which enables the prediction to be accomplished within merely 1 second. The CFD simulation that comprises the pre-processing of the geometric CAS modeling, the numerical simulation for four beat cycles, and the post-processing of the computed results, however, being run at Intel Core I5-9400 2.9 GHz × 4 CPU, takes approximately 2 hours on the server, indicates that the computational cost of the CFD simulation can be reduced by approximately 7200 times.

In addition, we carried out a consistent analysis of the DL- and CFD-based results to examine the prediction performance and capability of clinical application. We calculated the averaged flow velocities, i.e., the mean values of velocities at all points of the narrowest cross-sections of the stenoses on ICA and CCA, based on the preoperative and postoperative testing set models. Correlations between DL- and CFD-based average velocities are compared in terms of Velocity-CFD and Velocity-DL, as depicted in Fig. 4-7 of the scatter plot of the preoperative models with $r = 0.9471$, $P < 0.001$ (Fig. 4-7-A), and the scatter plot of the postoperative models with $r = 0.9584$, $P < 0.001$ (Fig. 4-7-B), respectively. Obviously, good consistency is observed between the DL-based predictions and the CFD-based simulations equally in the preoperative and postoperative datasets.

4.4 Discussion

In this study, we proposed a DL strategy for the first time to predict the 3D and unsteady hemodynamics of stenotic carotid arteries before and after surgical treatments (i.e., cavity

change). Error analysis results show that the DL strategy can achieve high-accuracy hemodynamic prediction (ERR<12.5%) while reducing computational cost by 7200 times, which demonstrates the clinical potential and practical capability of the DL strategy in predicting complex hemodynamics for stenotic arteries while reducing the computational cost and simplifying the operation process.

Table 4-4: Comparison of ML- and DL-based methods on hemodynamic prediction

Method	Predicting objective	Subject number	Data size	Data format	Performance
Current DL-based strategy	3D CAS unsteady hemodynamics	298	1000	High resolution point cloud	MRE < 12.5%, NAME < 7.5%
ML approach (Itu et al)	Fractional flow reserve (FFR) value	87	12000	Geometric parameter	Accuracy = 99.7%
Deconvolution Network (Guo et al)	2D steady flow	None	400000	Low resolution pixels	MRE < 3%
CNNs model (Su et al)	2D unsteady WSS distribution	small	2000	Low resolution pixels	MAE < 2.5%
DNNs model (Liang et al)	3D thoracic aorta hemodynamics	25	729	Low resolution meshes	NMAE<6.5%

As summarized in Table 4, the previous studies on predicting flow fields or hemodynamic parameters based on ML or DL methods are limited to either 2D and reduced

models or simplified 3D models but with no applications to the complex CAS. Itu et al. reported an ML-based model to predict the FFR parameter [18] but with a reduced-order model, which is highly targeted but limited in its application scope. Guo et al. presented a deconvolutional network (CNN)-based model for the prediction of 2D and/or 3D flow fields [23] by developing a dimensionality-reduction model, however, which can cause the information loss of flow fields because the data normalization process introduces considerable noises, needing larger datasets and hence much more computational cost. By generating a large number of idealized blood vessel models based on a small size of clinical datasets and employing a convolutional neural network, Su et al. achieved the 2D real-time wall shell stress (WSS) prediction [172], but their model did not take account for the realistic spatial geometric information. Recently, Liang et al. built up 3D idealized thoracic aorta models but used merely 80,100 nodes for model segmentation and normalization of the human thoracic aorta [24], which was combined with a DL method. Even though a high-resolution prediction of 3D hemodynamics was achieved, the small-scale dataset of subjects and the utilization of a fixed mesh set for different geometric models largely constrained the flexibility and accuracy of the simulations.

Compared with previous ML- and DL-based studies, this study first manifested in larger clinical datasets, which could demonstrate better generality in terms of capabilities in clinical application. And besides, we used two formats of point cloud datasets that can flexibly characterize the stenosis/ cavity geometry and carotid flow fields while employing a double input-sampling network structure for feature extraction and 3D hemodynamic prediction. The mesh-independent test result demonstrated that it is sufficient to accurately characterize the geometry of stenotic carotid artery models at a suitable resolution. The variability of point clouds regarding quantity and spatial coordinates is conducive to accurately characterizing different complex models that vary from a preoperative artery to a

postoperative artery, which previous DL studies cannot handle. For instance, a stenotic model contained approximately 40,000 cavity points and 220,000 fluid points. And to match the point cloud's characteristics, the employed DL network could extract the geometric information from the cavity point cloud while obtaining the hemodynamic information from the fluid point cloud. Specifically, the network was separately constrained by the global geometric features of the overall blood cavity while guided by the local hemodynamic information. Thus, the combination of the point cloud and the DL network could effectively introduce spatial relationships by stitching the two modules and then realizing point-by-point hemodynamic prediction of a carotid artery.

For the ERR results, the stenotic model was higher than the cavity changed model (Table 3), which may be due to the difference in the flow field and complexity of the narrow location. In our CAS models, the number of fluid points in the lesion area of the artery accounted for approximately 10% of the entire model, which means that the ERRs of the entire model was mainly determined by the stenosis part. In addition, flow field changes in the stenosis due to a narrow lumen, as well as secondary flow near the bifurcation site, lead to large changes in the flow field at the stenosis site. On the other hand, compared with the healthy model, the lesion model (CAS) has a larger range regardless of the velocity field and the pressure field, resulting in the ERRs in the stenotic part being more sensitive to flow field changes. Taking the above factors into consideration, the ERRs of diseased arteries, i.e., the CAS models, were higher than those of healthy arteries (the whole model), and the ERRs of the lesioned and bifurcated areas of the models were the highest.

The limitations of this study mainly lie in the insufficient number of clinical patients and the related pathological information. These limitations are reflected in the following: First, 720 augmented models were constructed through morphological modification of the carotid artery models based on the original dataset of the 280 patients but without apparent

CAS features, which was conducted by adjusting the seven primary parameters of the diameters of CCA, ICA, and ECA, the bifurcation angle between ICA and CCA, the stenosis location, the number of stenoses, the stenosis severity, and the stenosis length base on. Thus, it is necessary to enlarge the original dataset by recruiting more patients with recognizable CAS diseases to enhance the efficiency, stability, and accuracy of the DL training analysis. Second, the lesion generated for constructing the stenotic artery is idealistic and thus ignores the diversity in stenoses such as asymmetric type, multiple contiguous types, etc. Therefore, a comprehensive analytical study on simultaneously validating the applicability and ability of our DL strategy for patients with different types of stenosis will be explored in our future studies by expanding the sample size of real clinical data. Third, instead of imposing personalized boundary conditions on each artery, we employed a general boundary condition for the CFD simulations and then selected only one time instant of the CFD results for the DL dataset generation. Moreover, owing to solely focusing on the cavity change while ignoring the influences of surgical treatments, we neither utilized the arterial models treated by carotid endarterectomy nor a balloon or a vascular stent for expanding the narrowed artery. Therefore, like the postoperative scars, the thickness of an actual vascular stent, and the interaction between stents and blood vessels that we did not include in our study [9], which in turn may impact the reasonably of hemodynamic results and lead to potential errors. Finally, our study only chose the artery portion near the carotid bifurcation as the object of interest. It did not account for the cerebral artery and facial artery parts downstream of the ICA and the ECA, respectively, as well as the cardiovascular artery upstream of the CCA, which will be evaluated in our future study.

In summary, this study aimed to employ a flexible data format to represent high-resolution geometric stenotic arteries while proposing a suitable DL network and substantially achieved an accurate prediction of hemodynamic results of carotid stenotic

arteries before and after surgical treatments. Therefore, with the high goal of applying our DL strategy to real-time clinical revascularization surgery guidance, improvement of our strategy prediction performance and applicability through optimizing our DL methods with larger datasets will be our next research target.

4.5 Conclusion

In this study, we proposed a simulation-based framework to achieve DL-based hemodynamic prediction of normal and diseased carotid arteries. Through establishing high-quality point cloud datasets combined with an advanced DL network, the DL-based methodology is verified capable of achieving high accurate DL predictions, which are well consistent with computational fluid dynamic (CFD) simulations while dramatically reducing computational costs. This points to the capability and feasibility of the DL-based strategy for fast and accurately predicting the hemodynamics of carotid artery stenosis (CAS) before and after surgical treatments.

Chapter V

Conclusions and outlooks

5.1 Summary of contributions

In this thesis, we propose novel machine learning (ML)- and deep learning (DL)-based strategies for the evaluation and treatment of cardiovascular diseases (CVDs). These ML and DL methods overcome the challenges that traditional methods cannot address, such as the unclear quantitative relationships between cardiac function and pulse wave signals, blood supply capability of patients with heart failure and pulse wave signals, and the high computational cost of computational fluid dynamic (CFD) simulations for obtaining the hemodynamics of carotid artery stenosis (CAS) before and after surgical treatments.

In Chapter I, we introduce the harmful effects, diagnosis, and treatments of the cardiovascular diseases that we focus on with ML, DL, and CFD, especially the methods we employ for AI-based analysis.

In Chapter II: For the first time, we propose an ML strategy that enables a fast yet accurate noninvasive prediction of cardiac function parameters based on pulse waves. The feasibility and potential of pulse wave-based prediction of physiological and pathological CVD conditions in clinical applications are revealed. Based on a database of 412 subjects, we selected three parameters - arterial compliance, total peripheral resistance, and stroke volume - as important indicators reflecting cardiac function. Two subject groups were created to represent different datasets. The independent sample t-test confirmed that our subject groups could represent the typical physiological characteristics of the corresponding population. Our ML model is validated through consistency analysis of the ML-predicted three cardiovascular function parameters with clinical measurements. The error analysis also proved its capability to achieve a high-accuracy prediction on TPR and SV for both the healthy-subject group (accuracy: 85.3%, 86.9%) and the CVD-subject group (accuracy: 88.3%, 89.2%).

In Chapter III: the promising potential of ML in predicting the blood supply capacity of

patients with HF through non-invasive pulse wave signal analysis was demonstrated. Utilizing a high-quality pulse wave dataset from 237patients with HF, we implemented and optimized two validated ML networks to predict crucial cardiovascular function parameters such as left ventricular ejection fraction (LVEF), left ventricular end-diastolic diameter (LVDd), left ventricular end-systolic diameter (LVDs), left atrial dimension (LAD), and peripheral oxygen saturation (SpO2). Statistical tests confirmed the consistency of our dataset with prior studies ($p > 0.05$), while error functions and Bland–Altman analysis demonstrated the accuracy and reliability of our ML models. This work highlights the significant clinical potential of ML methods in HF patient health monitoring and deterioration prevention, offering a novel, non-invasive approach for evaluating blood-supply capability.

In Chapter IV: the capability of the DL-based fast and accurate hemodynamic prediction of pre- and post-surgical treatments of CAS was underscored. Four point-cloud datasets generated from CFD simulation results for the prediction of hemodynamics in CAS pre- and post-surgical treatment models. A DL network with dual input-sampling channels was employed to align with the CFD-based point-cloud datasets. After training, the proposed DL strategy successfully unveiled correlations between transient blood flow characteristics and arterial geometry pre- and post-CAS surgery. Computational costs were remarkably reduced by 7,200 times, with DL-based predictions well-aligned with CFD simulations. This study underscores the potential of a CFD-driven, DL-based approach for predicting 3D transient hemodynamics associated with CAS pre- and post-treatment, offering a valuable tool for ischemic stroke diagnosis and prognosis of surgical treatments.

5.2 Outlook

In this thesis, AI approaches including ML and DL have been verified to play a crucial

role in the diagnosis and prognosis of cardiovascular diseases, assisting in health monitoring and treatment guiding. Our future work will focus on two primary aspects: the expansion of the dataset and the optimization of the network structure.

For Chapter II and Chapter III, our first aim is to expand the dataset in terms of size and scope, incorporating a more diverse range of clinical parameters and patient demographics. This will enhance the generalizability and flexibility of our findings and may enable classification of heart failure patients considering specific cardiovascular diseases. We also plan to include clinically important indicators, such as B-type natriuretic peptide, which are currently absent from our dataset. Furthermore, we intend to refine our Machine Learning models, improving their accuracy and predictive capabilities for a broader range of cardiac function parameters. This involves the exploration of the group classification of healthy and cardiovascular disease (CVD) individuals while quantitatively evaluating the severity of specific CVDs.

For Chapter IV, our goal is to develop a more comprehensive and realistic approach to our carotid artery stenosis (CAS) models. This involves expanding our original dataset with more patients having recognizable CAS diseases, considering diverse types of stenosis, and applying personalized boundary conditions for each artery in our simulations. We also aim to include the effects of real surgical treatments in our models, such as the thickness of a vascular stent, and the interaction between stents and blood vessels. Lastly, we plan to broaden our area of interest to other parts of the artery system, such as the cerebral artery and facial artery parts downstream of the internal carotid artery and the external carotid artery, as well as the cardiovascular artery upstream of the common carotid artery.

Bibliography

[1] A. Halliday, R. Bulbulia, L.H. Bonati, J. Chester, A. Cradduck-Bamford, R. Peto, H. Pan, J. Potter, H.H. Eckstein, B. Farrell, Second asymptomatic carotid surgery trial (ACST-2): a randomised comparison of carotid artery stenting versus carotid endarterectomy, The Lancet. 398 (2021) 1065–1073.

[2] P. Moresoli, B. Habib, P. Reynier, M.H. Secrest, M.J. Eisenberg, K.B. Filion, Carotid stenting versus endarterectomy for asymptomatic carotid artery stenosis: a systematic review and meta-analysis, Stroke. 48 (2017) 2150–2157.

[3] W.J. Powers, A.A. Rabinstein, T. Ackerson, O.M. Adeoye, N.C. Bambakidis, K. Becker, J. Biller, M. Brown, B.M. Demaerschalk, B. Hoh, Guidelines for the early management of patients with acute ischemic stroke: 2019 update to the 2018 guidelines for the early management of acute ischemic stroke: a guideline for healthcare professionals from the American Heart Association/American Stroke , Stroke. 50 (2019) e344–e418.

[4] L.H. Bonati, J. Dobson, R.L. Featherstone, J. Ederle, H.B. van der Worp, G.J. de Borst, P.T.M. Willem, J.D. Beard, T. Cleveland, S.T. Engelter, Long-term outcomes after stenting versus endarterectomy for treatment of symptomatic carotid stenosis: the International Carotid Stenting Study (ICSS) randomised trial, The Lancet. 385 (2015) 529–538.

[5] J. Wang, L. Guo, R.N. Holdefer, Y. Zhang, Q. Liu, Q. Gai, W. Zhang, Intraoperative neurophysiology and transcranial doppler for detection of cerebral ischemia and hyperperfusion during carotid endarterectomy, World Neurosurg. 154 (2021) e245–e253.

[6] J.E. Doenges, A.B. Reed, Vascular surgery presence in carotid endarterectomy YouTube videos, J Vasc Surg. 72 (2020) 1453–1456.

[7] M.A. Darwal, K.M. Liebman, M.J. Binning, Carotid Artery Angioplasty and Stenting: 2-Dimensional Operative Video, Operative Neurosurgery. 19 (2020) E595–E596.

[8] A.N. Kazantsev, N.N. Burkov, Y.N. Zakharov, V.G. Borisov, R.Y. Lider, M.S. Bayandin, A.I. Anufriev, Personalized brain revascularization: computer modeling of the reconstruction zone for carotid endarterectomy, Khirurgiia (Sofiia). (2020) 71–75.

[9] L. Xu, F. Liang, B. Zhao, J. Wan, H. Liu, Influence of aging-induced flow waveform variation on hemodynamics in aneurysms present at the internal carotid artery: a computational model-based study, Comput Biol Med. 101 (2018) 51–60.

[10] W. Fu, Z. Gu, X. Meng, B. Chu, A. Qiao, Numerical simulation of hemodynamics in stented internal carotid aneurysm based on patient-specific model, J Biomech. 43 (2010) 1337–1342.

[11] Y. Han, J. Xia, L. Jin, A. Qiao, T. Su, Z. Li, J. Xiong, H. Wang, Z. Zhang, Computational fluid dynamics study of the effect of transverse sinus stenosis on the blood flow pattern in the ipsilateral superior curve of the sigmoid sinus, Eur Radiol. 31 (2021) 6286–6294.

[12] Y. Fu, A. Qiao, Y. Yang, X. Fan, Numerical simulation of the effect of pulmonary vascular resistance on the hemodynamics of reoperation after failure of one and a half ventricle repair, Front Physiol. 11 (2020) 207.

[13] R. Yamaguchi, G. Tanaka, H. Liu, Effect of elasticity on flow characteristics inside intracranial aneurysms, Int J Neurol Neurother. 3 (2016) 49.

[14] P.H. Winston, Artificial intelligence, Addison-Wesley Longman Publishing Co., Inc., 1984.

[15] M.C. Polson, J.J. Richardson, Foundations of intelligent tutoring systems, Psychology

Press, 2013.

[16] A.S. Sultan, M.A. Elgharib, T. Tavares, M. Jessri, J.R. Basile, The use of artificial intelligence, machine learning and deep learning in oncologic histopathology, Journal of Oral Pathology & Medicine. 49 (2020) 849–856.

[17] R. Cuocolo, M. Caruso, T. Perillo, L. Ugga, M. Petretta, Machine learning in oncology: a clinical appraisal, Cancer Lett. 481 (2020) 55–62.

[18] L. Itu, S. Rapaka, T. Passerini, B. Georgescu, C. Schwemmer, M. Schoebinger, T. Flohr, P. Sharma, D. Comaniciu, A machine-learning approach for computation of fractional flow reserve from coronary computed tomography, J Appl Physiol. 121 (2016) 42–52.

[19] I. Goodfellow, Y. Bengio, A. Courville, Deep learning, MIT press, 2016.

[20] A.Y. Hannun, P. Rajpurkar, M. Haghpanahi, G.H. Tison, C. Bourn, M.P. Turakhia, A.Y. Ng, Cardiologist-level arrhythmia detection and classification in ambulatory electrocardiograms using a deep neural network, Nat Med. 25 (2019) 65–69.

[21] W. Chen, Y. Liu, Y. Li, H. Dang, Sacubitril/valsartan improves cardiac function in Chinese patients with heart failure: a real-world study, ESC Heart Fail. 8 (2021) 3783–3790.

[22] G. Li, K. Watanabe, H. Anzai, X. Song, A. Qiao, M. Ohta, Pulse-wave-pattern classification with a convolutional neural network, Sci Rep. 9 (2019) 1–11.

[23] X. Guo, W. Li, F. Iorio, Convolutional neural networks for steady flow approximation, Proceedings of the ACM SIGKDD International Conference on Knowledge Discovery and Data Mining. 13-17-Augu (2016) 481–490. https://doi.org/10.1145/2939672.2939738.

[24] L. Liang, W. Mao, W. Sun, A feasibility study of deep learning for predicting hemodynamics of human thoracic aorta, J Biomech. 99 (2020) 109544.

[25] D.B. Santana, Y.A. Zócalo, R.L. Armentano, Integrated e-health approach based on vascular ultrasound and pulse wave analysis for asymptomatic atherosclerosis detection and cardiovascular risk stratification in the community, IEEE Transactions on Information Technology in Biomedicine. 16 (2012) 287–294. https://doi.org/10.1109/TITB.2011.2169977.

[26] I.B. Wilkinson, I.R. Hall, H. MacCallum, I.S. Mackenzie, C.M. McEniery, B.J. Van der Arend, Y.E. Shu, L.S. MacKay, D.J. Webb, J.R. Cockcroft, Pulse-wave analysis: Clinical evaluation of a noninvasive, widely applicable method for assessing endothelial function, Arterioscler Thromb Vasc Biol. 22 (2002) 147–152. https://doi.org/10.1161/hq0102.101770.

[27] T. Weber, M.F. O'Rourke, E. Lassnig, M. Porodko, M. Ammer, M. Rammer, B. Eber, Pulse waveform characteristics predict cardiovascular events and mortality in patients undergoing coronary angiography, J Hypertens. 28 (2010) 797–805.

[28] G. Li, X. Song, A. Qiao, M. Ohta, Research on arterial stiffness status in type 2 diabetic patients based on pulse waveform characteristics, CMES - Computer Modeling in Engineering and Sciences. 117 (2018) 143–155. https://doi.org/10.31614/cmes.2018.04100.

[29] M. Zhaohui, J. Bai, S. Wang, Frequency Domain Analysis of Pulse Oximeter signal of Hypertension patients, Beijing Biomedical Engineering. 21 (2002) 1–4.

[30] T. Suzuki, Y. Suzuki, J. Okuda, R. Minoshima, Y. Misonoo, T. Ueda, J. Kato, H. Nagata, T. Yamada, H. Morisaki, Cardiac output and stroke volume variation measured by the pulse wave transit time method: a comparison with an arterial pressure-based cardiac output system, J Clin Monit Comput. 33 (2019) 385–392.

[31] T. Thenappan, K.W. Prins, R. Cogswell, S.J. Shah, Pulmonary hypertension secondary to heart failure with preserved ejection fraction, Canadian Journal of

Cardiology. 31 (2015) 430–439.

[32] J.E. Trammel, A. Sapra, Physiology, Systemic Vascular Resistance, (2020).

[33] S. Meyers, D. Todd, I.M.R. Wright, L. Gortner, G. Reynolds, Non-invasive assessment of cardiac output with portable continuous-wave Doppler ultrasound, (2008).

[34] M. Tachibana, T. Miyoshi, K. Osawa, N. Toh, H. Oe, K. Nakamura, T. Naito, S. Sato, S. Kanazawa, H. Ito, Measurement of epicardial fat thickness by transthoracic echocardiography for predicting high-risk coronary artery plaques, Heart Vessels. 31 (2016) 1758–1766. https://doi.org/10.1007/s00380-016-0802-5.

[35] C. Wei-Wei, G.A.O. Run-Lin, L.I.U. Li-Sheng, Z.H.U. Man-Lu, W. Wen, W. Yong-Jun, W.U. Zhao-Su, L.I. Hui-Jun, G.U. Dong-Feng, Y. Yue-Jin, China cardiovascular diseases report 2015: a summary, J Geriatr Cardiol. 14 (2017) 1.

[36] F. Prattichizzo, L. La Sala, L. Rydén, N. Marx, M. Ferrini, P. Valensi, A. Ceriello, Glucose-lowering therapies in patients with type 2 diabetes and cardiovascular diseases, Eur J Prev Cardiol. 26 (2019) 73–80.

[37] D. Muller, R. Agrawal, H.-R. Arntz, How sudden is sudden cardiac death, Circulation. 114 (2006) 1146–1150.

[38] E. Marijon, A. Uy-Evanado, F. Dumas, N. Karam, K. Reinier, C. Teodorescu, K. Narayanan, K. Gunson, J. Jui, X. Jouven, Warning symptoms are associated with survival from sudden cardiac arrest, Ann Intern Med. 164 (2016) 23–29.

[39] S.Y. Lee, K.J. Song, S. Do Shin, K.J. Hong, Epidemiology and outcome of emergency medical service witnessed out-of-hospital-cardiac arrest by prodromal symptom: Nationwide observational study, Resuscitation. 150 (2020) 50–59.

[40] R.S. Rosenson, H.B. Brewer, B.J. Ansell, P. Barter, M.J. Chapman, J.W. Heinecke, A. Kontush, A.R. Tall, N.R. Webb, Dysfunctional HDL and atherosclerotic

cardiovascular disease, Nat Rev Cardiol. 13 (2016) 48–60. https://doi.org/10.1038/nrcardio.2015.124.

[41] A.A. Inamdar, A.C. Inamdar, Heart failure: diagnosis, management and utilization, J Clin Med. 5 (2016) 62.

[42] S.D. Cagle, N. Cooperstein, Coronary artery disease: diagnosis and management, Primary Care: Clinics in Office Practice. 45 (2018) 45–61.

[43] L. Stoner, J.M. Young, S. Fryer, Assessments of arterial stiffness and endothelial function using pulse wave analysis, Int J Vasc Med. 2012 (2012).

[44] R.R. Townsend, H.R. Black, J.A. Chirinos, P.U. Feig, K.C. Ferdinand, M. Germain, C. Rosendorff, S.P. Steigerwalt, J.A. Stepanek, Clinical use of pulse wave analysis: proceedings from a symposium sponsored by North American Artery, The Journal of Clinical Hypertension. 17 (2015) 503–513.

[45] S. Kurasawa, S. Koyama, H. Ishizawa, K. Fujimoto, S. Chino, Verification of non-invasive blood glucose measurement method based on pulse wave signal detected by FBG sensor system, Sensors. 17 (2017) 2702.

[46] C.E. Hann, J.G. Chase, T. Desaive, C.B. Froissart, J. Revie, D. Stevenson, B. Lambermont, A. Ghuysen, P. Kolh, G.M. Shaw, Unique parameter identification for cardiac diagnosis in critical care using minimal data sets, Comput Methods Programs Biomed. 99 (2010) 75–87.

[47] B. Saugel, K. Kouz, T.W.L. Scheeren, G. Greiwe, P. Hoppe, S. Romagnoli, D. de Backer, Cardiac output estimation using pulse wave analysis-physiology, algorithms, and technologies: a narrative review, Br J Anaesth. (2020).

[48] D. Wu, S. Wang, J. Xie, B. Mao, B. Li, C. Jin, Y. Feng, G. Li, Y. Liu, Hemodynamic Mechanism of Coronary Artery Aneurysm High Occurrence on Right Coronary Artery, Front Physiol. 11 (2020) 323.

[49] B. Li, K. Xu, J. Liu, B. Mao, N. Li, H. Sun, Z. Zhang, X. Zhao, H. Yang, L. Zhang, A Numerical Model for Simulating the Hemodynamic Effects of Enhanced External Counterpulsation on Coronary Arteries, Front Physiol. 12 (2021) 467.

[50] X. Zhang, H. Haneishi, H. Liu, Multiscale modeling of the cardiovascular system for infants, children, and adolescents: Age-related alterations in cardiovascular parameters and hemodynamics, Comput Biol Med. 108 (2019) 200–212.

[51] X. Zhang, S. Noda, R. Himeno, H. Liu, Cardiovascular disease-induced thermal responses during passive heat stress: an integrated computational study, Int J Numer Method Biomed Eng. 32 (2016) e02768.

[52] A. Işın, C. Direkoğlu, M. Şah, Review of MRI-based brain tumor image segmentation using deep learning methods, Procedia Comput Sci. 102 (2016) 317–324.

[53] G. Li, H. Wang, M. Zhang, S. Tupin, A. Qiao, Y. Liu, M. Ohta, H. Anzai, Prediction of 3D Cardiovascular hemodynamics before and after coronary artery bypass surgery via deep learning, Commun Biol. 4 (2021) 1–12. https://doi.org/10.1038/s42003-020-01638-1.

[54] I. Ullah, M. Hussain, H. Aboalsamh, An automated system for epilepsy detection using EEG brain signals based on deep learning approach, Expert Syst Appl. 107 (2018) 61–71.

[55] G. Li, J. Ji, J. Ni, S. Wang, Y. Guo, Y. Hu, S. Liu, S.-F. Huang, Application of deep learning for predicting the treatment performance of real municipal waste water based on one-year operation of two anaerobic membrane bioreactors, Science of the Total Environment. (2021) 118160. https://doi.org/10.1016/j.scitotenv.2021.151920.

[56] W. Liu, Z. Wang, X. Liu, N. Zeng, Y. Liu, F.E. Alsaadi, A survey of deep neural network architectures and their applications, Neurocomputing. 234 (2017) 11–26.

[57] T.-E. Chen, S.-I. Yang, L.-T. Ho, K.-H. Tsai, Y.-H. Chen, Y.-F. Chang, Y.-H. Lai,

S.-S. Wang, Y. Tsao, C.-C. Wu, S1 and S2 heart sound recognition using deep neural networks, IEEE Trans Biomed Eng. 64 (2016) 372–380.

[58] O. Trojnarska, L. Szczepaniak-Chicheł, M. Gabriel, A. Bartczak-Rutkowska, J. Rupa-Matysek, A. Tykarski, S. Grajek, Arterial stiffness and arterial function in adult cyanotic patients with congenital heart disease, J Cardiol. 70 (2017) 62–67.

[59] M.F. O'Rourke, D.E. Gallagher, Pulse wave analysis., J Hypertens Suppl. 14 (1996) S147-57.

[60] H.-T. Wu, C.-H. Lee, C.-E. Chen, A.-B. Liu, Predicting arterial stiffness with the aid of ensemble empirical mode decomposition (EEMD) algorithm, in: 2010 IEEE International Conference on Wireless Communications, Networking and Information Security, IEEE, 2010: pp. 179–182.

[61] X. Zhang, Y. Shang, D. Guo, T. Zhao, Q. Li, X. Wang, A more effective method of extracting the characteristic value of pulse wave signal based on wavelet transform, J Biomed Sci Eng. 9 (2016) 9–19.

[62] Y. Katsuragawa, H. Ishizawa, Non-invasive blood pressure measurement by pulse wave analysis using FBG sensor, in: 2015 IEEE International Instrumentation and Measurement Technology Conference (I2MTC) Proceedings, IEEE, 2015: pp. 511–515.

[63] V. Hartmann, H. Liu, F. Chen, Q. Qiu, S. Hughes, D. Zheng, Quantitative comparison of photoplethysmographic waveform characteristics: effect of measurement site, Front Physiol. 10 (2019) 198.

[64] K. Takazawa, H. Kobayashi, I. Kojima, A. Aizawa, M. Kinoh, Y. Sugo, M. Shimizu, Y. Miyawaki, N. Tanaka, A. Yamashina, Estimation of central aortic systolic pressure using late systolic inflection of radial artery pulse and its application to vasodilator therapy, J Hypertens. 30 (2012) 908–916.

[65] F. Chang, W. Hong, T. Zhang, J. Jing, X. Liu, Research on wavelet denoising for pulse signal based on improved wavelet thresholding, in: 2010 First International Conference on Pervasive Computing, Signal Processing and Applications, IEEE, 2010: pp. 564–567.

[66] D.P. Kingma, J. Ba, Adam: A method for stochastic optimization, ArXiv Preprint ArXiv:1412.6980. (2014).

[67] G.Y. Zou, Confidence interval estimation for the Bland–Altman limits of agreement with multiple observations per individual, Stat Methods Med Res. 22 (2013) 630–642.

[68] X. Ying, An overview of overfitting and its solutions, in: J Phys Conf Ser, IOP Publishing, 2019: p. 22022.

[69] M. Li, M. Soltanolkotabi, S. Oymak, Gradient descent with early stopping is provably robust to label noise for overparameterized neural networks, in: International Conference on Artificial Intelligence and Statistics, PMLR, 2020: pp. 4313–4324.

[70] D. Giavarina, Understanding bland altman analysis, Biochem Med (Zagreb). 25 (2015) 141–151.

[71] A. Markina, A. Fedotov, Spectral method of photoplethysmogram processing for screening of atherosclerosis, J Biomed Photonics Eng. 3 (2017) 020305. https://doi.org/10.18287/jbpe17.03.020305.

[72] M.P. Turakhia, M. Desai, H. Hedlin, A. Rajmane, N. Talati, T. Ferris, S. Desai, D. Nag, M. Patel, P. Kowey, Rationale and design of a large-scale, app-based study to identify cardiac arrhythmias using a smartwatch: The Apple Heart Study, Am Heart J. 207 (2019) 66–75.

[73] Z.I. Attia, P.A. Noseworthy, F. Lopez-Jimenez, S.J. Asirvatham, A.J. Deshmukh, B.J. Gersh, R.E. Carter, X. Yao, A.A. Rabinstein, B.J. Erickson, An artificial intelligence-enabled ECG algorithm for the identification of patients with atrial fibrillation during

sinus rhythm: a retrospective analysis of outcome prediction, The Lancet. 394 (2019) 861–867.

[74] M. Zabihi, A.B. Rad, S. Kiranyaz, M. Gabbouj, A.K. Katsaggelos, Heart sound anomaly and quality detection using ensemble of neural networks without segmentation, in: 2016 Computing in Cardiology Conference (CinC), IEEE, 2016: pp. 613–616.

[75] E.D. Luczak, L.A. Leinwand, Sex-based cardiac physiology, Annu Rev Physiol. 71 (2009) 1–18.

[76] V. Regitz-Zagrosek, G. Kararigas, Mechanistic pathways of sex differences in cardiovascular disease, Physiol Rev. 97 (2017) 1–37.

[77] A. Qiao, H. Zhang, J. Xia, Approach to the flow rate distribution of coronary branches in the calculation of fractional flow reserve, Molecular & Cellular Biomechanics. 16 (2019) 35.

[78] P. Porapakkham, P. Porapakkham, H. Zimmet, B. Billah, H. Krum, B-type natriuretic peptide–guided heart failure therapy: a meta-analysis, Arch Intern Med. 170 (2010) 507–514.

[79] N. Rodondi, I. Locatelli, D. Aujesky, J. Butler, E. Vittinghoff, E. Simonsick, S. Satterfield, A.B. Newman, P.W.F. Wilson, M.J. Pletcher, Framingham risk score and alternatives for prediction of coronary heart disease in older adults, PLoS One. 7 (2012) e34287.

[80] B. Bozkurt, A. Coats, H. Tsutsui, A Report of the Heart Failure Society of America, Heart Failure Association of the European Society of Cardiology, Japanese Heart Failure Society and Writing Committee of the Universal Definition of Heart Failure Consensus Conference., Eur J Heart Fail. (2021).

[81] H. Butrous, S.L. Hummel, Heart failure in older adults, Canadian Journal of

Cardiology. 32 (2016) 1140–1147.

[82] G. Savarese, L.H. Lund, Global public health burden of heart failure, Card Fail Rev. 3 (2017) 7.

[83] P.A. McKee, W.P. Castelli, P.M. McNamara, W.B. Kannel, The natural history of congestive heart failure: the Framingham study, New England Journal of Medicine. 285 (1971) 1441–1446.

[84] P. Ponikowski, A.A. Voors, S.D. Anker, H. Bueno, J.G.F. Cleland, A.J.S. Coats, V. Falk, J.R. González-Juanatey, V.-P. Harjola, E.A. Jankowska, 2016 ESC Guidelines for the diagnosis and treatment of acute and chronic heart failure, Kardiologia Polska (Polish Heart Journal). 74 (2016) 1037–1147.

[85] J.S. Burchfield, M. Xie, J.A. Hill, Pathological ventricular remodeling: mechanisms: part 1 of 2, Circulation. 128 (2013) 388–400.

[86] M. Yildiz, A.A. Oktay, M.H. Stewart, R. V Milani, H.O. Ventura, C.J. Lavie, A. Aimo, G. Vergaro, A. González, A. Barison, J. Lupón, V. Delgado, A.M. Richards, R.A. de Boer, T. Thum, H. Arfsten, Cardiac remodelling–Part 2: Clinical, imaging and laboratory findings. A review from the Study Group on Biomarkers of the Heart Failure Association of the European Society of Cardiology, Prog Cardiovasc Dis. 24 (2022) 944–958.

[87] P. Martens, H. Beliën, M. Dupont, W. Mullens, Insights into implementation of sacubitril/valsartan into clinical practice, ESC Heart Fail. 5 (2018) 275–283.

[88] W.W. Parmley, Pathophysiology of congestive heart failure, Am J Cardiol. 55 (1985) A9–A14.

[89] J. Bauersachs, Heart failure drug treatment: the fantastic four, Eur Heart J. 42 (2021) 681–683.

[90] C.W. Yancy, M. Jessup, B. Bozkurt, J. Butler, D.E. Casey, M.H. Drazner, G.C.

Fonarow, S.A. Geraci, T. Horwich, J.L. Januzzi, 2013 ACCF/AHA guideline for the management of heart failure: a report of the American College of Cardiology Foundation/American Heart Association Task Force on Practice Guidelines, J Am Coll Cardiol. 62 (2013) e147–e239.

[91] S.D. Solomon, N. Anavekar, H. Skali, J.J. V McMurray, K. Swedberg, S. Yusuf, C.B. Granger, E.L. Michelson, D. Wang, S. Pocock, Influence of ejection fraction on cardiovascular outcomes in a broad spectrum of heart failure patients, Circulation. 112 (2005) 3738–3744.

[92] A.C. of E. Physicians, Ultrasound guidelines: emergency, point-of-care and clinical ultrasound guidelines in medicine, Ann Emerg Med. 69 (2017) e27–e54.

[93] W. Lesyuk, C. Kriza, P. Kolominsky-Rabas, Cost-of-illness studies in heart failure: a systematic review 2004–2016, BMC Cardiovasc Disord. 18 (2018) 1–11.

[94] M. Urbich, G. Globe, K. Pantiri, M. Heisen, C. Bennison, H.S. Wirtz, G.L. Di Tanna, A systematic review of medical costs associated with heart failure in the USA (2014–2020), Pharmacoeconomics. 38 (2020) 1219–1236.

[95] V.N. Agbor, N.A.B. Ntusi, J.J. Noubiap, An overview of heart failure in low-and middle-income countries, Cardiovasc Diagn Ther. 10 (2020) 244.

[96] M. Martirosyan, K. Caliskan, D.A.M.J. Theuns, T. Szili-Torok, Remote monitoring of heart failure: benefits for therapeutic decision making, Expert Rev Cardiovasc Ther. 15 (2017) 503–515. https://doi.org/10.1080/14779072.2017.1348229.

[97] K. Guk, G. Han, J. Lim, K. Jeong, T. Kang, E.-K. Lim, J. Jung, Evolution of wearable devices with real-time disease monitoring for personalized healthcare, Nanomaterials. 9 (2019) 813.

[98] K. Sughimoto, K. Okauchi, D. Zannino, C.P. Brizard, F. Liang, M. Sugawara, H. Liu, K. ichi Tsubota, Total Cavopulmonary Connection is Superior to Atriopulmonary

Connection Fontan in Preventing Thrombus Formation: Computer Simulation of Flow-Related Blood Coagulation, Pediatr Cardiol. 36 (2015) 1436–1441. https://doi.org/10.1007/s00246-015-1180-y.

[99] K. Sughimoto, J. Levman, F. Baig, D. Berger, Y. Oshima, H. Kurosawa, K. Aoki, Y. Seino, T. Ueda, H. Liu, K. Miyaji, Machine learning predicts blood lactate levels in children after cardiac surgery in paediatric ICU, Cardiol Young. (2022) 1–8. https://doi.org/10.1017/S1047951122000932.

[100] X. Song, Y. Liu, S. Wang, H. Zhang, A. Qiao, X. Wang, Noninvasive Hemodynamic Diagnosis based on Nonlinear Pulse Wave Theory Applied to Four Limbs, Front Bioeng Biotechnol. 11 (n.d.) 348.

[101] O.T. Inan, P.F. Migeotte, P. Kwang-Suk, M. Etemadi, K. Tavakolian, R. Casanella, J. Zanetti, J. Tank, I. Funtova, G.K. Prisk, seismocardiography: a review of recent advances. Biomedical and Health Informatics, IEEE Journal Of. 19 (2015) 1414–1427.

[102] E. O'Brien, G. Parati, G. Stergiou, Ambulatory blood pressure measurement: what is the international consensus?, Hypertension. 62 (2013) 988–994.

[103] M. Cikes, S.D. Solomon, Beyond ejection fraction: an integrative approach for assessment of cardiac structure and function in heart failure, Eur Heart J. 37 (2016) 1642–1650.

[104] M. Elgendi, R. Fletcher, Y. Liang, N. Howard, N.H. Lovell, D. Abbott, K. Lim, R. Ward, The use of photoplethysmography for assessing hypertension, NPJ Digit Med. 2 (2019) 60.

[105] R. Nuzzo, Statistical errors, Nature. 506 (2014) 150.

[106] R. Li, K. Sughimoto, X. Zhang, S. Wang, H. Liu, Impacts of respiratory fluctuations on cerebral circulation: a machine-learning-integrated 0-1D multiscale hemodynamic

model, Physiol Meas. (2023).

[107] J.K. W., T.S. Jessica, G.B. S., S. Khader, M. Riccardo, A. Mohsin, A. Euan, D.J. T., Artificial Intelligence in Cardiology, J Am Coll Cardiol. 71 (2018) 2668–2679. https://doi.org/10.1016/j.jacc.2018.03.521.

[108] S. Grigorescu, B. Trasnea, T. Cocias, G. Macesanu, A survey of deep learning techniques for autonomous driving, J Field Robot. 37 (2020) 362–386.

[109] Y. Guo, G. Li, T. Mabuchi, D. Surblys, T. Ohara, T. Tokumasu, Prediction of nanoscale thermal transport and adsorption of liquid containing surfactant at solid-liquid interface via deep learning, J Colloid Interface Sci. (2022).

[110] G. Li, X. Song, H. Wang, S. Liu, J. Ji, Y. Guo, A. Qiao, Y. Liu, X. Wang, Prediction of Cerebral Aneurysm Hemodynamics With Porous-Medium Models of Flow-Diverting Stents via Deep Learning, Front Physiol. (2021) 1513.

[111] D. Shen, G. Wu, H.-I. Suk, Deep learning in medical image analysis, Annu Rev Biomed Eng. 19 (2017) 221.

[112] S. Wang, D. Wu, G. Li, Z. Zhang, W. Xiao, R. Li, A. Qiao, L. Jin, H. Liu, Deep learning-based hemodynamic prediction of carotid artery stenosis before and after surgical treatments, Front Physiol. 13 (2023) 2674.

[113] Y. LeCun, Y. Bengio, G. Hinton, Deep learning, Nature. 521 (2015) 436–444.

[114] M. Mittal, L.M. Goyal, S. Kaur, I. Kaur, A. Verma, D.J. Hemanth, Deep learning based enhanced tumor segmentation approach for MR brain images, Appl Soft Comput. 78 (2019) 346–354.

[115] N. Noorbakhsh-Sabet, R. Zand, Y. Zhang, V. Abedi, Artificial intelligence transforms the future of health care, Am J Med. 132 (2019) 795–801.

[116] A. Bhandary, G.A. Prabhu, V. Rajinikanth, K.P. Thanaraj, S.C. Satapathy, D.E. Robbins, C. Shasky, Y.-D. Zhang, J.M.R.S. Tavares, N.S.M. Raja, Deep-learning

framework to detect lung abnormality–A study with chest X-Ray and lung CT scan images, Pattern Recognit Lett. 129 (2020) 271–278.

[117] G. Li, J. Ji, J. Ni, S. Wang, Y. Guo, Y. Hu, S. Liu, S.-F. Huang, Y.-Y. Li, Application of deep learning for predicting the treatment performance of real municipal wastewater based on one-year operation of two anaerobic membrane bioreactors, Science of The Total Environment. 813 (2022) 151920.

[118] S. Wang, D. Wu, G. Li, X. Song, A. Qiao, R. Li, Y. Liu, H. Anzai, H. Liu, A machine learning strategy for fast prediction of cardiac function based on peripheral pulse wave, Comput Methods Programs Biomed. 216 (2022) 106664.

[119] M.G. Neto, L.F.G. Duarte, E. de Sousa Rodrigues Jr, H.S. Bittencourt, N.G. Dos Santos, B.C. David, E. da Silva Lima, H.F.C. Dos Reis, Effects of noninvasive ventilation with bilevel positive airway pressure on exercise tolerance and dyspnea in heart failure patients, Hellenic Journal of Cardiology. 59 (2018) 317–320.

[120] S.E. Lee, H.-Y. Lee, H.-J. Cho, W.-S. Choe, H. Kim, J.-O. Choi, E.-S. Jeon, M.-S. Kim, K.-K. Hwang, S.C. Chae, Reverse J-curve relationship between on-treatment blood pressure and mortality in patients with heart failure, JACC Heart Fail. 5 (2017) 810–819.

[121] G. Zhao, Y. Li, L. Cui, X. Li, Z. Jin, X. Han, E. Fang, Y. Gao, D. Zhou, H. Jiang, Increased circulating cathepsin K in patients with chronic heart failure, PLoS One. 10 (2015) e0136093.

[122] L. Xie, Q.-Y. Xu, X.-Q. Zheng, J.-H. Xue, J.-J. Niu, T.-C. Yang, Evaluation of the efficacy of four anti-SARS-CoV-2 antibodies after vaccination using kits from two manufacturers: A prospective, longitudinal, cohort study at 11 serial time points within 160 days, Int Immunopharmacol. (2022) 109285.

[123] N.K. Chauhan, K. Singh, A review on conventional machine learning vs deep learning,

in: 2018 International Conference on Computing, Power and Communication Technologies (GUCON), IEEE, 2018: pp. 347–352.

[124] Y. Li, S. Carabelli, E. Fadda, D. Manerba, R. Tadei, O. Terzo, Machine learning and optimization for production rescheduling in Industry 4.0, The International Journal of Advanced Manufacturing Technology. 110 (2020) 2445–2463.

[125] G. Huang, Z. Liu, L. Van Der Maaten, K.Q. Weinberger, Densely connected convolutional networks, in: Proceedings of the IEEE Conference on Computer Vision and Pattern Recognition, 2017: pp. 4700–4708.

[126] J. Schmidt-Hieber, Nonparametric regression using deep neural networks with ReLU activation function, The Annals of Statistics. 48 (2020) 1875–1897.

[127] L. Razzaq, M. Farooq, M.A. Mujtaba, F. Sher, M. Farhan, M.T. Hassan, M.E.M. Soudagar, A.E. Atabani, M.A. Kalam, M. Imran, Modeling viscosity and density of ethanol-diesel-biodiesel ternary blends for sustainable environment, Sustainability. 12 (2020) 5186.

[128] A. De Myttenaere, B. Golden, B. Le Grand, F. Rossi, Mean absolute percentage error for regression models, Neurocomputing. 192 (2016) 38–48.

[129] A. Carkeet, Exact parametric confidence intervals for Bland-Altman limits of agreement, Optometry and Vision Science. 92 (2015) e71–e80.

[130] S. Scolletta, L. Bodson, K. Donadello, F.S. Taccone, A. Devigili, J.-L. Vincent, D. De Backer, Assessment of left ventricular function by pulse wave analysis in critically ill patients, Intensive Care Med. 39 (2013) 1025–1033.

[131] S. Valenti, G. Volpes, A. Parisi, R. Pernice, S. Stivala, L. Faes, A. Busacca, A silicon photomultiplier-based analog front-end for DC component rejection and pulse wave recording in photoplethysmographic applications, in: 2022 IEEE International Symposium on Medical Measurements and Applications (MeMeA), IEEE, 2022: pp.

1–6.

[132] M. Doerr, S. Weber, R. Birkemeyer, L. Leonardi, C. Winterhalder, C.J. Raichle, N. Brasier, T. Burkard, J. Eckstein, iPhone App compared with standard blood pressure measurement–The iPARR trial, Am Heart J. 233 (2021) 102–108.

[133] A.S. Vischer, J. Rosania, T. Socrates, C. Blaschke, J. Eckstein, Y.-M. Proust, G. Bonnier, M. Proença, M. Lemay, T. Burkard, Comparability of a Blood-Pressure-Monitoring Smartphone Application with Conventional Measurements—A Pilot Study, Diagnostics. 12 (2022) 749.

[134] N.R. Hill, C. Arden, L. Beresford-Hulme, A.J. Camm, D. Clifton, D.W. Davies, U. Farooqui, J. Gordon, L. Groves, M. Hurst, Identification of undiagnosed atrial fibrillation patients using a machine learning risk prediction algorithm and diagnostic testing (PULsE-AI): Study protocol for a randomised controlled trial, Contemp Clin Trials. 99 (2020) 106191.

[135] N. Sahni, G. Simon, R. Arora, Development and validation of machine learning models for prediction of 1-year mortality utilizing electronic medical record data available at the end of hospitalization in multicondition patients: a proof-of-concept study, J Gen Intern Med. 33 (2018) 921–928.

[136] K. Nagpal, D. Foote, Y. Liu, P.-H.C. Chen, E. Wulczyn, F. Tan, N. Olson, J.L. Smith, A. Mohtashamian, J.H. Wren, Development and validation of a deep learning algorithm for improving Gleason scoring of prostate cancer, NPJ Digit Med. 2 (2019) 48.

[137] V. Hachinski, Stroke and potentially preventable dementias proclamation: updated world stroke day proclamation, Stroke. 46 (2015) 3039–3040.

[138] X. Zhang, L. Zheng, M. Luo, C. Shu, E. Wang, Evaluation of particle shape, size and magnetic field intensity for targeted delivery efficiency and plaque injury in treating

atherosclerosis, Powder Technol. 366 (2020) 63–72.

[139] J. Pan, X. Li, Y. Peng, Remote ischemic conditioning for acute ischemic stroke: dawn in the darkness, Rev Neurosci. 27 (2016) 501–510.

[140] D. Barthels, H. Das, Current advances in ischemic stroke research and therapies, Biochimica et Biophysica Acta (BBA)-Molecular Basis of Disease. 1866 (2020) 165260.

[141] A.N. Alagöz, B.A. Acar, T. Acar, A. Karacan, B.E. Demiryürek, Relationship between carotid stenosis and infarct volume in ischemic stroke patients, Med Sci Monit. 22 (2016) 4954.

[142] W. Brinjikji, J. Huston, A.A. Rabinstein, G.-M. Kim, A. Lerman, G. Lanzino, Contemporary carotid imaging: from degree of stenosis to plaque vulnerability, J Neurosurg. 124 (2016) 27–42.

[143] Y. Kubota, Y. Hanaoka, J. Koyama, Y. Fujii, T. Ogiwara, K. Ito, T. Horiuchi, T-configuration stent placement for carotid bifurcation stenosis co-existing with ipsilateral intracranial stenosis: a case report and literature review, Journal of Stroke and Cerebrovascular Diseases. 30 (2021) 105472.

[144] D.F. Bandyk, Follow-up after carotid endarterectomy and stenting: What to look for and why, in: Semin Vasc Surg, Elsevier, 2020: pp. 47–53.

[145] F. Liang, M. Oshima, H. Huang, H. Liu, S. Takagi, Numerical Study of Cerebroarterial Hemodynamic Changes Following Carotid Artery Operation: A Comparison between Multiscale Modeling and Stand-Alone Three-Dimensional Modeling, J Biomech Eng. 137 (2015). https://doi.org/10.1115/1.4031457.

[146] K. Matsuura, W.W. Jin, H. Liu, G. Matsumiya, Computational fluid dynamics study of the end-side and sequential coronary artery bypass anastomoses in a native coronary occlusion model†, Interact Cardiovasc Thorac Surg. 26 (2018) 583–589.

https://doi.org/10.1093/icvts/ivx376.

[147] H. Liu, F. Liang, J. Wong, T. Fujiwara, W. Ye, K. Tsubota, M. Sugawara, Multi-scale modeling of hemodynamics in the cardiovascular system, Acta Mechanica Sinica. 31 (2015) 446–464.

[148] Q. Hou, K. Tao, T. Du, H. Wei, H. Zhang, S. Chen, Y. Pan, A. Qiao, A computational analysis of potential aortic dilation induced by the hemodynamic effects of bicuspid aortic valve phenotypes, Comput Methods Programs Biomed. (2022) 106811.

[149] M.L. Rizzini, A. Candreva, C. Chiastra, E. Gallinoro, K. Calò, F. D'Ascenzo, B. De Bruyne, T. Mizukami, C. Collet, D. Gallo, Modelling coronary flows: impact of differently measured inflow boundary conditions on vessel-specific computational hemodynamic profiles, Comput Methods Programs Biomed. (2022) 106882.

[150] R.S. Driessen, I. Danad, W.J. Stuijfzand, P.G. Raijmakers, S.P. Schumacher, P.A. van Diemen, J.A. Leipsic, J. Knuuti, S.R. Underwood, P.M. van de Ven, A.C. van Rossum, C.A. Taylor, P. Knaapen, Comparison of Coronary Computed Tomography Angiography, Fractional Flow Reserve, and Perfusion Imaging for Ischemia Diagnosis, J Am Coll Cardiol. 73 (2019) 161–173. https://doi.org/10.1016/j.jacc.2018.10.056.

[151] X. Yin, X. Huang, Q. Li, L. Li, P. Niu, M. Cao, F. Guo, X. Li, W. Tan, Y. Huo, Hepatic hemangiomas alter morphometry and impair hemodynamics of the abdominal aorta and primary branches from computer simulations, Front Physiol. 9 (2018) 334.

[152] A. Polanczyk, M. Podgorski, T. Wozniak, L. Stefanczyk, M. Strzelecki, Computational fluid dynamics as an engineering tool for the reconstruction of hemodynamics after carotid artery stenosis operation: A case study, Medicina (B Aires). 54 (2018) 42.

[153] M. Albadawi, Y. Abuouf, S. Elsagheer, S. Ookawara, M. Ahmed, Predicting the onset of consequent stenotic regions in carotid arteries using computational fluid dynamics, Physics of Fluids. 33 (2021) 123106.

[154] M. Conti, C. Long, M. Marconi, R. Berchiolli, Y. Bazilevs, A. Reali, Carotid artery hemodynamics before and after stenting: A patient specific CFD study, Comput Fluids. 141 (2016) 62–74.

[155] D. Bluestein, Utilizing Computational Fluid Dynamics in cardiovascular engineering and medicine—What you need to know. Its translation to the clinic/bedside, Artif Organs. 41 (2017) 117.

[156] A. Taebi, Deep Learning for Computational Hemodynamics: A Brief Review of Recent Advances, Fluids. 7 (2022). https://doi.org/10.3390/fluids7060197.

[157] V. Sklet, Exploring the capabilities of machine learning (ML) for 1D blood flow: Application to coronary flow, (2018).

[158] M. Sarabian, H. Babaee, K. Laksari, Physics-informed neural networks for improving cerebral hemodynamics predictions, ArXiv Preprint ArXiv:2108.11498. (2021).

[159] N. Singh, A.R. Moody, I. Roifman, D.A. Bluemke, A.E.H. Zavodni, Advanced MRI for carotid plaque imaging, Int J Cardiovasc Imaging. 32 (2016) 83–89.

[160] D. Gallo, D.A. Steinman, U. Morbiducci, An insight into the mechanistic role of the common carotid artery on the hemodynamics at the carotid bifurcation, Ann Biomed Eng. 43 (2015) 68–81.

[161] Spatial Team, The Main Benefits and Disadvantages of Point-Cloud Modeling, (2019).

[162] C.R. Qi, H. Su, K. Mo, L.J. Guibas, PointNet: Deep learning on point sets for 3D classification and segmentation, Proceedings - 30th IEEE Conference on Computer Vision and Pattern Recognition, CVPR 2017. 2017-Janua (2017) 77–85.

https://doi.org/10.1109/CVPR.2017.16.

[163] J. Kresslein, P. Haghighi, J. Park, S. Ramnath, A. Sutradhar, J.J. Shah, Automated cross-sectional shape recovery of 3D branching structures from point cloud, J Comput Des Eng. 5 (2018) 368–378.

[164] J.B. Thomas, L. Antiga, S.L. Che, J.S. Milner, D.A. Hangan Steinman, J.D. Spence, B.K. Rutt, D.A. Steinman, Variation in the carotid bifurcation geometry of young versus older adults: implications for geometric risk of atherosclerosis, Stroke. 36 (2005) 2450–2456.

[165] R.F. Smith, B.K. Rutt, A.J. Fox, R.N. Rankin, Geometric characterization of stenosed human carotid arteries, Acad Radiol. 3 (1996) 898–911.

[166] K. Spanos, G. Petrocheilou, C. Karathanos, N. Labropoulos, D. Mikhailidis, A. Giannoukas, Carotid bifurcation geometry and atherosclerosis, Angiology. 68 (2017) 757–764.

[167] L. Goubergrits, K. Affeld, J. Fernandez-Britto, L. Falcon, Geometry of the human common carotid artery. A vessel cast study of 86 specimens, Pathology-Research and Practice. 198 (2002) 543–551.

[168] D. Lopes, H. Puga, J.C. Teixeira, S.F. Teixeira, Influence of arterial mechanical properties on carotid blood flow: Comparison of CFD and FSI studies, Int J Mech Sci. 160 (2019) 209–218. https://doi.org/10.1016/j.ijmecsci.2019.06.029.

[169] H. Gharahi, B.A. Zambrano, D.C. Zhu, J.K. DeMarco, S. Baek, Computational fluid dynamic simulation of human carotid artery bifurcation based on anatomy and volumetric blood flow rate measured with magnetic resonance imaging, Int J Adv Eng Sci Appl Math. 8 (2016) 46–60.

[170] M. Raissi, A. Yazdani, G.E. Karniadakis, Hidden fluid mechanics: Learning velocity and pressure fields from flow visualizations, Science (1979). 367 (2020) 1026–1030.

[171] M. Ghahremani, B. Tiddeman, Y. Liu, A. Behera, Orderly disorder in point cloud domain, in: European Conference on Computer Vision, Springer, 2020: pp. 494–509.

[172] B. Su, J. Zhang, H. Zou, D. Ghista, T. Le, C. Chin, Generating wall shear stress for coronary artery in real-time using neural networks: Feasibility and initial results based on idealized models, Comput Biol Med. 126 (2020) 104038.

Acknowledgements

In completing my doctoral journey, I am immensely grateful for the countless individuals and experiences that have enriched my life and research.

First and foremost, I would like to express my deepest gratitude to my advisor, Professor Hao Liu. Four years ago, he provided me with the incredible opportunity to pursue my PhD at Chiba University. He has been a constant source of guidance and support, both academically and personally. I fondly recall the countless hours he devoted to discussing my first academic paper with me, meticulously reviewing each word and idea, which ultimately sharpened my critical thinking and writing skills.

I am also deeply grateful to the members of my defense committee for their valuable input and willingness to dedicate their time to my graduation pre-defense. I extend my appreciation to Professor Qiao Aike and Professor Liu Youjun for their assistance throughout my research journey.

During my four years in Japan, I have been fortunate to forge lasting friendships and connections with classmates like Wang Jinxin, Li Ruichen, Sun Jianwei, Rong Jiaxin, Xue Yujing, Hiraki Yuto, etc. The memories we've shared will always be treasured.

I owe a debt of gratitude to my parents, whose unwavering support, both emotionally and financially, has been integral to my success. I am equally thankful for my girlfriend Wu Dandan, whose encouragement and companionship have been indispensable in helping me complete my doctoral research.

In writing this acknowledgment, I hope to express my heartfelt thanks to all those who have been instrumental in my journey while maintaining a unique perspective. In the end of my doctoral study, there are so many people and things to acknowledgement.

Publications and presentations

Publications in academic journals (peer-reviewed):

1. Wang, S., Wu, D., Li, G., Song, X., Qiao, A., Li, R., Liu, Y., Anzai, H., and Liu, H. (2022). A machine learning strategy for fast prediction of cardiac function based on peripheral pulse wave. *Computer Methods and Programs in Biomedicine*, *216*, 106664.
2. Wang, S., Wu, D., Li, G., Zhang, Z., Xiao, W., Li, R., Qiao, A., Jin, L., Liu, H. (2023). Deep learning-based hemodynamic prediction of carotid artery stenosis before and after surgical treatments. *Frontiers in Physiology*, *13*, 2674.
3. Wang, S., Ryohei O., Wu D., Aoki K., Kato, H., Iwahana T., Okada S., Kobayashi Y., Liu H. Machine Learning-driven, Pulse Wave-based Evaluation of the Blood-supply Capability of Heart Failure Patients. *Computer Methods and Programs in Biomedicine* (Under review)
4. Wang, S., Wu, D., Li, G., Peng, K., Mu, Y., Ohta, M., Anzai, H., and Qiao, A. (2022). Finite element analysis of the mechanical performance of a zinc alloy stent with the tenon-and-mortise structure. *Technology and Health Care*, *30*(2), 351-359.
5. Wu, D., Wang, S., Xie, J., Mao, B., Li, B., Jin, C., and Liu, Y. (2020). Hemodynamic mechanism of coronary artery aneurysm high occurrence on right coronary artery. *Frontiers in Physiology*, *11*, 323.
6. Song, X., Liu, Y., Wang, S., Zhang, H., Qiao, A., and Wang, X. (2023). Noninvasive Hemodynamic Diagnosis based on Nonlinear Pulse Wave Theory Applied to Four Limbs. *Frontiers in Bioengineering and Biotechnology*, *11*, 348.
7. Li, R., Sughimoto, K., Zhang, X., Wang, S., and Liu, H. (2023). Impacts of respiratory

fluctuations on cerebral circulation: a machine-learning-integrated 0-1D multiscale hemodynamic model. *Physiological Measurement*. 44.3 (2023): 035013.

8. Li, R., Sughimoto, K., Zhang, X., Wang, S., Hiraki, Y., and Liu, H. (2022). Impact of Respiratory Fluctuation on Hemodynamics in Human Cardiovascular System: A 0-1D Multiscale Model. *Fluids*, *7*(1), 28.

Presentations:

1. Wang, S., Li, R., Liu Hao., “機械学習を用いた脈波による心機能の予測.” 日本機械学会 2021 度年次大会，千葉， 2021/09/08.
2. Wang, S., Li, R., and Liu, H., “Fast Prediction of Cardiac Function Based on Pulse Wave via Machine Learning Method.” The 7th International Conference on Computational and Mathematical Biomedical Engineering (CMBE22). 2022/06/27, Milano, Italy. (Oral presentation)